Mechanistic-Based Procedure for the Early Opening of Concrete Pavements

by

Katelyn Kosar

Bachelor's Degree in Civil Engineering, West Virginia University, 2017

Submitted to the Graduate Faculty of the

Swanson School of Engineering in partial fulfillment

of the requirements for the degree of

Doctor of Philosophy

University of Pittsburgh

2023

UNIVERSITY OF PITTSBURGH

SWANSON SCHOOL OF ENGINEERING

This dissertation was presented

by

Katelyn Kosar

It was defended on

March 22, 2023

and approved by

Julie Vandenbossche, PhD, Professor, Department of Civil and Environmental Engineering,

Amir Alavi, PhD, Professor, Department of Civil and Environmental Engineering,

Jeff Roesler, PhD, Professor, Department of Civil Engineering, University of Illinois

Dissertation Director: Lev Khazanovich, PhD, Professor, Department of Civil and Environmental Engineering

Mechanistic-Based Procedure for the Early Opening of Concrete Pavements

Katelyn Kosar, PhD

University of Pittsburgh, 2023

Determining the opening time for a concrete pavement is a critical decision. Longer construction time may negatively affect the contractor and funding government agency by increasing construction cost and the travelling public by increasing the time lost to drivers due to congestion or detours. However, opening early can be detrimental to short- and long-term pavement performance. If a pavement has not had the time to reach the strength needed to carry the expected traffic load, performance issues are possible and the chance of failure or damage increases the earlier a pavement is opened.

Current criteria for opening a concrete pavement to traffic are empirically derived and often outdated with most transportation agencies using an age and strength requirement. The existing criteria do not account for time of construction, design features, early age traffic load conditions, climate conditions, edge support conditions, and other factors that affect early age pavement performance. The current methods also ignore the effect early opening has on the long-term performance. This limits the accuracy of cost-benefit decisions for the life of the pavement when considering when to open to traffic and causes conservative opening times that unnecessarily extend construction and road closure. To address these limitations, this study aimed to improve flexibility and efficiency in traffic opening criteria without compromising pavement performance.

The accurate determination and prediction of in-place concrete strength during early-age development until it achieves design strength is a crucial element of the early opening process. To achieve this, a procedure was proposed that combines nondestructive maturity and ultrasound

tomography methods to improve early-age concrete strength evaluation. This approach leverages the predictive capabilities of the maturity method along with the accuracy and efficiency of ultrasonic testing to obtain maximum information on in-situ concrete strength development during early ages. The combined nondestructive test procedure involves evaluating the shear wave velocity and using the maturity method to predict concrete strength development for a specific location and construction month, enabling users to make informed decisions on when to perform early-age procedures.

A mechanistic-based model for prediction of pavement damage due to early pavement opening was also proposed. The procedure accounts for site conditions and pavement characteristics creating a simplified but accurate model for stress estimations. Web tools were published to implement the developed procedures for easy public use. This provides users with the probability of damage occurring for an alternative opening strength beyond the conservative, generalized state criteria. Users can move forward with procedures based on the conditions of their individual project and increase their allowable construction efficiency.

The results of the recently conducted full scale and laboratory tests conducted by the Minnesota Department of Transportation as well as the University of Pittsburgh Impactful Resilient Infrastructure Science and Engineering (IRISE) public/private research consortium were used to calibrate and validate the methods developed in this study.

Table of Contents

List of Tables

List of Figures

Preface

Thank you everyone who made this possible and gave me so much support. A special thank you to my amazing advisor, Dr. Lev Khazanovich, and knowledgeable committee, Dr. Julie Vandenbossche, Dr. Amir Alavi, and Dr. Jeff Roesler. Thanks is also needed to MnROAD, PennDOT, FHWA, IRISE and Golden Triangle for providing the resources for the field and laboratory experiments and my fellow graduate students who gave their time and effort to help with the large scale data collection required for this research. I am grateful I had the opportunity to work with and know this incredible group.

A final thank you to my wonderful friends, family, and fiancé, Alex. Your support is unparalleled, and I would not be where I am today without you all.

1.0 Introduction

1.1 Problem Statement and Research Objectives

Minimizing roadway closure due to construction and rehabilitation is a modern demand of commercial and passenger traffic. Work zones, and the resulting road closure, can have a significant effect on the overall network. Road closures lead to inconveniences for users including time lost to congestion or alternate routes, confusion caused by detours, and a greater potential for accidents [1]. The increase in idling cars also increases CO_2 emissions [2]. Traffic management plans are currently in use to reduce the effect on users by creating efficient detours and construction schedules [3]. Unfortunatly, reducing adverse effects for users commonly results in construction occurring alongside moving traffic making pavement construction especially hazardous. In 2018, there were 755 fatalities in work zone crashes; 124 of which were construction workers [4].

These effects are evident for highway work zones, but urban road closures have additional concerns. Often urban roads must be fully closed for construction requiring detours and alternative routes. This may divert traffic to roads that are not accustomed to or designed for the increased level of traffic, affecting the quality of other pavements and impacting different drivers in the network [3]. Furthermore, non-drivers, such as public transportation users, can also be affected as work zones may interrupt bus routes or restrict access to local businesses.

Lingering work zones have monetary effects on all involved. For contractors, the duration of construction determines costs of equipment and labor. For road owners and users, a life cycle cost considers the negative effects on the road user through a user cost. User cost includes vehicle operating (fuel, oil, maintenance, etc.), delay (speed loss, detours, etc.), and crash costs [5,6].

User costs can be significant depending on the work zone conditions [5]. A brief analysis examined how work zones on urban roads impact user costs. Simply closing one block in downtown Pittsburgh may result in a user cost of about $65 per hour, with most of the cost incurred on passenger vehicles. The same closure averaged an 11% travel delay on the entire downtown network. This demonstrates the importance of short construction time in urban areas. This example had a short work zone length in a grid network with simple detours; however, more complex situations quickly increase the user costs. Even a few hours saved can lead to a significant reduction in user costs.

Since work zones for pavement construction or maintenance can rarely be avoided, the length of time required to complete the work is a major consideration. Concrete pavement construction fundamentally takes longer than asphalt pavement construction. Asphalt pavements rely on the base layer to provide the strength necessary to carry the traffic load therefore they can open to traffic when the asphalt cools. In concrete pavements, the traffic load is carried by the concrete which requires time to gain the necessary strength. This aspect of concrete pavement allows for a longer service life but requires a longer construction time when compared to asphalt. Often concrete pavement engineers use alternative materials or additives to reduce the time of construction by increasing the rate of strength gain. However, these high early strength mixtures change concrete properties and tend to be expensive.

Minor modifications in scheduling are easily implemented and are effective methods to shorten construction times for both conventional and high early strength concrete. Minimal alterations to scheduling may result in a significant decrease in roadway closure time and can be applied to all levels of traffic and concrete mixture designs. Construction is expensive making time a precious commodity. Proper scheduling is necessary to efficiently shorten construction time.

Productive testing and scheduling can result in a reduction of any delays in early age construction procedures; however, it must be done without jeopardizing pavement performance.

Reducing the construction time of concrete pavements has been a research focus for many years with a variety of successful results that primarily focus on improving concrete mixtures. One aspect of construction that is viable for shortening regardless of mixture is the time a pavement cures before traffic is allowed on the new pavement. Opening a pavement to traffic at the earliest strength allowable can reduce construction time, improve driver satisfaction, and reduce the probability of premature pavement failures. However, there is a delicate balance that needs to be maintained regardless of concrete developments. Opening a pavement early can be detrimental to short- and long-term pavement performance. Since concrete strength must be sufficient to carry the expected traffic load or risk early failure, the risk of damage increases the earlier a pavement is opened. Allowing traffic earlier has the potential for performance issues that have more severe consequences that the negative impacts of a persisting work zone.

Concrete exposed to premature loading is susceptible to internal damage that lowers the durability of a pavement. This can affect shrinkage and compromise the microstructure of concrete which may not be evident immediately but can cause serious performance issues and shorten pavement life. Cracking and fatigue damage can occur immediately after opening [7]. Cracking is a common distress later in pavement life and often maintenance costs to fix damage are expected and accounted for when determining the life cycle cost. However, the need to address this issue so early after construction is inconvenient and overall, avoidable. Joint damage is also possible from loading pavements too early. Early wheel loads can cause excessive bearing stresses on the dowel bars that can damage the concrete around the reinforcement. This is another distress that may not

be evident right away but will cause dowel looseness, compromise load transfer efficiency, and impact the ride quality.

The key to finding the optimum time to open to traffic is determining the strength at which the chance of pavement structural or serviceability damage occurring is small enough that the pavement is still deemed reliable to last the design life. This requires two aspects: accurate and rapid measurement of strength and flexible strength criteria able to adjust to individual roadways.

Early age concrete changes rapidly. Pavement engineers need quick and reliable information on in-situ concrete properties to make knowledgeable decisions on construction procedures such as removing forms, cutting joints, or opening a pavement to traffic. By improving the method of determining concrete strength, procedures can be performed as soon as criteria is met with minimal time lost to testing.

Another important consideration for reducing construction time is to adjust the current requirements for opening a pavement to traffic. Current criteria were empirically determined and conservative to remove the risk of damage caused by early loading on any pavement. Criteria must become flexible to consider individual pavement needs and increase the allowable construction schedule productivity.

This thesis will examine strength determination in the field and the criteria for opening to traffic which can reduce the negative impacts of a work zone, improving worker safety, user experience, and life cycle costs for the project. The purpose of this research is to develop a rational traffic opening criteria for concrete pavements that creates an efficient opening process without jeopardizing pavement performance.

The objectives of this research are:

1. Improve strength prediction using combined nondestructive testing procedures;

2. Predict pavement stress due to early loading using a mechanistic-based analysis;
3. Develop a procedure to analyze risk of damage from early loading times; and
4. Produce a tool for public use to suggest opening criteria for individual projects.

Traffic opening can occur once concrete strength is greater than loading stress. Improving the methods that determine strength and stress is critical to identifying the optimum traffic opening. Nondestructive testing is becoming common practice in various aspects of structural engineering. There are advantages and disadvantages of each nondestructive technology but combining processes can increase the accuracy and efficiency necessary for early age strength determination in the field. Calculated stresses must account for the factors affecting early age concrete. By utilizing a mechanistic-based analysis, an accurate approximation of stresses can be found under varying conditions for different projects.

After strength and stress values are established, a risk analysis can be used to determine at what strength the pavement performance is no longer in jeopardy. This analysis will consider a finer time and traffic loading scale than traditional long-term performance models to encompass the fast paced and variable nature of early age concrete. To utilize the new process outlined in this thesis, web tools were developed for field implementation.

1.2 Research Approach

The methods developed in this dissertation are used to determine the appropriate concrete strength needed for traffic opening without risking concrete pavement performance. This includes several field and laboratory experiments that explored the effect of opening a concrete pavement extremely early and the capabilities and limitations of modern nondestructive tests. The

experiences and data from these experiments were used to develop procedures that increase the efficiency of opening a concrete pavement to traffic.

1.3 Dissertation Organization

Chapter 1 describes the problem and introduces research objectives and approach.

Chapter 2 presents the literature review describing the current standards for opening a concrete pavement to traffic and existing practices for determining concrete strength in the field using destructive and nondestructive methods.

Chapter 3 presents a large-scale field test to determine the effect of opening a concrete pavement to traffic very early. This includes a finite element analysis to identify key factors affecting early age concrete performance and critical stresses.

Chapter 4 presents a laboratory and field experiment to evaluate the ability of two common nondestructive tests to accurately estimate early age concrete strength in the field and compare their proficiency for pavement construction use.

Chapter 5 presents potential improvements for evaluating concrete strength in the field using a procedure combining common nondestructive tests to best evaluate in-situ strength. This includes a laboratory experiment exploring the effect of specimen size on beam velocity measured by a linear array ultrasonic device, and potential reasonings for the phenomenon.

Chapter 6 presents a procedure for a mechanistic-based early opening damage analysis which determines the risk of premature pavement failure based on a chosen opening concrete strength and key factors affecting critical stresses.

Chapter 7 presents web tools for simplified general use that employs the damage analysis and combined nondestructive test procedures. This includes two separate web tools for national and regional use.

Chapter 8 summarizes key findings and outcomes completed in this dissertation and recommends future research.

2.0 Literature Review

2.1 Opening to Traffic Guidelines

The methods of determining concrete strength in the field are evolving to become more accurate and effective. However, strength measured in the field only confirms the set state opening to traffic criteria are met. This limits the achievable construction efficiency for any project to the efficiency of the opening criteria. The minimum requirement is the pavement has the strength required to support the predicted traffic load, but this is difficult to quantify in generalized state guidelines. This section will review the current state guidelines for opening a pavement to traffic and past research that aimed to improve opening criteria.

2.1.1 Current Criteria for Opening to Traffic

Opening times were originally arbitrary wait times which have since evolved into criteria based on concrete compressive or flexural strength [7,8]. Ideally, this criterion is the minimum strength required to carry the stress caused by the expected traffic loads. While the simple rule of strength greater than stress is understood and accepted, it is not currently used in practice when determining the opening-to-traffic guidelines. The strength necessary to carry traffic depends on numerous variables that change between pavements and locations. To reduce the complexity of the criteria, current values are purposely conservative and generalized to be applicable across a state.

Traffic opening criteria are often based on age, compressive strength, flexural strength, or a combination of these factors. Most states have at least an age and compressive strength requirement, although, the age requirement is often secondary so the pavement can be opened whenever the strength criteria is met. There is a lack of consistency in criteria values between states due to the empirical nature of the standards.

For opening conventional concrete to general traffic, the age, compressive strength, and flexural strength criteria ranges between 3 to 15 days, 2000 to 4000 psi, and 250 to 650 psi, respectively, between states (Appendix A). Often with the desire to open a pavement to traffic early, high early strength concrete is used instead of conventional concrete. High early strength concrete has its own set of criteria differing between states as well. For high early strength concrete, the age, compressive strength, and flexural strength criteria ranges between 4 to 24 hours, 1200 to 3500 psi, and 290 to 420 psi, respectively [9].

Several states are beginning to add other categories to their opening criteria. Pennsylvania requires various compressive or flexural strengths depending on slab thickness and length (Table 1) [10]. Alaska and Wisconsin change the age or strength needed to open to traffic depending on ambient temperature. Iowa, Minnesota, and Ohio have a range of opening strengths that depend on concrete layer thickness. Several states consider differing traffic levels offering separate conditions for construction and general traffic (Alabama, Indiana, Missouri, Nebraska, New York, Texas). Kentucky also considers traffic patterns by allowing a pavement to open after 72 hours of curing for residential traffic. California considers load location by allowing traffic at a flexural strength of 350 psi instead of 650 psi if traffic is kept away from the edge.

These additional considerations take an important step in improving opening to traffic criteria by accounting for some site-specific conditions that affect pavement performance. This

improves the opening process to a degree. However, there are few states with these considerations and each state only considers one or two factors.

Table 1: Strength criteria from PennDOT 408 [10]

Slab Thickness, in	Strength for Opening to Traffic, psi			
	Slab Length < 10 ft		Slab Length ≥ 10 ft	
	Compressive Strength	Flexural Strength (3rd point loading)	Compressive Strength	Flexural Strength (3rd point loading)
6.0	3000	490	3600	540
7.0	2400	370	2700	410
8.0	2150	340	2150	340
9.0	2000	275	2000	300
10.0 +	2000	250	2000	300

The existing criteria, regardless of the state, do not account for all critical factors that affect early age pavement performance and ignore the effect early opening has on long-term performance. This limits the accuracy of cost-benefit decisions for the pavement life when considering when to open to traffic. The guidelines are based purely on general long-term performance observations with caution not to load before the design strength is reached even if conditions may allow it. The limitations of current opening to traffic guidelines need to be addressed to improve construction scheduling efficiency.

Another restriction of current criteria is minimal distinction between traffic levels. The stresses applied by lightweight, or passenger, vehicles will be lower than heavy load vehicles. Smaller vehicles could be allowed on pavements before the strength criteria is reached without compromising long-term performance. This would limit the short-term traffic disruption caused by the construction. Only Kentucky currently considers this factor in their specifications.

The opening to traffic criteria must become more flexible to encompass the conditions and needs of individual projects. The current criteria are simply too rigid and general to truly be efficient and cost effective.

2.1.2 Past Research Aiming to Improve Traffic Opening Guidelines

Improving opening to traffic guidelines and criteria is not a new research topic as the desire to shorten construction time has always been a point of concern. Many research projects have approached this problem looking to clarify the allowable opening strength.

"Fast-Track Concrete Pavements" (1994) is an early publication on how to simply reduce construction time and road closure in a procedure they coined "fast track concrete pavement construction" [11]. This paper suggested many different avenues to shorten construction including using high early strength concrete, improving construction organization and planning, using nondestructive testing, and revising traffic opening criteria. They stated that proper strength criteria should depend on vehicle type and weight, number of loads, location of loads, elastic modulus of the concrete, pavement structure design, slab thickness, base and subbase properties, and edge support conditions. They recommended a few basic criteria using flexural strengths for light traffic and allowable edge loading but specified that no traffic should be allowed before joints are cut.

Cole and Okamoto (1995) aimed to change opening to traffic guidelines from generic times and strength chosen at the discretion of agencies to calculated flexural strengths that consider fatigue [12]. They recommended making criteria based on a range of common factors that can affect strength requirements including traffic loading, load location, moisture and temperature gradients, foundation properties, thickness, and road classification. This paper provided several tables of strength requirement recommendations. They also recommended the use of nondestructive testing to estimate strength in the field.

Olek et al. (2002) explored a maturity-based opening to traffic guideline for Indiana based on fatigue performance [7]. They conducted fatigue testing alongside maturity and strength

laboratory testing to develop fatigue – strength relationships and found that the current Indiana criteria are conservative. Olek et al. (2002) recommended opening to traffic criteria be based on fatigue curves for different ages, mixture designs, and curing conditions.

In a report by Yuan and Nazarian (2004) for the Texas Department of Transportation, the focus was on minimizing road closure time [13]. Seismic technologies, including the free-free resonant column test and Portable Seismic Pavement Analyzer, were tested alongside maturity to improve in situ field strength estimation. The study found that the seismic modulus showed a stronger correlation to strength compared to other methods. These seismic technologies are similar to current ultrasonic technologies used. Based on the findings, Yuan and Nazarian (2004) recommended the use of seismic modulus for guidelines on opening pavements to traffic, and identified the great potential of utilizing these nondestructive tests in combination.

Crovetti and Khazanovich (2005) determined a minimum strength requirement for opening to traffic using dowel bearing stress and key pavement design factors [14]. They recommended criteria based on dowel bar size since joint damage can cause significant reduction in pavement performance and life. The laboratory tests on the effect of early loading on concrete surrounding the dowel were inconclusive so no official criteria values were recommended. However, they did create a simplified procedure for critical dowel bearing stresses that aligned well with field data.

Ghafoori and Tays (2007) explored the abrasion resistance of fast track concrete paving [15]. They considered the early opening to traffic effects on abrasion resistance as this was a serious concern with prematurely loaded pavements. They concluded that increased cement content, curing time, and accelerating admixtures improves abrasion resistance; therefore, depending on the fast-track plan employed, abrasion may not be a concern.

Antico et al. (2015) discussed a project based in Indiana that focused on making more accurate opening to traffic criteria [16]. They considered the effect of wheel loadings on pavement behavior and made criteria based on pavement thickness, subgrade qualities, time-dependent elastic modulus, and time-dependent flexural strength. Antico et al. (2015) concluded that allowing pavements with thicker concrete layers to open at an earlier strength will not risk early age cracking, although this model did not consider environmental stresses.

Freeseman et al. (2016) reconsidered the opening criteria for Minnesota using a modified design guide framework [17]. Mechanistic-Empirical Pavement Design Guide (MEPDG) is a procedure for designing pavements that considers stress states and accumulated damage over the design period. Freeseman et al. (2016) adapted the MEPDG framework for fatigue cracking to calculate early-age damage. They created a program that used a MEPDG input file with additional early age information and provided cracking damage prediction based on opening times. This allowed the user to account for different site conditions and traffic opening times. They also recommended using nondestructive testing to estimate strength in the field.

Su et al. (2020) reported on a study based in Indiana that aimed to determine early age properties, and therefore traffic opening times, using electromechanical impedance coupled with piezoelectric sensors [18]. They were able to model concrete stiffness and compressive strength gain with accuracy using sensors imbedded in the field pavement. They did note that while the sensors are durable and sensitive, they are wired and imbedded which creates restrictions in data gathering.

These projects begin addressing the well-known concerns with early age concrete pavement construction procedures, specifically the opening to traffic guidelines. Current opening to traffic criteria uses set standard opening values based on each DOT's digression but early

research suggested set values based on generalized pavement characteristics [7,11,12,14]. To further individualize guidelines, models based on some pavement design and performance properties were developed [16,17]. Even more recently, studies are beginning to fully individualize opening criteria by creating strength relationships [18]. These projects form a solid foundation for further improvement to traffic opening criteria for concrete pavements. However, there are certain limitations with these studies that this research aims to address, including accurate, individualized models, portable data collection, and overall user friendliness.

2.2 Destructive Testing

Early age construction procedures, including opening to traffic, are scheduled and performed based on set strength criteria. This considers the load carrying capacity of a pavement to ensure it is capable of supporting predicted traffic loads. Destructive testing is the conventional method of strength measurement and criteria due to its simple procedure and direct strength measurement. Destructive methods determine strength by purposely failing specimens to determine mechanical properties of concrete [19]. For use in the field, it involves pouring separate specimens using the same concrete used in the field to test at certain ages in a laboratory.

Compressive strength is the most common strength test in the field due to the small specimen size and simple process. However, this test only indirectly evaluates concrete resistance to cracking. Another popular destructive test is flexural strength. This is more representative of a pavement since it simulates a pavement bending under a vehicle load making flexural strength a better indicator of cracking resistance. Flexural strength testing creates a tensile stress state along the bottom of the beam similar to what a pavement experiences under traffic and environmental

loading but it is more involved and complex than the compressive strength test. For either destructive method, testing needs to be done several times at specific ages to properly establish strength gain. Each time increment needs multiple measurements to establish a representative value [20–22].

Regardless of whether compressive or flexural strength testing is used, there are drawbacks to destructive testing. Destructive testing requires separate specimens which may not represent the pavement as they are not experiencing the same conditions. This excludes the effect of time of construction, design features, early age traffic load conditions, climate conditions, edge support conditions, or any other factors that are irreplicable in laboratory but affect pavement performance [11]. There can also be variability within the pavement due to small environmental changes, concrete mixture changes, or placement differences that are not captured by separate sampling [14].

Destructive testing has practical issues as well. Preparing for and performing destructive testing can be labor intensive and time consuming creating a limit on the number of feasible specimens and test ages. This can restrict the data available for decision-making especially at early ages. Destructive testing can also have a high variability due to differences between specimens, operators, or laboratories. This variation is considered in the ASTM standards for each destructive test where the tolerance for multi-laboratory testing is higher than for a single operator.

Destructive testing is lacking for rapid construction projects since it takes time to perform and there are a limited number of avalible specimens. This can leave a gap in productive construction between when the pavement reaches the required strength and when the specimens are tested. Gathering additional information on pavement strength gain and variability needs to be addressed to improve construction scheduling efficiency.

The limitations of destructive testing have led to other methods being used in conjunction to improve concrete pavement strength gain monitoring.

2.3 Nondestructive Testing

Concerns with destructive testing encouraged the research and implementation of nondestructive testing. Nondestructive testing allows the user to inspect, monitor, or test systems without removing survivability of the structure [19]. Nondestructive testing is already commonly used in pavement and structural engineering for estimating in-situ concrete strength and quality control [8,12]. Although destructive testing is still widely used by Departments of Transportation, nondestructive testing is gaining popularity. Many departments have begun accepting nondestructive methods as acceptable measurements of strength to be used for traffic opening criteria. These progressive circumstances indicate an ideal time to update strength determination methods in the field to utilize the latest technologies available.

Nondestructive testing is performed directly on the concrete with minimal or no impact on the structure. This accounts for the effect of environmental, boundary, or curing conditions that may not be repeatable in a laboratory but are critical to determine early age concrete properties [14]. Nondestructive testing empirically correlates concrete properties to measured variables which estimates properties without requiring material failure [8,19].

There are various methods that can measure or estimate a variety of concrete properties including moisture content, density, thickness, and elastic modulus [8]. Each nondestructive method involves different technologies, some imbedded within the pavement, attached to the surface, or a portable machine that allows testing to occur directly on the pavement. Far fewer

specimens are needed in the field in comparison to destructive tests. Destructive tests require dozens of specimens while nondestructive tests may only need a few to confirm relationships developed in the laboratory. Nondestructive methods often have small time-steps for data collection allowing more data to be obtained. Another advantage for many methods of nondestructive testing is portability. Multiple locations on a slab can be monitored to account for variability within a single slab, monitor the strength of critical stress locations, or check areas flagged for potential defects. This can allow for a larger, in-situ area to be analyzed to better identify the abilities of the entire constructed section.

Recent advances in technology have created an opportunity for a wider range of testing devices that evaluate different concrete parameters with increased accuracy. A few popular methods include maturity, ultrasonic tomography, ground penetrating radar, electromechanical impedance, and sounding methods [23]. These methods can determine a variety of parameters including durability, damage, and strength. This study focuses on two used for strength estimation: maturity and ultrasonic testing. The maturity method is a well-established technology for concrete strength assessment. Ultrasonic tomography is regularly used for quality control and is growing in popularity for strength estimation.

2.3.1 Maturity

The maturity method is a nondestructive test used to evaluate the strength development of cementitious materials using the combined effects of time and temperature [24]. Concrete forms when water and cement mix in a process called hydration. As hydration products form, they act as a glue to change the concrete mixture into a single system. This reduces permeability and porosity while increasing concrete strength (Figure 1a). Hydration is dependent on temperature and

moisture in the system. Moisture can cause a significant reduction in hydration if the relative humidity is below 80% [25]. While moisture is important, generally it is easily controlled and kept as high as possible during curing to encourage constant hydration. Temperature is more difficult to control. Hydration is an exothermic reaction and has a natural heat evolution. The amount of heat released by the mixture during hydration is an indicator of the amount of hydration products. Therefore, there is a correlation between heat generated by the mixture and developed strength. Monitoring the temperature of concrete will indicate the hydration level as shown in Figure 1b.

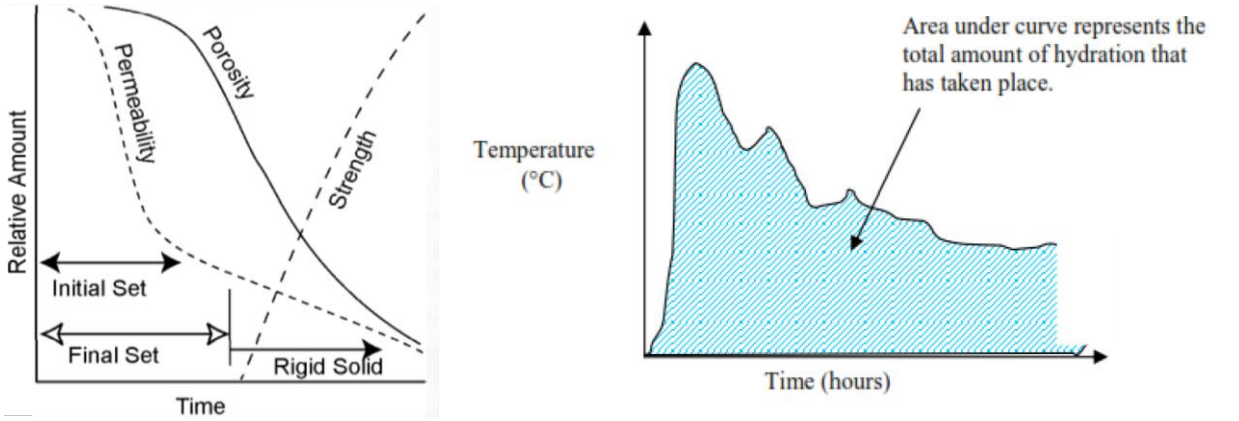

Figure 1: Change in (a) durability, density, and strength [26] **and (b) temperature** [23] **as concrete hardens.**

The dependence of hydration on temperature is the basis of the maturity method. Maturity is defined as the product of concrete age and temperature or the equivalent age at a specified temperature [14,19]. To define maturity of a concrete mixture, specimens in a laboratory are monitored for temperature while regularly measuring for concrete strength using destructive testing. The temperature and strength data is correlated to create a unique maturity – strength relationship for the mixture [24]. This relationship can be used in the field to estimate the strength of in-situ pavement using temperature sensors imbedded in the slab at representative locations [14,19]. The correlation between the heat generated by the mixture and the developed strength allows for easier strength monitoring for future use of the same concrete mixture without the need for separate sampling at the construction site.

The important aspect of maturity is the predictive ability of the maturity – strength relationship. Temperature data is predictable based on historical data on ambient temperature and heat of hydration. Since maturity is a function of temperature, temperature models create a reasonable prediction of maturity and therefore strength. This is a major benefit in scheduling early age construction practices and a key advantage to maturity.

Maturity has been used for many years to reliably estimate concrete strength [13,14,17,19,27–31] and has an ASTM standard for consistent use [32]. Maturity was initially explored as a means of strength estimation for opening concrete pavements to traffic in the early 2000's. Crovetti and Khazanovich (2005) developed an opening to traffic guideline based on dowel bar size and maturity [14]. Olek et al. (2002) and Mancio et al. (2004) explored maturity as a new criteria for Indiana and California, respectively [7,29]. Nazarian, Yuan, and Medichetti (2003) and Yuan and Nazarian (2004) also explored using maturity for opening strength guidelines [13,31]. Since then, maturity has been regularly used in the field and recent studies have been expanding maturity use into modern mixtures. Mynarcik (2013) applied maturity procedures readily used in pavements to industrial floors [30]. Soutsous et al. (2020 and 2021) used maturity to accurately explore the strength gain rates of modern mixtures such as adiabatically cured and fly ash [27,33]. Hong et al. (2020) used maturity to understand the effect of temperature on setting time and stiffness [28]. So far, 64% of the considered states, 29 out of 45, have changed their specifications to accept maturity as an appropriate estimation of strength (Figure 2).

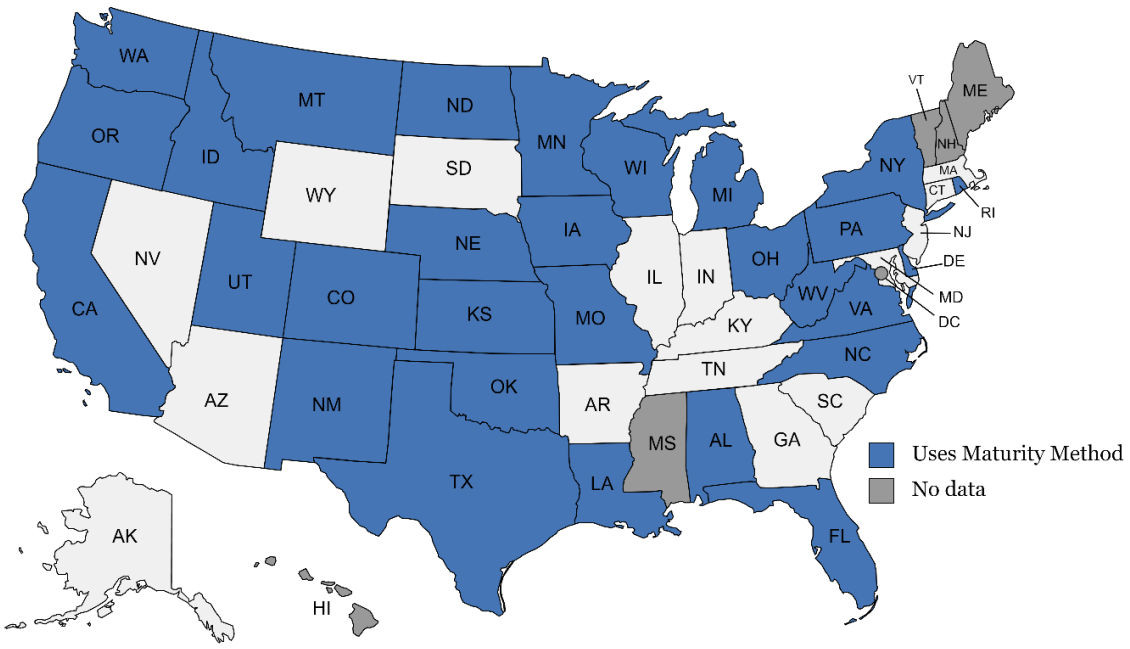

Figure 2: State departments with maturity in their guidelines as an acceptable estimation of strength

To use the maturity method, a maturity meter (or temperature sensors) and a data logger are needed along with the apparatuses to test either flexural or compressive strength. Calculating maturity in Celsius-hour is preferred over Fahrenheit-hour for easier computation. In a laboratory, either compressive or flexural strength can be used for correlation. ASTM Standard C1074 dictates fifteen specimens are required for testing with at least two containing temperature sensors which allows for five days of testing. Three specimens are tested at each desired age as with standard destructive testing and the specimens containing temperature sensors are tested on the last day.

There are several benefits specific to the maturity method. Temperature correlates very well to hydration, creating an accurate and reliable estimation of strength. Temperature monitoring also has small time-steps, providing continuous strength estimation that reduces time delays and improves timing of early age construction procedures such as joint cutting, form removal, and opening to traffic. Maturity is performed the same in a laboratory and in the field and includes the effect of different environmental and curing conditions. Once maturity is properly calibrated,

variability in predicting strength development is reduced when compared to destructive methods [34]. The major advantage is the ability of the maturity – strength relationship to utilize predictive temperature models which can be used to improve construction scheduling and guide future procedures.

Despite the general acceptance of maturity for strength estimation, there are limitations. The maturity – strength relationsip is mixture specific and especially sensitive to changes in the mixture. Under a contractors' discretion, concrete mixture changes are possible and can include changes in water-to-cement ratio, aggregate, cement type, or more, all of which can invalidate the relationship. This is especially critical with high early strength concrete pavements because the mixture design or curing method is often modified to make the mixture more workable [35].

Permanent temperature sensor locations limit the area monitored. Field use assumes that the location of the sensors is representative of the entire pavement [14,19]. However, this only considers the conditions immediately surrounding the sensor, ignoring potential discontinuities along the pavement or errors in placement during consolidation or curing [23]. Increasing the amount of temperature sensors in the pavement is possible but it can become expensive. Maturity is also based on the assumption of continuous hydration [35]. It is unable to evaluate the effect of curing on moisture retention and if the moisture levels are not adequate, the maturity – strength relationship would no longer be valid [23].

Other studies have observed inconsistencies in the accuracy of strength estimation using maturity. Mancio et al. (2004) found that while estimated early age strength for conventional concrete was similar to measured values, estimated strength for high early strength concrete was consistently high [29]. Okamoto and Whiting (1994) concluded that maturity has the potential to significantly underestimate very early age strength but will become more accurate after about eight

hours of curing [34]. Nandhini and Karthikeyan (2021) observed inconsistencies (both over- and underestimating of strength) depending on mix type and maturity – strength relationship used [36].

Despite potential limitations, maturity is a common choice to reliably monitor strength gain in concrete. Once properly prepared, maturity is an accurate and low labor method for estimating in-situ concrete strength.

2.3.2 Maturity – Strength Relationship

Properly establishing the relationship is necessary for accurate strength estimations of each concrete mixture relationship is unique. The procedure to determine the maturity curve is briefly detailed below and should be conducted in accordance with ASTM C1074 [32]. Relationships are mixture-specific and separate maturity testing must be performed for every mixture design.

Step 1: Obtain Temperature Data

Temperature sensors are placed in the center of at least two cylinder and two beam specimens. These specimens will be monitored as strength testing continues as normal on other specimens. The final day of strength testing will use the monitored specimens.

Step 2: Calculating the Maturity Index

The Nurse-Saul method, described in ASTM C1074, is commonly used in the maturity – strength relationship by computing the concrete maturity index or time-temperature factor (*TTF*) using laboratory temperature data and the following equation.

$$TTF = \sum (T_{PCC,m} - T_0)\Delta t \qquad \textbf{(2-1)}$$

where *TTF* is the temperature-time factor at age *t*, degree-days or degree-hours; Δt is a time interval, days or hours; $T_{PCC,m}$ is the mean concrete temperature during the time interval Δt, °C; and T_0 is the datum temperature, °C (standard values are 14°F or -10°C).

Step 3: Obtaining Strength Data

Compressive or flexural strength data is gathered alongside temperature data. ASTM C1074 highlights five required days of testing (1, 3, 7, 14, and 28), but additional times can be added if necessary [32]. At least fifteen cylinder or beam specimens are needed so that three specimens are tested each time increment to establish the average compressive or flexural strength for that age.

Step 4: Creating the Maturity – Strength Relationship

The temperature and strength data is correlated to create a unique maturity – strength relationship for the mixture. Temperature correlates very well to hydration, so when properly calibrated, temperature provides an accurate indication of strength. There are several relationships that could be used if desired depending on the representation of the strength data. The following equations are common examples of maturity – strength relationships:

$$M_r = a_m \ln TTF - b_m \quad \textbf{(2-2)}$$

$$f'_c = c_m \ln TTF - d_m \quad \textbf{(2-3)}$$

OR

$$M_r = M_{ru} e^{-\left(\frac{a_m}{TTF}\right)^{bm}} \quad \textbf{(2-4)}$$

$$f'_c = f'_{cu} e^{-\left(\frac{c_m}{TTF}\right)^{d_m}} \quad \textbf{(2-5)}$$

where M_r is the flexural strength (modulus of rupture), psi; M_{ru} is the ultimate expected flexural strength, psi; f'_c is the compressive strength, psi; f'_{cu} is the ultimate expected compressive strength, psi; a_m, b_m, c_m, and d_m are calibration coefficients.

For the first function, a simple regression is used to determine the coefficients for the specific mixture. To determine the calibration coefficients for the second function, the following steps should be taken.

a) Transform Equation (2-4) into Equation (2-6):

$$ln\, ln \frac{M_{ru}}{M_r} = b_m\, ln\, a_m - b_m\, ln\, TTF \equiv \alpha_1 + \alpha_2\, ln\, TTF \quad \textbf{(2-6)}$$

b) Compute $ln\, TTF$ and $ln\, ln \frac{M_{ru}}{M_r}$. Perform a linear regression with $ln\, TTF$ as an independent variable and $ln\, ln \frac{M_{ru}}{M_r}$ as a dependent variable to determine coefficient α_1 and α_2.

c) Determine the coefficients of the maturity – flexural strength relationship using the following equations:

$$a_m = e^{-\frac{\alpha_1}{\alpha_2}}$$

$$b_m = -\alpha_2$$

To utilize maturity in the field, temperature sensors are placed in the pavement during pouring in a position where they are fully surrounded by concrete to monitor the temperature and calculate the maturity index. The maturity of the concrete pavement then uses the maturity – strength relationship to determine the estimated strength of the pavement at that time [14,19].

2.3.3 Ultrasonic Testing

While ultrasound technology has been used to analyze internal characteristics of objects from a variety of fields, it is still an emerging technology in the pavement industry. Ultrasonic tomography uses penetrating, mechanical waves that propagate through the material and cause a measurable energy disturbance. The wave energy diminishes as they travel and reflect off acoustic

differences between materials in the scanned cross section. The waves can be analyzed to detect internal boundaries or determine material properties. This method is known to have a lower variability than other nondestructive tests because it is unaffected by moisture or constraint conditions [37,38].

This method has been used for a wide variety of testing. Quality control tests are commonly performed using ultrasonic waves. The boundary and inclusion reflections create a 3D reconstruction of the cross section allowing the user to check pavement thickness or dowel bar placement and locate damage or delamination. This is an appealing aspect in pavement construction and quality control. Hoegh et al. (2011) used linear-array ultrasonic tomography to determine slab thickness, reinforcement location, and internal distresses [39]. Hoegh et al. (2013) used ultrasonic tomography to classify joint damage and found this method to be more accurate than traditional methods [40]. Vancura et al. (2013) used ultrasonic tomography to check pavement thickness in multiple locations over a project with accuracy [41]. Choi et al. (2016) used ultrasonic shear wave tomography to identify cracks and delamination in pavements [42]. Salles et al. (2019) used ultrasonic tomography to identify incipient cracks in concrete slabs [43]. Salles et al. (2021) used shear wave velocity to inspect concrete pavements prior to rehabilitation [44].

Another aspect of ultrasonic testing is the ability to estimate material properties through acoustic impedance measurement, which will be utilized in this study through ultrasonic wave velocity. This is a common procedure that has been used by numberous studies in the past. Brozovsky, Matejka, and Martinec (2005) used ultrasonic pulse and an impact hammer to determine the compressive strength of interlocking paving blocks [45]. Cho et at. (2007) used nondestructive techniques to estimate in-situ strength through shear wave velocity relationship with the elastic modulus of concrete [37]. Akcaozoglu et al. (2013) used ultrasonic wave velocity

as an indicator of density and elastic properties and saw potential for compressive strength estimation on concrete containing waste PET lightweight aggregate [46]. Liu et al. (2014) monitored the hardening process of mortor and concrete using ultrasonic wave velocity [47]. Hannachi and Guetteche (2014) encouraged using ultrasonic pulse velocty to for elastic modulus, compostition, and density. They recommended utilizing correlation tests to estimate compressive strength as well [48]. Mandal et al. (2015) used ultrasonic velocity to estimate flexural strength and constraint modulus of cement stabilized materials. They also explored the effect of density, curing time, and binder content on wave velocity [49]. Zou and Meegoda (2018) characterized the microstructure of cement paste using ultrasonic wave velocity [50]. Bompan and Haach (2018) used ultrasonic wave velocity to estimate the stress state of concrete specimens [51]. Ridengaoqier et al. (2021) used ultrasonic wave velocity to estimate porosity of previous concrete and proposed a procedure for field use [52].

Ultrasonic testing originally required a solution that ensured full contact between the device and pavement surface. Modern devices use dry point contact that requires no surface preparation, increasing the efficiency of data collection. In recent years, noncontact ultrasonic devices have been explored to expedite the scanning process, however, there are still hurtles to overcome in this technology. There are reported issues of low signal-to-noise ratio and a drastic loss of energy when traveling through air [53]. Nevertheless, studies have begun exploring how noncontact could be used with concrete structures by changing the type of waves used, for example leaky Rayleigh waves. Several studies have explored noncontact methods for damage location [54–56]. Hong et al. (2020) used contactless ultrasonic testing to study concrete stiffening behavior [28]. Tran et. al. (2020) used leaky Rayleigh waves to determine setting time for joint sawing [57]. These studies hold a promising continuation of ultrasonic testing to farther increase efficiency of

data collection. Despite the technological advancements, this dissertation will utilize dry point contact technology as it is more established in industry and has less complex utilization at this time.

Ultrasonic testing uses the velocity of a direct arrival wave to determine material properties. For structures only accessible from one side, like a pavement, the pulse-echo method is used (Figure 3). At least one transmitter and one receiver are positioned a set distance apart. Linear array devices have many contact points, each able to send and receive waves to increase scan accuracy through redundancies [44,58,59]. Transmitters emit a pulse at a specified frequency that propogate through the concrete pavement to a receiver that records the echo [8,39,60]. Figure 4 shows a sample time history for a device receiver. The signal arrival time is evident by the increase in amplitude. For concrete, the pulse frequency is typically between 20 – 150 kHz, often 50 kHz.

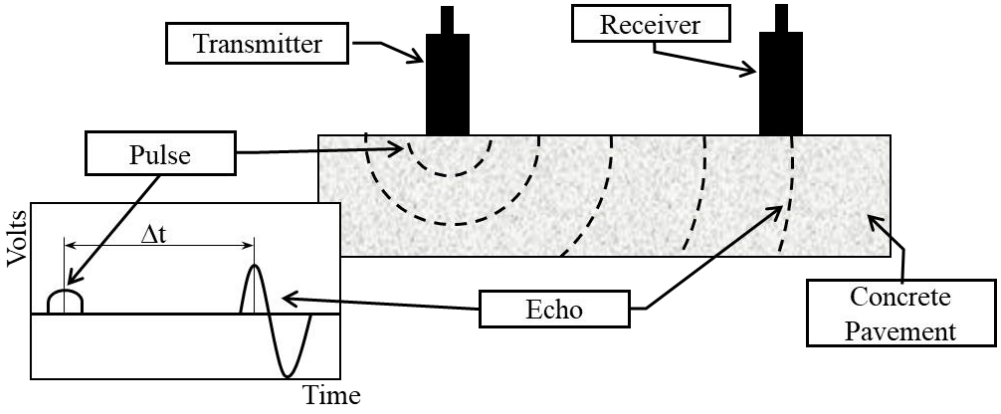

Figure 3: Pulse-echo method used in ultrasonic devices

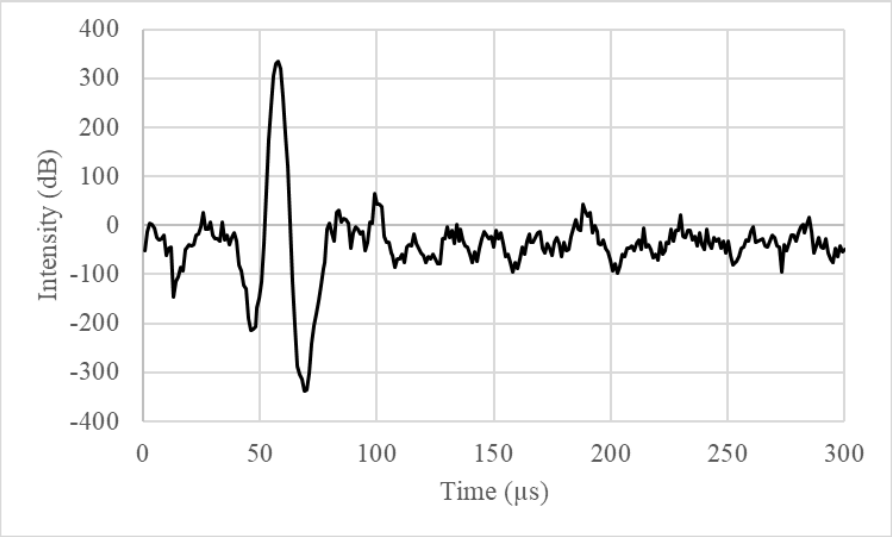

Figure 4: Example impulse time history.

The received signal can be analyzed to determine differences in material properties or defects [39]. Since the distance between transmitters and receivers is set, the arrival time - the time it takes for the wave to be received - can be used to calculate the wave velocity. Figure 5 shows the resulting signal analysis for a linear array device which displays the arrival times for multiple sensor distances. The trendline slope is the wave velocity for that scan in mm/µs. The wave velocity for the trendline shown in Figure 5 is 2.65 mm/µs or 2653 m/s.

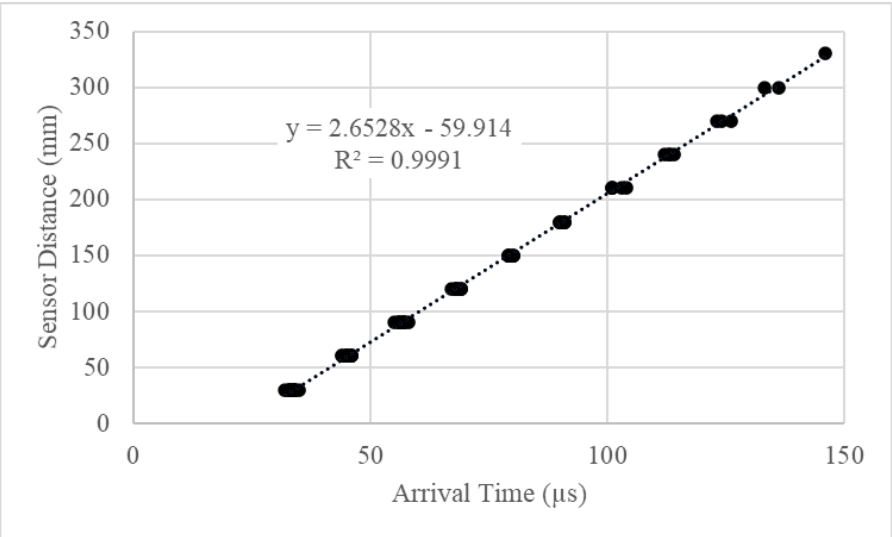

Figure 5: Example of arrival signal analysis to determine wave velocity

Calculating wave velocity is typically performed internally by the device and displayed on the screen. A linear array device, A1040 MIRA from Acoustic Control Systems, Saarbrücken, Germany, was used in this study. This device records shear wave velocity, a 3D reconstruction of the pavement directly below the scan, and the time history profiles [39,60]. Each scan only takes a few seconds to perform. Figure 6 shows an example of MIRA's immediate output screen.

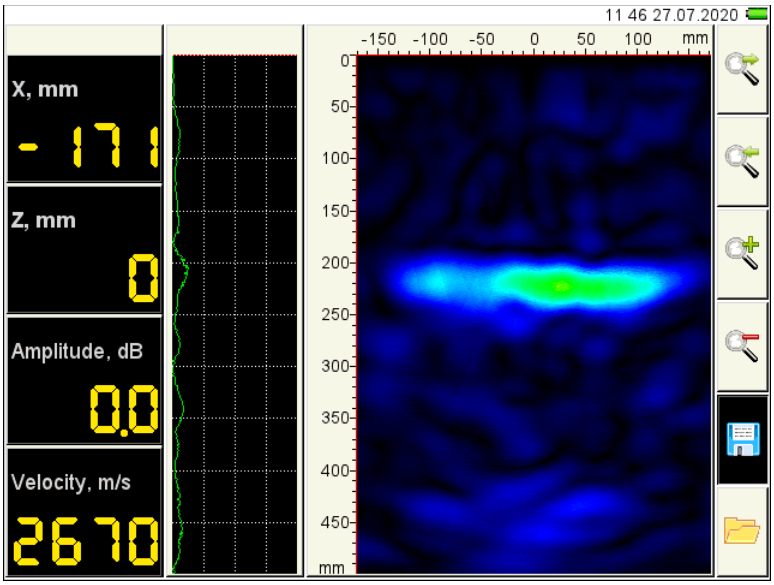

Figure 6: Example of display screen on MIRA device

Ultrasonic waves can include pressure, shear, surface, or flexural depending on the technology and method used [23]. Two ultrasonic mechanical wave types, pressure and shear, are especially common in modern ultrasonic testing but have different characteristics. They have unique wave shapes and energy that change the allowable penetration depth or material type.

Pressure waves are a type of body wave also known as p-waves, primary, compressive, or longitudinal waves. Pressure waves contain an area of higher density or compression as shown in Figure 7a. They are faster than other wave types and contain the least amount of energy. This allows them to travel through solids, liquids, and gas, and therefore devices can be ground- or air-coupled. However, this also limits penetration depth and the amount of pore water in a system

can affect pressure wave propagation [28,61]. There are many ultrasonic devices available that use pressure waves and many conclusions made in this study are valid for pressure wave devices as well. However, in this dissertation another type of body wave, shear wave, is primarily used and considered.

Shear waves, also known as s-waves, transverse waves, or secondary waves, contain an area of higher amplitude as shown in Figure 7b. They are slower than pressure waves, about 60% of the speed depending on the Poisson's ratio of the concrete, which restricts this wave to solids [60–62]. However, shear waves have more energy than pressure waves which allows for deeper penetration [61,63]. Shear waves have less backscatter and signal attenuation when compared to pressure waves reducing variability in measurements [60,61]. The ultrasonic shear wave device to be primarily used in this project is a A1040 MIRA from Acoustic Control Systems (Figure 8).

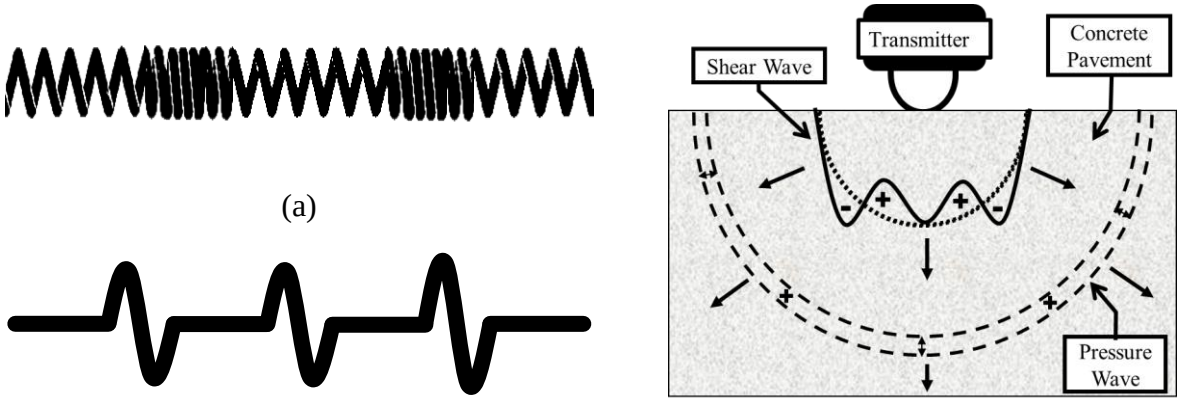

(a) (b) (c)

Figure 7: Shape of (a) pressure waves and (b) shear waves and (c) their shape as they travel through a concrete pavement

Figure 8: Ultrasonic devices that use shear waves

Ultrasonic testing has an accurate and direct correlation to concrete stiffness. Wave velocity is theoretically related to several concrete material properties: elastic modulus (E), Poisson's ration (υ), and density (ρ) [37]. Equations (2-7) and (2-8) calculate the velocity for pressure (V_p) and shear (V_s) waves. Elastic modulus, or stiffness, is the ability of a material to resist elastic deformation or the amount of deflection under a load. This material property increases as strength increases and has several simple, empirical relations to strength. The direct relationship wave velocity has with stiffness, and therefore empirical relationship to concrete strength, is a significant advantage because wave velocity can estimate strength accurately through laboratory correlations.

$$V_p = \sqrt{\frac{E(1-\upsilon)}{\rho(1+\upsilon)(1-2\upsilon)}} \quad \textbf{(2-7)}$$

$$V_s = \sqrt{\frac{E}{2\rho(1+\upsilon)}} \quad \textbf{(2-8)}$$

When the same coarse aggregate is used, wave velocity is independent of temperature, moisture, curing, or constraint conditions and has a lower variability compared to other nondestructive tests [13,37,38]. Cement type used, water-to-cement ratio, and any additives have

a small influence on wave velocity meaning minor changes to the mixture in the field will not have a significant impact on the wave velocity – strength relationship [13]. Data collection takes little time as no coupling agent or surface preperation is needed on modern devices. Ultrasonic devices are portable and do not require permanent sensors so testing can be conducted at multiple locations at the discretion of the user. This allows for more autonomy in scanning so variability within the pavement can be identified, critical stress locations can be montired, or potential defects can be flagged [39]. If these potential issues are identified during initial construction, corrections can be made to increase pavement uniformity and performance.

Both maturity and ultrasonic testing have been used in early age strength estimation, but ultrasonic testing has been found to be more accurate than maturity at early ages [13,37,38]. The improved accuracy, in combination with the mobility, makes ultrasonic testing preferable for early age field use.

There are several limitations to ultrasonic testing. Concrete is a heterogenetic material, therefore the different material properties can affect the wavelength and create variability [19]. Linear array devices such as MIRA address this issue and reduce measurement variability. MIRA has 48 dry point contact transducers located on the bottom of the device to emit and receive signals in 12 linear array channels. This linear array design increases the repeatability of ultrasonic testing over a traditional single transducer and receiver arrangement. However, when using linear array ultrasonic devices on small specimens, the edge conditions can affect wave propagation. This creates discrepancies when relating laboratory specimens to in-situ pavements of the same concrete mixture and age. A major limitation is strength can only be estimated for the time of the scan. Accurate temperature modeling allows maturity to predict future strengths, but no such

model exists for wave velocity. Wave velocity provides no information on how the pavement will continue to gain strength.

2.3.4 Wave Velocity – Strength Relationship

The equations for wave velocity show the direct relationship between wave velocity and stiffness but for strength it is recommended to do preconstruction laboratory testing for more accurate wave velocity – strength relationships for the mixture. To determine the shear wave velocity – strength curve, there must be flexural testing in conjunction with ultrasonic scans. This procedure is outlined below.

Step 1: Obtaining Beam Strength and Wave Velocity Data

Strength and wave velocity data must be collected from beam specimens that use a similar concrete mixture as the slab in question. The beam must first be scanned using the ultrasonic device to determine the average wave velocity at the beam age. Immediately following the scan, the beam should be tested for flexural strength. Adjustments to the collected data points for velocity can be made to improve the accuracy of the beam velocity and avoid the effect of vertical edges. This will be further explored in a later chapter.

At least fifteen beam specimens are needed so that three specimens are tested each time increment to establish the average strength for that day. Testing days include 1, 3, 7, 14, and 28 days. Third and center point loading, ASTM C78 and C293 respectively, are procedures that can be used to determine the flexural strength of simple beams [20,21].

Step 2: Creating the Wave Velocity – Strength Relationship

To develop the relationship between strength and shear wave velocity, the ultimate flexural strength must be estimated (M_{ru}). The relationship to describe the shear wave velocity - flexural strength relationship is assumed:

$$M_r = M_{ru} \times e^{a_s V_s + b_s} \quad \textbf{(2-9)}$$

where V_s is the shear wave velocity, m/s; and a_s and b_s are coefficients depending on the concrete mix properties.

To obtain the coefficients of this relationship, a_s and b_s, a linear regression should be performed with V_s as the independent variable and $ln\frac{M_r}{M_{ru}}$ as the dependent variable using strength data collected in Step 1.

2.4 Summary

The efficiency of construction is limited to the efficiency of the opening to traffic criteria. Currently, state guidelines are purposefully conservative and generalized to be applicable across the entire state. Certain states are categorizing their requirements to consider some early age performance factors, however, no state accounts for multiple critical early age performance factors, the effect on long term performance, and only one considers individual projects' traffic patterns. Improvements are needed to identify the minimum allowable strength needed to carry the traffic load for individual pavements and bring flexibility to opening to traffic criteria.

Strength determination for meeting opening criteria is currently measured using destructive testing which is a direct measurement of specimen mechanical properties. However, destructive

testing is insufficient for field use as it does not properly represent the conditions in the field, and it requires excessive time and labor. This has encouraged movement to nondestructive methods since they are performed directly on the structure with no loss in serviceability. Nondestructive tests measure a specific variable depending on the method that is empirically correlated to concrete properties.

Maturity is a nondestructive method defined as the equivalent age at a specified temperature and correlates concrete hydration and temperature to strength. This method results in an accurate and predictive maturity – strength relationship. The relationship is very dependent on consistency in the mixtures and will not be representative if there are changes to the mixture or curing conditions in the field. Some studies have observed inconsistencies in the accuracy of the relationship at early ages.

Ultrasonic testing is a nondestructive method that measures velocity of mechanical waves transmitted through the concrete. The wave velocity can be directly correlated to the elastic modulus and therefore has an accurate relationship to concrete strength. When the same coarse aggregate is used, wave velocity is independent of temperature, moisture, curing, or constraint conditions and has a lower variability compared to other nondestructive tests. Ultrasonic devices are portable and quick to use to better examine concrete variability. These devices were designed to be used on larger concrete surfaces and have difficulty with the vertical edges on a beam specimen limiting laboratory use. Each ultrasonic scan only considers the strength at the time of the scan with no indication of future strength gain.

3.0 Influencing Factors on Opening Strength

To improve traffic opening strength criteria, factors influencing pavement performance and critical stresses must first be identified. The purpose of this chapter is to explore extremely early concrete pavement loading and identify when and why distress or failure occurs using a large scale field experiment. Several aspects of an early loaded pavement were monitored with a focus on ride quality and joint performance to quantify potential early age damage. This was used to identify factors affecting critical stress occurring in the concrete layer.

3.1 Laboratory and Field Testing

3.1.1 Cell Specifications

Testing was performed at MnROAD, the Minnesota Department of Transportation (MnDOT) cold weather pavement testing facility. This is a pavement test track that allows for heavily monitored large scale testing for multiple research projects at once.

To evaluate the effect of early loading on pavement damage, six test cells were constructed on MnROAD's low volume road in July 2017 (Figure 9) [64]. The tested area was a total distance of 565 feet and cell lengths are slightly varied: Cells 124, 224, 324, 424, 524, and 624 are lengths 120, 120, 130, 115, 60, and 20 feet, respectively. Paving started from east to west, where Cell 624 was paved first and Cell 124 last. The cells were designed as 6-inch-thick concrete slabs with 1 inch diameter dowels and sawed, non-skewed joints established at 15-foot intervals (Figure 10).

The dense graded aggregate base was 6 in thick. The concrete layer thickness was measured by MITSCAN-T2 and varied between 5.8 and 6.6 inches. The concrete mixture used for the each cell meets the requirements of a 3A21 traditional contractor mix with conventional pozzolanic substitution [64]. The mixture is shown in Table 2.

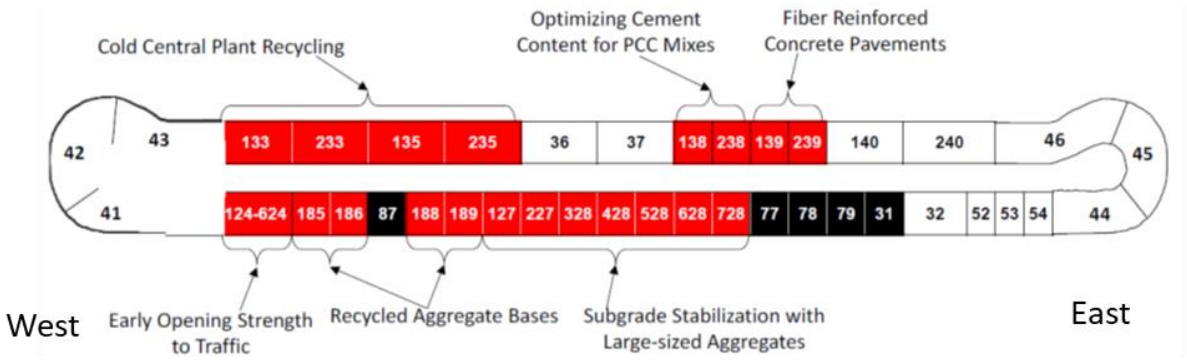

Figure 9: MnROAD Low Volume Road sections [64]

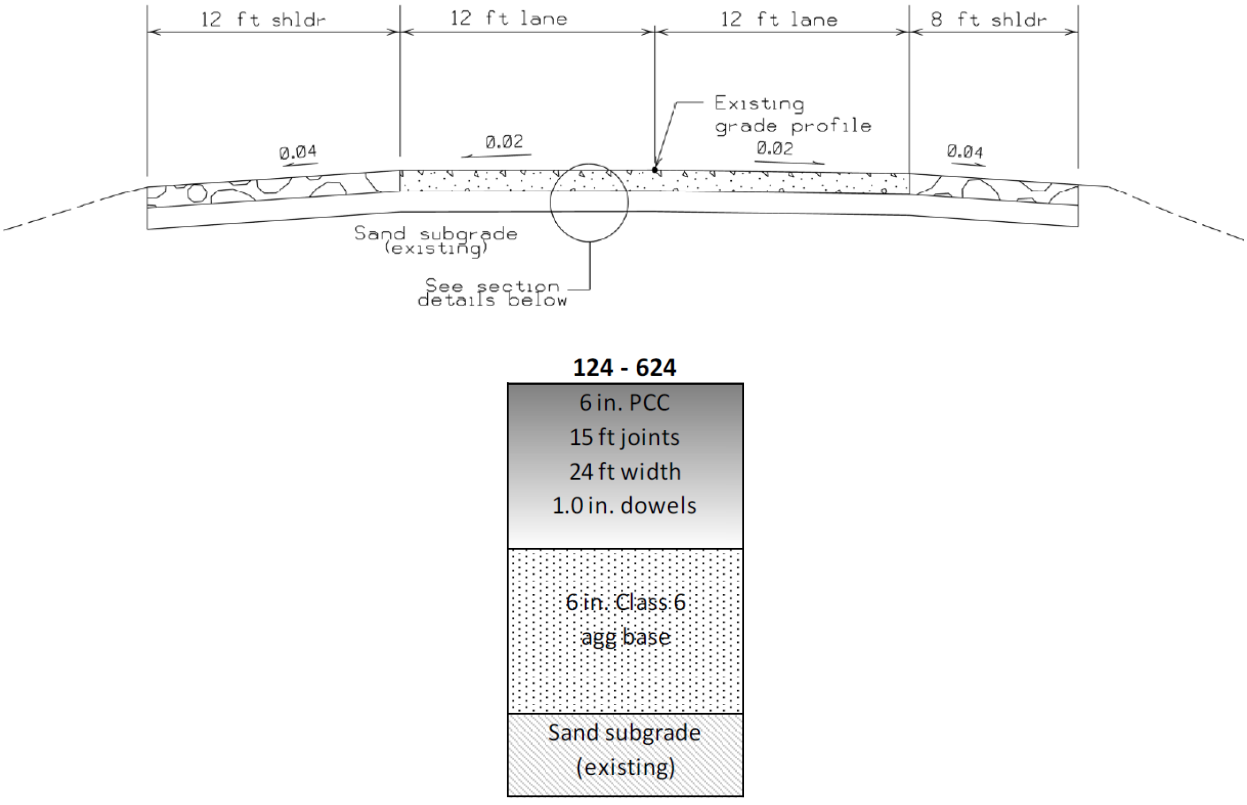

Figure 10: Concrete pavement section design (Cells 124-624) [64]

Table 2: Mix design for test cells [64]

Mix	Air (%)	Water (lbs)	Cement (lbs)	Fly Ash (lbs)	w/c	Fine Agg. (lbs)	Coarse Agg. #1	Coarse Agg. #2	Coarse Agg. #3
MR-3A21 124-624	7.0	228	400	170	0.40	1173	562	1015	305

3.1.2 Preconstruction Laboratory Testing

Laboratory testing, including concrete strength and maturity testing, was performed by American Engineering Testing, Inc. (AET). AET cast concrete specimens using the same concrete mixture design as the MnROAD Cells 124-624. Compressive and flexural testing was conducted 6 hours, 12 hours, 1 day, 2 days, 3 days, 4 days, 5 days, and 7 days after the specimens were cast. The temperature of the concrete specimens during curing varied between 23 and 30°C.

To enable strength determination of concrete cured under different temperature conditions, AET computed concrete maturity at the time of specimen testing using the Nurse-Saul method as described in ASTM C 1074 (Equation (2-1)) [32]. Figure 11 shows development of compressive and flexural strengths for various maturity levels. This was used to develop relationships between concrete strength and maturity using the relationship shown in Equations (2-2) and (2-3). Trendlines and corresponding predictive equations are also shown in Figure 11**.** These relationships were used to determine early loading times and estimate strength at time of loading.

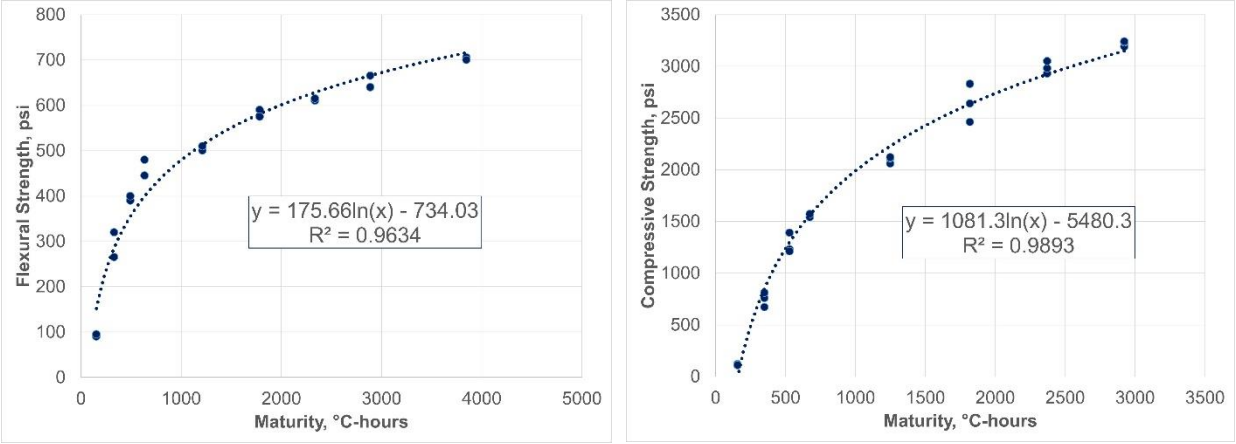

Figure 11: Predicted verses measured flexural (left) and compressive (right) strength gain

3.1.3 Early Loading of MnROAD Cells

The MnROAD cells were loaded much earlier than any current opening criteria suggests with varying circumstances. To consider different severities, two different vehicles were used for early loading: an unloaded 31,000-lb MnDOT snowplow truck and a 9,400-lb pickup truck. The inside lane of the cells was loaded by the snowplow and the outside lane was loaded by the pickup truck. Each loading contained one forward and one backward pass with the specified loading vehicle as shown in Figure 12. Cells 124, 224, 324, and 424 received 8, 6, 4, and 2 load passes, respectively. Cell 524 served as a control slab and was not loaded on the first day. Joint sawing occurred after the second loading.

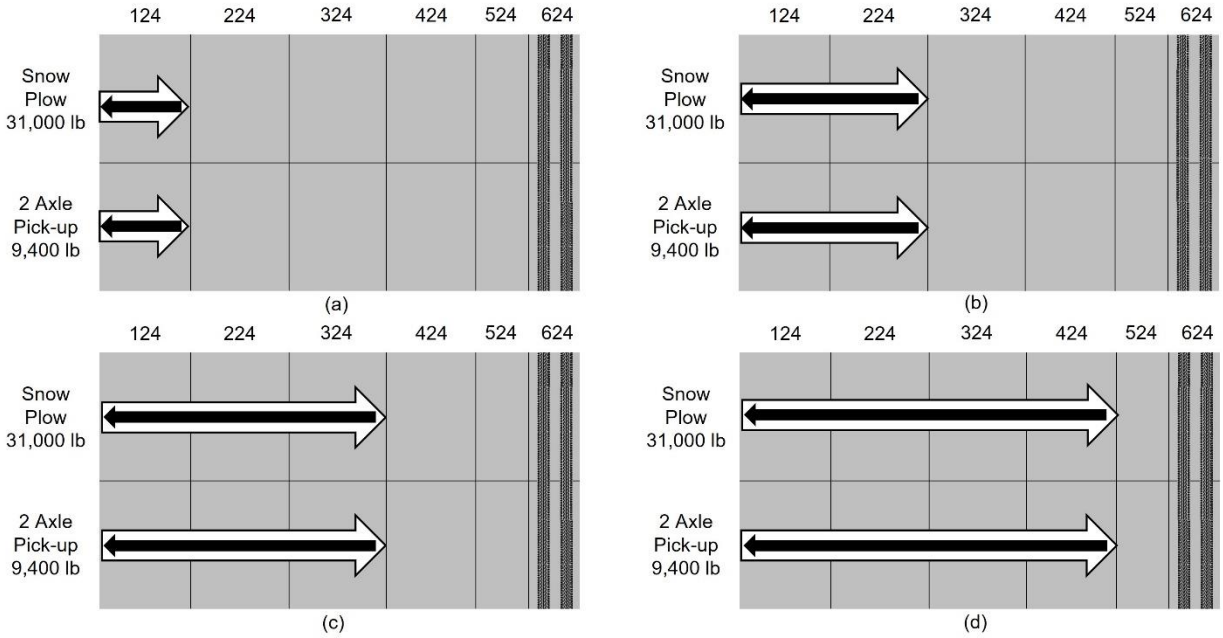

Figure 12: Primary loading scheme for early loading

The maturity – strength curves presented in Figure 11 were used to determine concrete strength at the time of loading. The first loading of Cell 124 was conducted when the maturity reached 100°C-hr, approximately 3 hours after paving, when the flexural strength was estimated to be just 73 psi. The final loading, which was performed on Cells 124-424, was performed when the maturity reached 400°C-hr, approximately 10 hours after paving, when the flexural strength was approximately 318 psi. For this pavement structure, MnDOT standard specifications recommends a flexural strength of 500 psi [65]. Loading sequences with corresponding maturity and flexural strengths are shown in Table 3.

Since the summer of 2017, all sections have been loaded with approximately 10,000 ESALs per year, standard for MnROAD's low volume test track.

Table 3: Loading sequencing for each maturity level.

Cell x24 Early Loading Sequence		
Maturity (Deg-Hr)	Flexural Strength (psi)	Load applied to lanes
100	73	1st load on Cell 124 (forward and back)
200	196	1st load on Cell 224, 2nd load on Cell 124
300	267	1st load on Cell 324, 2nd load on Cell 224, 3rd load on Cell 324
400	318	1st load on Cell 424, 2nd load on Cell 324, 3rd load on Cell 224, 4th load on Cell 124

Cell 624 was loaded by a 9,400-lb pickup truck traversing the slab approximately 2 hours after paving while the concrete was still plastic (Figure 13). This was done to study the impact that visible ruts impart when drivers erroneously drive on freshly placed concrete. The remaining cells did not show any visible damage after early loading.

Figure 13: Damage in Cell 624 due to early loading

3.2 Long-Term Damage Analysis of MnROAD Cells

The MnROAD cells were heavily monitored for temperature, dynamic strains caused by loading, static strains caused by the environment, warp and curl measurements, strength, durability, ultrasonic tomography (MIRA), international roughness index, falling weight

deflectometer testing, and petrographic data. This section will highlight key data and conclusions. Tests not fully discussed here measured no damage initiation or had inconclusive results. Full analysis of those tests is presented in Khazanovich, Kosar, and Li (2021) [66].

An extensive analysis of pavement performance using nondestructive testing and imbedded sensors could not identify any damage associated with early loading. An analysis of ride quality and falling weight deflectometer data collected over four years after paving was used to detect any damage that could have been revealed long-term that may be attributed to early loading.

3.2.1 Concrete Maturity and Strength at Time of Loading

The target loading times were based on concrete strength and maturity testing performed in a laboratory as was shown in Table 3. The actual concrete maturity at the time of loading was determined using maturity meters in the field. Table 4 presents the pavement age at each loading application. Table 5 presents measured maturity values for each cell and load application.

Table 4: Concrete pavement age at the time of each load application for the inner lane (IL) and outer lane (OL)

Age at Loading (hrs)						
	Loaded Cells				Control	Tire Rut
	124 IL	224 IL	324 IL	424 IL	524 IL	624 IL
	124 OL	224 OL	324 OL	424 OL	524 OL	624 OL
Paving Time	12:15	11:15	10:40	9:50		
Paired Repetition 1	3.00	4.00	4.55	5.40		2 hr
Paired Repetition 2	4.25	5.25	5.80	6.65		
Paired Repetition 3	6.55	7.55	8.10	8.95		
Paired Repetition 4	8.15	9.15	9.70	10.55		

Table 5: Actual concrete maturity at time of loading

Level	Load/ Rep	Loaded Cells			
31000 lb	SNOWPLOW → ←	124 IL	224 IL	324 IL	424 IL
9400 lb	PICK-UP → ←	124 OL	224 OL	324 OL	424 OL
		Maturity Level (°C-hr)			
	Paired Repetition 1	99.1	133.3	146.5	175.5
	Paired Repetition 2	144.8	181.0	194.4	225.6
	Paired Repetition 3	236.2	273.6	289.4	325.9
	Paired Repetition 4	304.1	341.6	360.8	401.8

The maturity data was used to determine concrete strength at time of loading using the results of concrete strength and maturity testing performed by AET as discussed in the previous section with the maturity – strength relationship visualized in Figure 14. It can be observed that the predictive equation for flexural strength is unreliable for maturity lower than 1000 ^{o}C-hrs. Figure 15 shows the trendline and predictive equation when only early maturity data were used. It can be observed that this predictive equation yields a more realistic estimation of concrete strength.

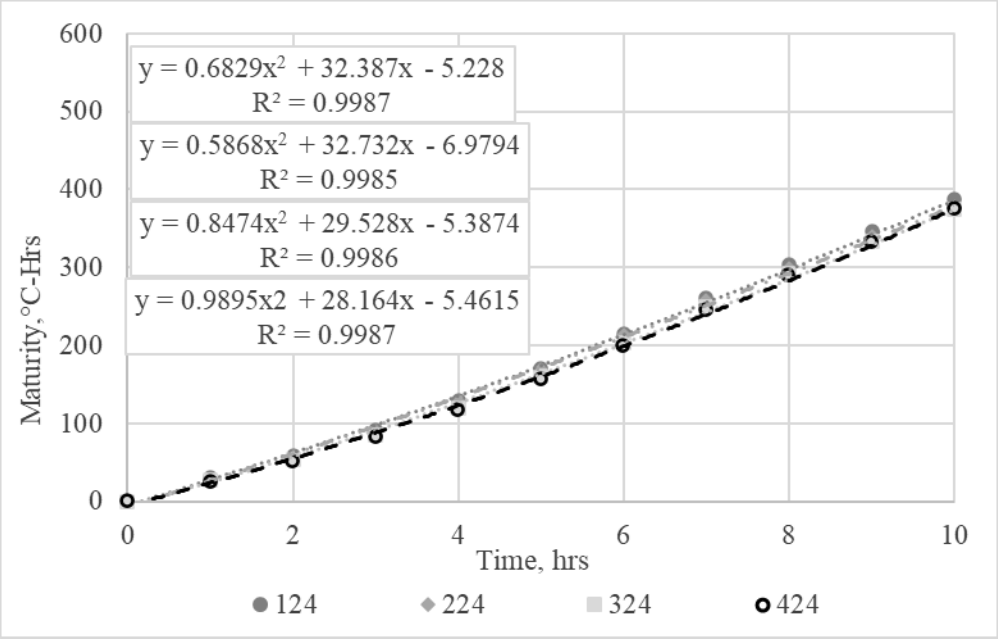

Figure 14: Measured concrete maturity vs elapsed time and corresponding regression equations

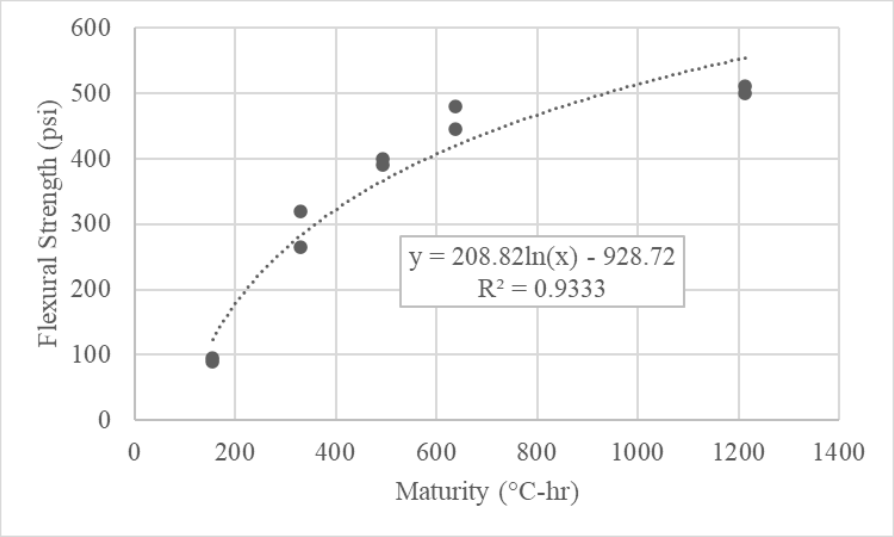

Figure 15: Concrete flexural strength vs maturity for low maturity levels

Analysis of maturity and strength data suggests that concrete in Cell 124 had reached compressive strength of 430 psi and flexural strength of 210 psi only after the time of the third loading; concrete in Cell 224 had reached flexural strength of 290 psi only at the time of the fourth loading, and Cell 424 reached flexural strength 320 psi at the time of fourth loading.

Table 6: In-place concrete flexural strength at loading estimated from maturity data

Level	Load/ Rep	Loaded Cells			
31000 lb	SNOWPLOW → ←	124 IL	224 IL	324 IL	424 IL
9400 lb	PICK-UP → ←	124 OL	224 OL	324 OL	424 OL
		Flexural Strength (psi)			
	Paired Repetition 1	73.3			
	Paired Repetition 2	139.9	179.1		
	Paired Repetition 3	225.9	251.7	261.6	
	Paired Repetition 4	270.3	290.7	300.3	319.2

3.2.2 Analysis of Ride Quality

Ride quality is the user experience of the pavement based on ride roughness. It is an important consideration in pavement construction and there are often disincentives to constructing pavements with poor serviceability. The international roughness index (IRI) is a commonly used

measurement and criteria to quantify ride quality. IRI reports pavement surface deviations as they impact vehicle suspension, typically summarized in inches/mile. Higher IRI values indicate a rougher pavement surface. In this study, a 3K Laser Line sensor was used to measure continuous profiles along the left and right wheel path of each lane and the resulting profiles were processed to report IRI.

Since this field test was performed in Minnesota, the MnDOT IRI criteria for a typically loaded pavement will be used as a comparison base as shown in Table 7 [67]. MnDOT uses the Ride Quality Index (RQI) as their serviceability criteria. RQI is the combination of IRI measurements and user opinion to better account for rider comfort. Equations exist to convert IRI to RQI for concrete and asphalt pavements. Table 7 shows the original RQI and verbal ratings determined by the user and the IRI criteria back calculated from the conversion equation for concrete pavements [67]. To be considered a good pavement in Minnesota, the IRI value must be less than 105 in/mile. If the pavement has an IRI greater than 170 in/mile, repair or reconstruction is necessary [65].

Table 7: IRI and RQI categories and ratings

IRI Rating	RQI Rating	Verbal Rating
55 >	4.1 – 5.0	Very Good
104 – 55	3.1 – 4.0	Good
169 – 105	2.1 – 3.0	Fair
255 – 170	1.1 – 2.0	Poor
255 <	0.0 – 1.0	Very Poor

Between July 2017 and August 2020, roughness profiles were measured a total of thirteen times for each cell for the inside and outside lanes, respectively, as shown in Figure 16 and Figure 17. As expected, Cell 624, the cell with visible rut marks, showed the highest IRI. Although Cell 524, which acted as a control and was therefore not exposed to early loading, exhibited significantly worse IRI for both inside and outside lanes than the remaining cells that were exposed

to early loading. Since IRI was measured consecutively at a specific driving speed, this unexpected increase could be due to the equipment having residual vibrations when scanning Cell 524 from the exceptionally rough ride of Cell 624. Both these cells were also significantly shorter than the remaining cells which could have provided less time for the equipment to settle from the excessive vibrations. Therefore, the extremely poor ride quality measurements for Cell 624 could have affected the ride quality measurements for Cell 524 even though the actual roughness of Cell 524 may be lower.

The remaining cells, Cell 124-424, show significant variability with a minor increase in IRI with time indicating no significant decline in serviceability for early loaded cells. These cells remain well below the 105 in/mile limit for a good pavement in Minnesota. The inside lane of Cell 124 initially exhibited a higher IRI than Cells 224, 324, and 424 possibly showing some effect of early loading since Cell 124 was loaded earliest. However, it has no significant deterioration and by the end of the observation period, IRI measurements of the most early loaded cell (Cell 124) are congruent to the cell with latest early loading (Cell 424). For the outside lane, Cells 124 and 224 are consistently higher than Cells 324 and 424, about 20 in/mile, indicating a potential effect of early loading. However, all cells did not have a significant decline in serviceability and stayed within the limit for a good pavement.

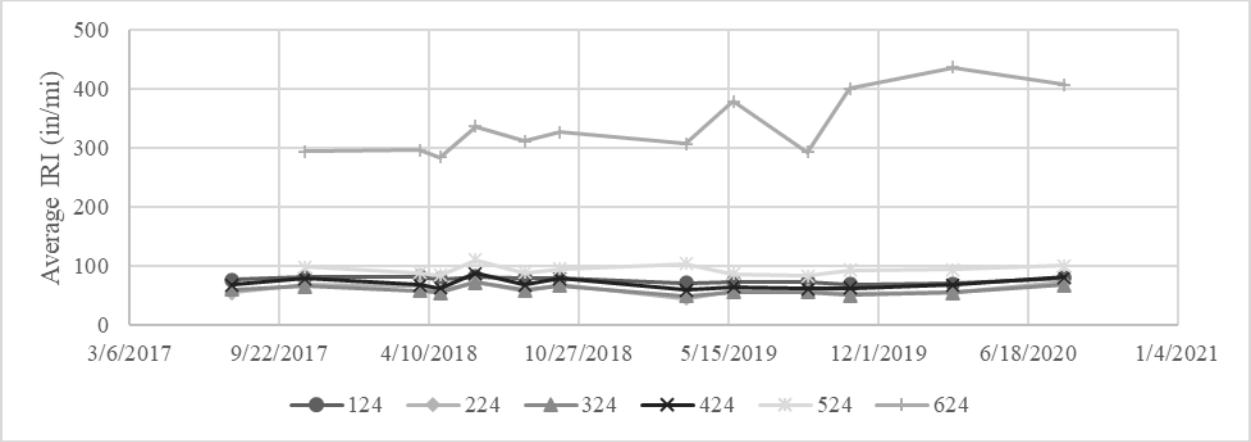

Figure 16: Average IRI of the inside lane

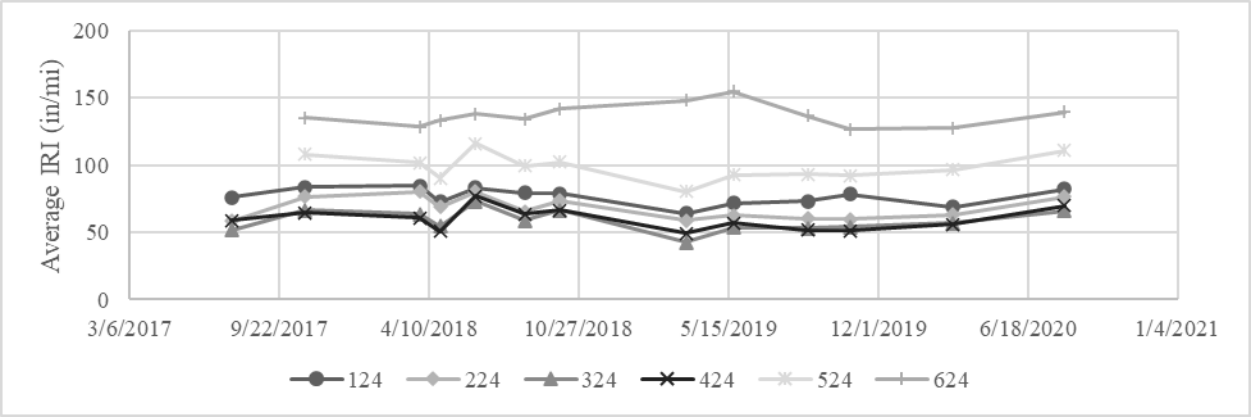

Figure 17: Average IRI of the outside lane

Figure 18 shows a comparison of IRI measurements from outside and inside lanes for Cell 124. This shows that although the inside lane was loaded at a very early age with a heavier truck, there was little difference in ride quality between the lanes. Figure 19 shows a similar side by side comparison for Cell 424 which was only loaded after the flexural strength reached 318 psi. This cell showed a greater difference in measured IRI than Cell 124. The difference in IRIs for these two lanes does not vary significantly between the measurements.

These observations lead to the conclusion that changes in ride quality over time for Cells 124, 224, 324, and 424 cannot be attributed to the early loading of these cells.

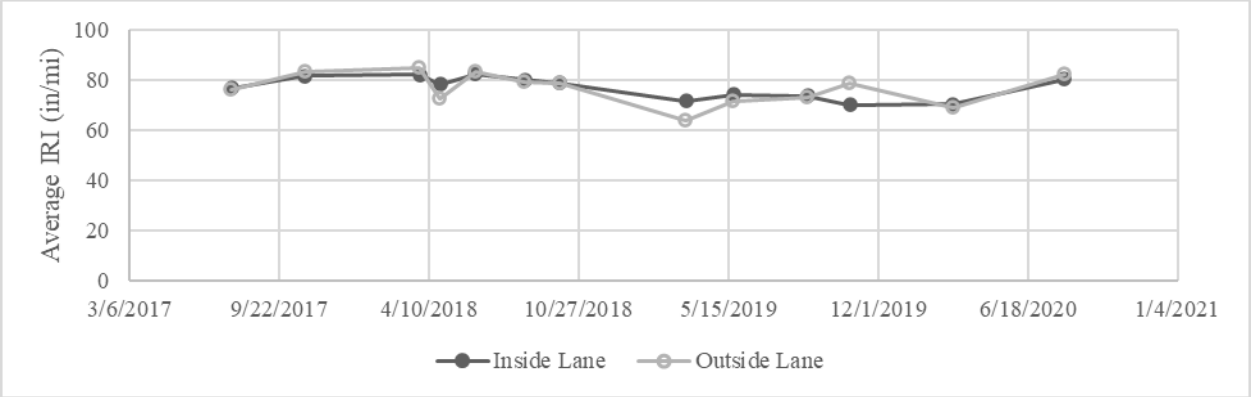

Figure 18: Average IRI for Cell 124

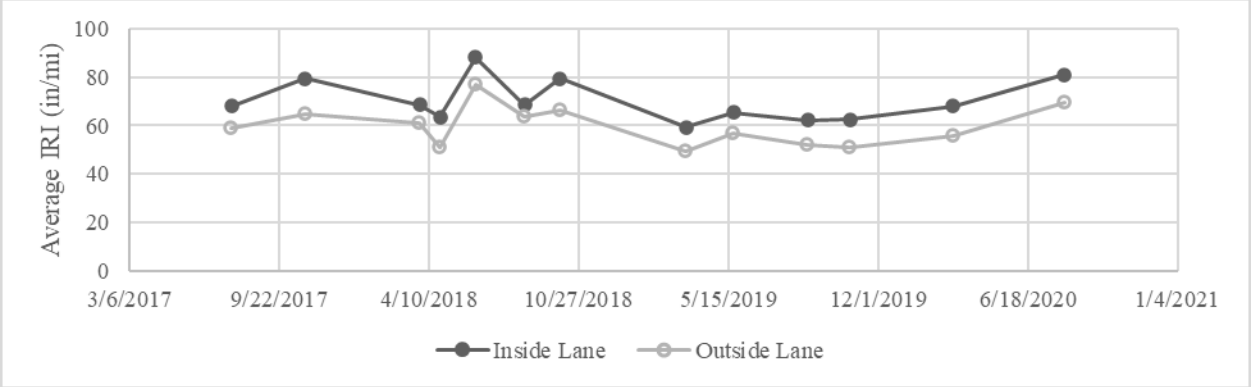

Figure 19: Average IRI for Cell 424

3.2.3 Analysis of Joint Performance

Joint performance is an important consideration in pavement construction, especially when considering early opening. If the pavement structure is not mature enough for loading, excess stresses occur in dowel bars and cause damage in the surrounding concrete that reduces performance. Load transfer efficiency (LTE) and differential deflections were used to quantify transverse joint performance and possible damage when exposed to early loading. LTE is the ratio of deflection of the unloaded slab to deflection of the loaded slab. LTE is a typical comparison, but it may exaggerate the degree of damage as a ratio of two small deflections can be

misrepresented. Differential deflections are the difference between the deflection of the unloaded slab and the loaded slab. This provides an actual deflection measurement for each joint to better judge the severity. This data is collected using falling weight deflectometer (FWD) data gathered by MnDOT. FWD testing uses a mechanically controlled load plate placed tangentially to the joint edge. The loaded and unloaded slab joint deflections were each measured under the center of the load plate (6 inches away from the joint).

FWD testing was conducted nine times between October 2017 and April 2021 on two joints in Cells 124-424 for both inside and outside lanes. Testing was performed for the approach slab and the leave slab surrounding the joint. Cells 524 and 624 had short lengths, 60 and 20 feet, which did not allow for full FWD testing. Only one joint was able to be tested for Cell 524 and none for Cell 624. Figure 20 and Figure 21 show the LTE for the inside and outside lanes, respectively. There was significant seasonal variability which is due to the expansion or contraction of concrete during changes in temperature causing the joint to become tighter or wider. This variability ranges between 70% and 95%, which is still an adequate load transfer level.

In September 2017, about three months after construction, LTE for the inside lane where heavier load was applied was higher than the outside lane. Also, Cells 124 and 224 showed similar or higher LTEs than Cells 324 and 424. This indicates that early loading by either size vehicle did not have a significant effect on initial joint performance.

As observed in Figure 20, LTEs for Cells 124 and 224 become lower over time than LTEs for Cells 324 and 424. The control cell, Cell 524, had LTEs slightly higher than others. This could potentially indicate a negative effect of early loading on dowel bar performance. However, further analysis of Figure 21 shows that on April 14, 2021, the measured LTE for the outside lane of Cell 424 was similar to the inside lane of Cells 124 and 424. This indicates that other factors, such as

construction, material quality, or environmental factors may have a greater influence on the LTE than early loading.

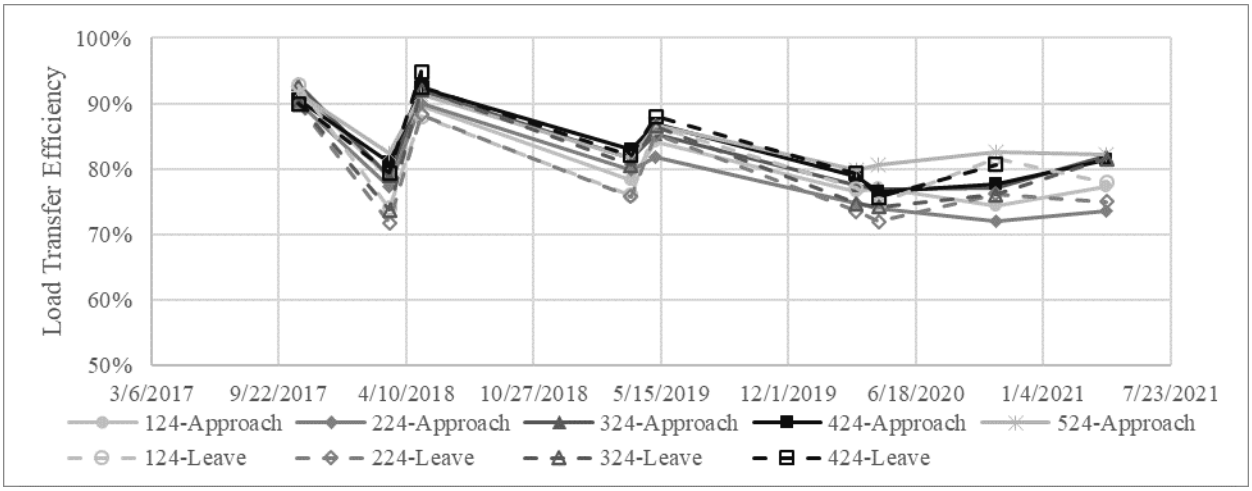

Figure 20: Load transfer efficiency for the inside lane

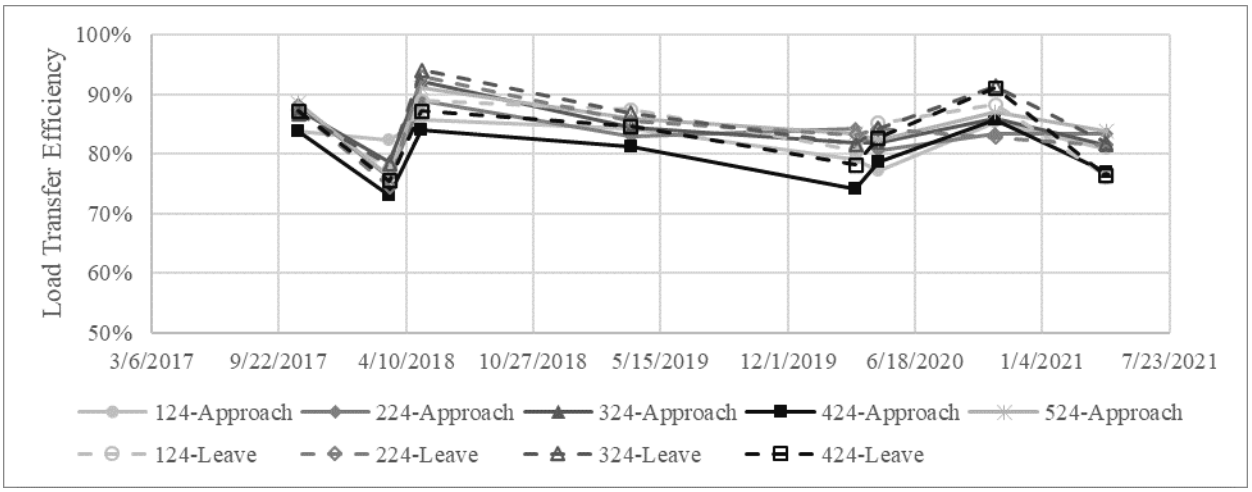

Figure 21: Load transfer efficiency for the outside lane

Differential deflections were also considered for this analysis. As observed in Figure 22, there is a clear difference between the inside and outside lanes. The inside lane, with the heavier load application, began with a higher differential deflection but quickly fell to meet and then further fell below the outside lane. This indicates there may be other contributing factors than the effect of vehicle load size. Earlier loaded cells had minimal differences to cells loaded later indicating no significant effect from early loading. Regardless of trends shown in Figure 22, the

worst differential deflection recorded was only 0.16 mm (0.006 inches) and most are below 0.1 mm (0.004 inches). Differential deflections are not considered problematic until 0.25 mm (0.01 inches) is reached. All cells in both lanes maintained low differential deflections providing good joint performance.

It can be concluded that analysis of FWD and IRI data did not find any of indications damage in Cells 124-424 that could be directly attributed to early opening.

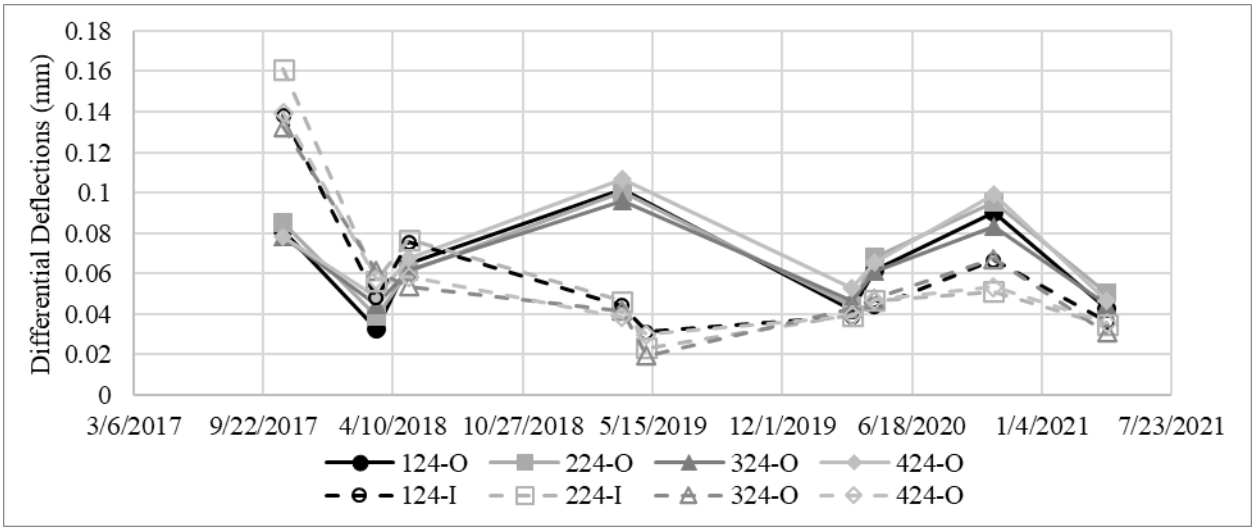

Figure 22: Differential deflections for each cell

3.3 Finite Element Analysis

A general principle of structures is if stress is greater than strength, failure can occur. However, in a pavement, when tensile stress reaches flexural strength it does not necessarily mean failure. The flexural strength of a pavement is estimated using a simply supported beam which has a less effective stress distribution than a slab on grade. Therefore, the flexural strength of an in-situ pavement will be greater than that measured with the laboratory method [68,69]. The flexural

strength of concrete slabs has been found to be 1.3 to 3.5 times higher than beam specimens of the same concrete mixture [70]. There is also greater strength variability in a slab at critical locations that can affect stresses in the concrete especially at early ages [23]. Since only six slabs were tested, it is possible that strength was higher at critical locations from favorable conditions.

To further investigate, a finite element analysis using ISLAB2000 was performed to estimate stresses that could have been experienced by MnROAD cells due early age loading by the MnDOT snowplow truck. The snowplow was simulated using two separate loadings by a 11-kip single axle and a 20-kip tandem axle. Different load locations and temperature gradients were used to examine potential stress states. A pavement structure similar to the MnROAD cells was created in ISLAB2000 using the following properties:

- Slab thickness: 6 in
- Concrete modulus of elasticity: 3,000,000 psi
- Poisson's ratio: 0.15
- Concrete coefficient of thermal expansion: 5.0E-6 1/°F
- Unit weight: 0.087 lb/in^3
- Base thickness: 6 in
- Base modulus of elasticity: 40,000 psi
- Interface condition between the concrete slab and base: unbonded
- Transverse joint spacing: 15 ft
- Subgrade stiffness: 250 psi/in
- Lane-shoulder joint LTE: 20%
- Linear temperature distribution through the slab thickness; the difference between the top and bottom concrete surfaces: 10°F or 0°F

- Axle type: single
- Axle weight: 12,000 lb or 18,000 lb
- Wheel tire pressure: 100 psi
- Wheel aspect ratio (length-to-width ratio): 1
- Axle position (distance from the slab/shoulder joint): 0 in or 12 in

The first simulation considers loading at the pavement edge at mid-slab with a 10°F temperature difference between the top and bottom of the concrete layer. Figure 23 shows the resulting longitudinal stresses. The critical stresses were directly under the load at the edge of the pavement which is a probable location for failure in a slab. The combination of a positive temperature differential and single axle load (11-kip) placed at the slab/shoulder joint causes the highest maximum stress (243 psi) at the bottom concrete surface. A heavier tandem axle load (20-kip) still causes a significant stress (205 psi) if it is placed at the slab edge in the presence of a positive temperature gradient. Recall the strengths at the time of loading ranged from 73-319 psi (Table 6). At the time of the first two loadings, the strength was well below these simulated stresses and therefore under these simulated conditions, damage is likely to initiate.

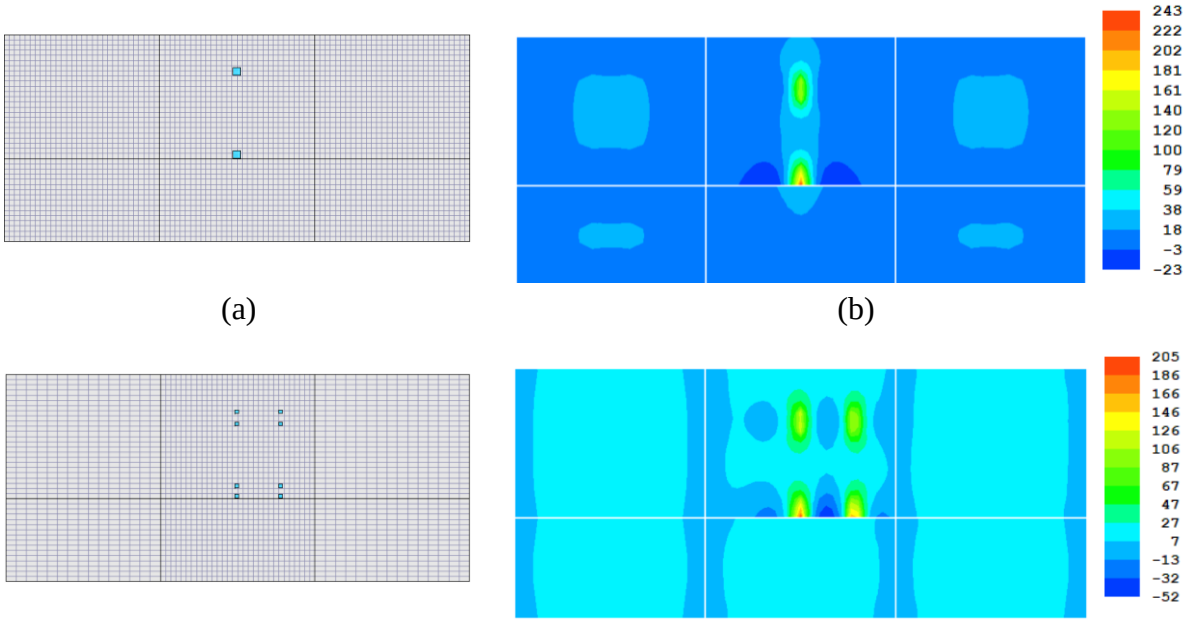

Figure 23: (a) ISLAB simulation with a single axle path on the edge with 10°F gradient with (b) bottom surface longitudinal stresses due to 11-kip single axle loading and (c) ISLAB simulation with a tandem axle path on the edge with 10°F gradient with (d) bottom surface longitudinal stresses due to 20-kip tandem axle loading.

During the field experiment, the snowplow wheels did not travel exactly at the slab edge. To simulate this, the wheel load location was moved 12 inches away from the slab edge while maintaining the axle loads and temperature gradient. As observed in Figure 24**,** moving load 12 inches away from the edge reduces the maximum stresses to 150 and 127 psi for 11-kip single axle and 20-kip tandem axle, respectively. Stresses dropped below 100 psi at the critical location on the mid-slab edge. This indicates the wheel path has significant contribution to decreasing damage and preventing early failure.

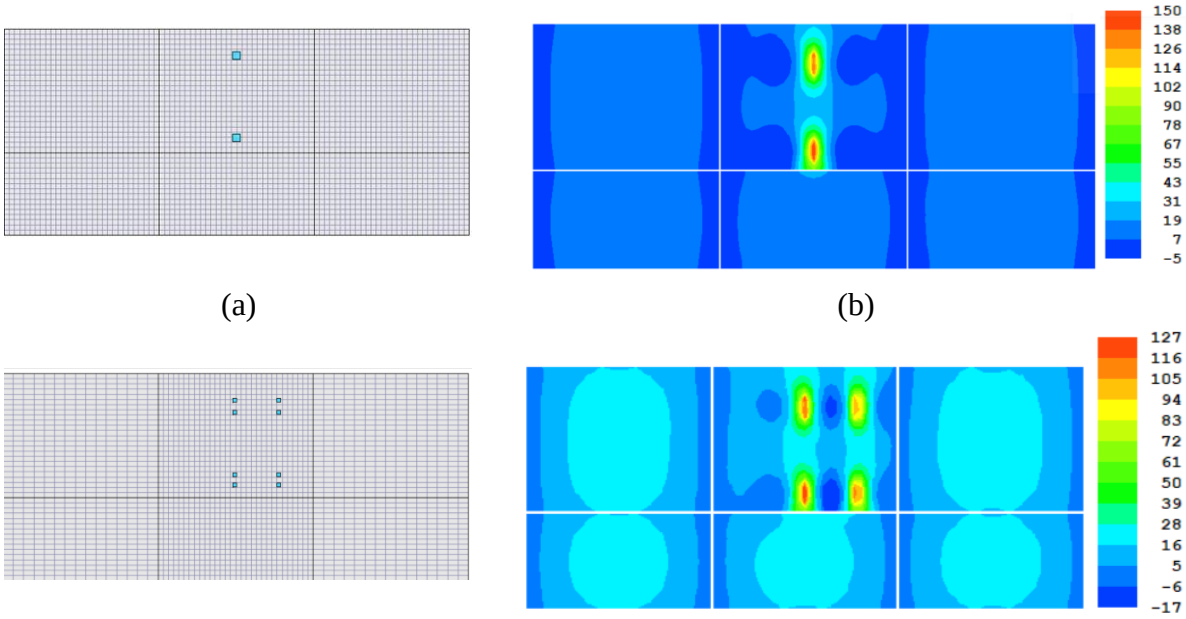

Figure 24: (a) ISLAB simulation with a single axle path 12 inches from the edge with 10°F gradient with (b) bottom surface longitudinal stresses due to 11-kip single axle loading and (c) ISLAB simulation with a tandem axle path 12 inches from the edge with 10°F gradient with (d) bottom surface longitudinal stresses due to 20-kip tandem axle loading.

When early loading was applied, the heat of concrete hydration was still affected by the temperature distribution through the slab thickness. Although early loading started about 3 pm, the temperature gradient was not necessarily high. To evaluate the effect of temperature difference on predicted stresses, the temperature gradient was changed from 10°F to 0°F. This caused maximum stresses to fall even lower: 132 and 110 psi for the single and tandem load, respectively (Figure 25). Changing the temperature gradient to a more favorable condition allows for an even greater decrease in critical stress at the slab edge with stresses dropping to below 75 psi. This is nearly the same as the pavement strength at the time of the first loading (73 psi) indicating that favorable conditions similar to this final simulation occurred during the MnROAD test explaining the lack of pavement damage. This clearly indicates the environmental conditions of loading have a critical effect on the concrete stresses alongside wheel path and axle loading.

The results of changing each loading condition are summarized in Table 8.

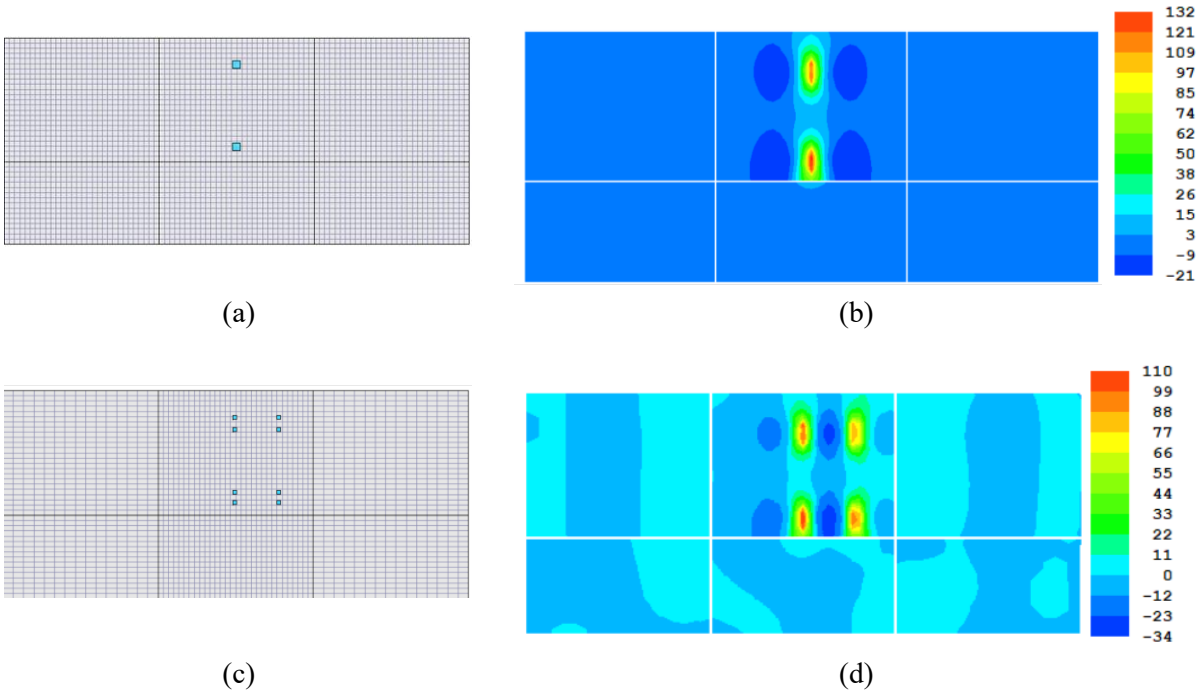

Figure 25: (a) ISLAB simulation with a single axle path 12 inches from the edge with 0°F gradient with (b) bottom surface longitudinal stresses due to 11-kip single axle loading and (c) ISLAB simulation with a tandem axle path 12 inches from the edge with 0°F gradient with (d) bottom surface longitudinal stresses due to 20-kip tandem axle loading.

Table 8: Summary of the effects of changing the conditions of loading

Axle Load	Estimated Maximum Stresses (psi)		
	10°F gradient on slab edge	10°F gradient 12 inches away from slab edge	0°F gradient 12 inches away from slab edge
11-kip	243	150	132
20-kip	205	127	110

This analysis shows that a favorable combination of loading conditions is a possible explanation for the absence of observable damage at the early loading field experiment. Repeating this experiment several times could potentially lead to damage under different conditions including a vehicle load closer to the edge, a positive temperature gradient in the concrete layer, or a lower concrete strength at critical locations caused by variability. Both individually and combined, these factors are shown to significantly affect critical slab stresses. To accurately evaluate the risk of

opening a concrete pavement to traffic earlier, it is important to estimate the chance of unfavorable conditions for axle load, wheel path, temperature gradient, pavement geometry, and strength variability.

3.4 Summary

This chapter focused on identifying factors influencing pavement performance and critical stresses occurring in a slab exposed to very early loading. A concrete pavement was loaded at four concrete strengths significantly earlier than standard criteria with two different vehicle loads. The pavement was heavily monitored for early age performance loss and was regularly tested over four years to examine long term pavement performance. Despite the extreme loadings and thorough monitoring, no damage could be directly attributed to early opening.

To understand the reasoning behind the lack of damage, a finite element model was made with similar parameters to the test pavement. The analysis examined the effect of axle load, wheel path, and temperature gradient on stresses occurring in the concrete layer. The worst-case scenario was under a 11-kip single axle load at the pavement edge with a 10°F temperature gradient. The resulting stresses were far above the concrete strength at the time of the earliest loadings. The best-case scenario was under a 20-kip tandem axle load moved away from the edge and without a temperature gradient. The stress from this simulation resulted in values similar to or below the strengths at the time of loading. Early age concrete has significant strength variability and therefore a critical location having more or less strength than the slab as a whole could control whether the pavement fails. The large-scale test must have been performed under favorable conditions and if the test were to be repeated, the same early loadings could potentially cause damage.

Each factor simulated in this model contributed to significant changes in concrete stress, especially at critical locations on the slab. To accurately determine the risk of damage due to early loading, it is crucial to estimate the chance of unfavorable conditions occurring specifically for axle load, wheel path, temperature gradient, pavement geometry and strength variability.

4.0 Nondestructive Methods' Field Performance on Early Age Concrete Mixtures

This chapter explores the accuracy of two common nondestructive tests when used on early age concrete to expedite onsite concrete strength determination. A laboratory and field evaluation of a concrete paving project was used to compare advantages and limitations of nondestructive tests for two common concrete mixtures used when rapid construction is required: high early strength (HES) concrete mixture and long-life concrete pavement (LLCP) mixture.

Modern conventional concrete has made significant advancements in strength and durability, but pavements still require several days of curing before traffic opening. HES mixtures shorten this significantly to about 7 hours after construction allowing for shorter construction and road closures [71]. HES mixtures are most commonly used to decrease construction time for rehabilitated concrete pavement and has competing closure times with asphalt pavement construction [72,73]. This is accomplished by using Type III cement, high cement content, low water to cement ratio, higher curing temperature, accelerating admixtures, or supplementary cementitious materials [72]. HES concrete obtains a specific strength at an earlier age than conventional concrete making HES ideal for cold weather conditions, rapid repairs, and fast track construction [72]. HES pavements are commonly opened to traffic within 24 hours of paving, and therefore the first day is the most critical for a successful pavement.

There is a potential for lower pavement performance and life span as potential misuse of materials and early age conditions is more likely. The issues with destructive testing highlighted earlier are amplified when using HES mixtures as strength testing is performed every few hours instead of days like conventional concrete. Due to a higher potential for last minute mixture changes or curing methods at the contractor's discretion, the Federal Highway Administration

(FHWA) suggests multiple tests to check HES pavement performance including strength development, durability, early stiffening, shrinkage, or temperature [35]. This increases the importance of using nondestructive testing but there are concerns over the accuracy of these tests at very early ages.

Maturity and ultrasonic testing were used to monitor both HES and conventional mixtures in laboratory and field applications. The results of this case study were discussed to evaluate the ability of the nondestructive tests to estimate very early age concrete strength for modern concrete mixtures when compared with traditional destructive testing and each other.

4.1 Field Study Site Description

The testing site (a work vehicle parking lot), shown in Figure 26, consists of multiple lanes of 12 × 12 ft dowelled Jointed Plain Concrete Pavement (JPCP). Construction began at 7:00 A.M. on July 13, 2020 in Imperial, Pennsylvania. Figure 27 shows photos from construction. The project consisted of an 8-inch-thick concrete pavement using HES mixture for the first lane and LLCP mixture for the remaining six lanes. On the first day, four lanes were paved about 1.5 hours apart. Due to the shape, the HES lane was constructed using fixed forms. A slipform paver was used for the LLCP lanes. A sprayed compound was used on each lane as the curing method. Joints were sawed approximately six to seven hours after paving.

Three slabs from the HES lane were monitored. Three slabs from the first LLCP lane (C1) were monitored (C1.1, C1.2, and C1.3) as well as one slab from each of the other two lanes (C2 and C3) (Figure 26). One HES slab and one LLCP slab were monitored for temperature to utilize the maturity method as described in ASTM C1074 [32]. Thermocouples were installed at two

locations shown in Figure 26: one at the slab center (TC) and another near the lane edge (TE). In addition to maturity data, shear wave velocity was measured at several locations on all monitored slabs: slab edge (TE), center (TC), corner right north (CRN), corner right south (CRS), corner left north (CLN), and corner left south (CLS). Monitoring several locations for each testing method allowed strength gain variability within the slab to be considered.

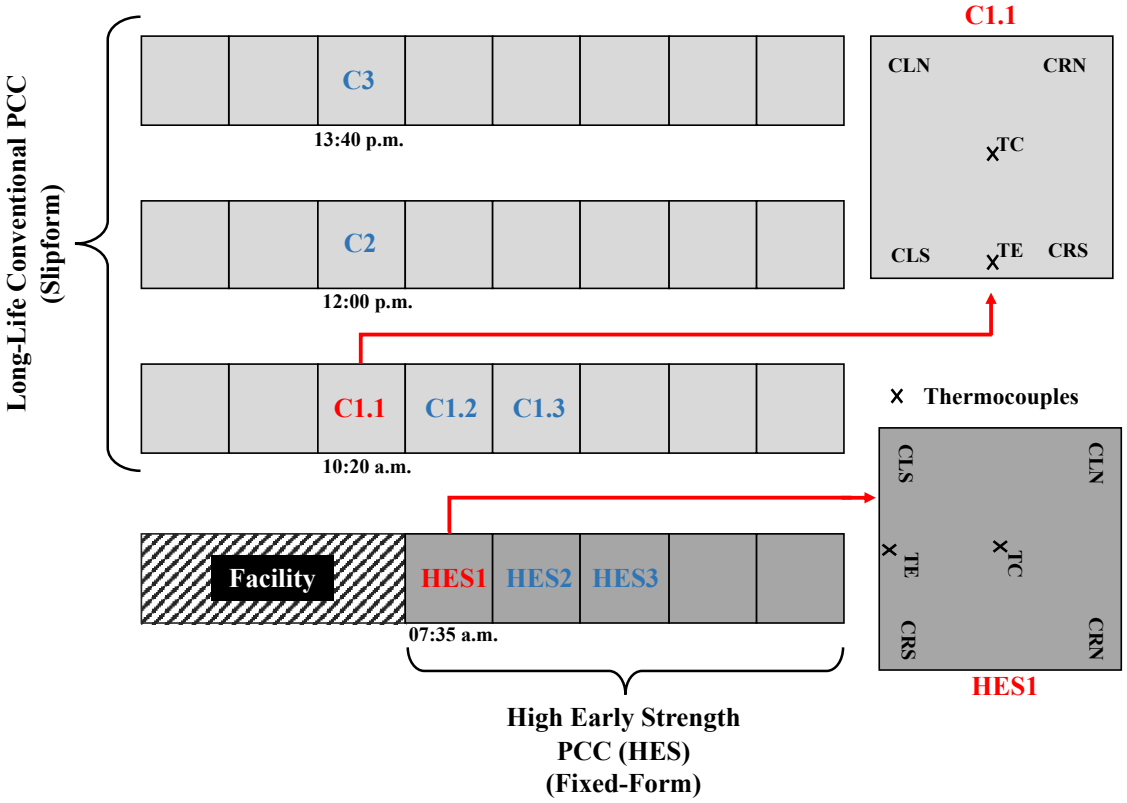

Figure 26: Testing site design with construction and instrumentation details

(a) HES

(b) HES

(c) HES

(d) LLCP

(e) LLCP

(f) LLCP

Figure 27: Construction of HES lane (a, b, and c) and of LLCP lanes (d, e, and f)

4.1.1 Concrete Mixtures

A summary of the mixture designs is provided in Table 9. The HES concrete mixture was designed to meet standards provided by Pennsylvania Department of Transportation (PennDOT) for a 7-hr accelerated mix design and the conventional concrete mix was designed to meet PennDOT requirements for LLCP. Both mixes used Type I/II Portland cement with Type F fly ash. The coarse aggregates included #57 limestone and #8 sandstone, and the fine aggregate was concrete sand.

Table 9: Mixture design details

	High Early Strength Mix	Long-Life Concrete Pavement Mix
Cement (lbs)	600	477
Pozzolan 1 (lbs)	150	134
Total Cementitious (lbs)	750	611
Coarse Aggregate 1 (lbs)	1309	1357
Coarse Aggregate 2 (lbs)	396	410
Total Coarse Aggregate (lbs)	1705	1767
Fine Aggregate (lbs)	1158	1161
Total Water (lbs)	236	249
W/C Ratio	0.315	0.408
Unit Weight (lbs/ft3)	142.93	141.03

4.2 Laboratory and Field Testing

Three types of strength testing were conducted for this experiment: destructive, maturity, and ultrasonic testing. Laboratory testing was performed on multiple cylinder and beam specimens of the same concrete mixtures used in the field to determine concrete strength at different ages. Maturity and ultrasonic data were collected on both laboratory specimens and slabs.

4.2.1 Laboratory Strength Testing

Standard destructive tests, compressive and flexural strength, were performed in a laboratory adjacent to the field site (Figure 28). Cylinder and beam specimens were cast using the same concrete poured in slabs HES1 and C1.1. Destructive tests followed ASTM standards C39, for compressive strength using 4 x 8-inch cylinders, and C78, for flexural strength using third-point loading [21,22].

(a) (b)

Figure 28: Conventional laboratory strength testing (a) compressive strength and (b) third-point loading for flexural strength

The HES mixture was tested for compressive strength at 3, 5, 7, and 24 hours after pouring. HES beam specimens were only tested for flexural strength at 7 hours which is the suggested opening time for the mixture. The LLCP mixture was tested for both compressive and flexural strength at 1, 3, 5, 7, 14, and 28 days after construction. Compressive strength (f'_c) and flexural strength (M_r) results are shown in Table 10.

.

For a conventional concrete mixture to meet PennDOT requirements, it must reach a compressive strength of 3000 psi in 72 hours and 3750 psi in 28 days [10]. The LLCP far exceeded these requirements reaching 3000 psi within 24 hours and 6219 psi at 28 days indicating a high-quality pavement. For a HES concrete mixture, PennDOT requires the concrete reach 1200 psi in less than 7 hours [9]. This requirement was also exceeded as the HES mixture reached 2484 psi in 7 hours. Both mixtures had an average compressive strength of 3000 psi within the first 24 hours indicating the mixtures will have a similar performance in this case study.

There was minimal strength development in the LLCP mixture between 3 and 5 days as shown in the small increase in compressive strength and the small reduction in flexural strength. These variations are not statistically significant therefore the concrete remained constant between 3 and 5 days.

PennDOT does not have a minimum flexural strength to open to traffic with conventional concrete. At 7 days, the LLCP mixture flexural strength was well over any state requirements at 819 psi. Several other states have HES specifications with flexural strength and recommend opening strengths ranging from 290 to 490 psi [9,74–77]. The recommended opening time for HES pavements is 7 hours, at which point the mixture reached a flexural strength of 361 psi which falls within the range of state criteria.

Table 10: Average and standard deviation for compressive strength testing in psi

	High Early Strength Mix		Long-Life Concrete Mix	
Test Time	Avg. f'_c	St. Dev. f'_c	Avg. f'_c	St. Dev. f'_c
3 hours	125	16	-	-
5 hours	951	43	-	-
7 hours	2484	73	-	-
1 day	3658	128	3311	145
3 days	-	-	4329	115
5 days	-	-	4426	106
7 days	-	-	5040	217
14 days	-	-	5237	440
28 days	-	-	6219	111

Table 11: Average and standard deviation for flexural strength testing in psi

	High Early Strength Mix		Long-Life Concrete Mix	
Test Time	Avg. M_r	St. Dev. M_r	Avg. M_r	St. Dev. M_r
7 hours	360.9	12.8	-	-
1 day	-	-	597.2	57.9
3 days	-	-	741.2	18.0
5 days	-	-	719.0	19.2
7 days	-	-	819.3	88.6
14 days	-	-	824.0	86.9
28 days	-	-	804.4	25.5

4.2.2 Maturity Testing

Maturity testing was conducted according to ASTM C1074 [32]. Type T thermocouples were used to measure the slab temperature. The thermocouples were installed in two locations on slabs HES1 and C1.1: one at slab center (TC) and another near the slab edge (TE) as illustrated in Figure 26. For each location, four thermocouples were installed: two at 1-inch below surface and the other two at mid-depth (Figure 29a). Temperature data collection began immediately after concrete placement using a CR 3000 datalogger manufactured by Campbell Scientific®. Slab temperature was recorded at 5-minute increments. Temperature sensors were also placed in the concrete cylinders (Figure 29b) and beams to allow for performance comparison between the slab

and laboratory specimens. The temperature data collected was used to calculate maturity of the concrete in the slabs and laboratory specimens.

(a) (b)

Figure 29: Thermocouple instrumentation in the (a) field and (b) laboratory

4.2.3 Ultrasonic Testing

Shear wave velocity was measured using a linear array ultrasonic tomography device called MIRA (Figure 30). Since MIRA scans do not require permanent instrumentation, require no surface preparation, and are quick to perform, tests were performed near the maturity sensor placements as well as several other locations on the slab (CLN, CRN, CLS, CRS, TE, and TC) as shown in Figure 26. This version of MIRA, provided by the FHWA, uses high frequency shear waves of 50,000 Hz. Transducers located on the bottom of the device emit and receive signals from 48 dry contact points arranged in 12 linear array channels. The reflected shear waves are recorded, stored, and analyzed for every scan in 66 signal time histories.

All ultrasonic measurements were performed in calibration mode, so the calculated shear wave velocity and subsurface reconstruction were recorded. Only shear wave velocity was considered in this case study.

Figure 30: Ultrasonic tomography device, MIRA

Ultrasonic testing began on the day of construction when the concrete had set enough to support walking, about 3 hours after placement (Figure 31) for slab HES1 and 5 hours for slab C1.1. Measurements were taken every 15 mins for one hour, then every 30 mins for 3 hours and, finally, every hour for the remainder of the workday. Due to the rapid concrete set and the short time intervals between scans, only one slab of each mixture was evaluated for the first 24 hours, HES1 and C1.1. Two measurements were taken at each location identified in Figure 26 for each time increment. Care was taken to avoid locations where dowel bars could interfere with the scan.

Ultrasonic testing was conducted 1, 2, 3, 5, 7, and 14 days after concrete placement. All slabs identified in Figure 26 were scanned at all locations for additional data. Shear wave velocity data for every measurement in slabs HES1 and C1.1 are presented in Appendix B. The first two scanned time increments for HES are excluded as the concrete was still in the initial stage of hardening and caused inconsistencies in the scan.

In the laboratory, ultrasonic testing was performed on beam specimens before flexural testing (Figure 31b). Concrete shear wave velocity was recorded three times on each side. Appendix C presents the full data.

(a) (b)

Figure 31: Ultrasonic testing in (a) the field and (b) laboratory

4.3 Results and Analysis for High Early Strength Concrete

Field and laboratory results for the HES mixture are presented in Figure 32 as maturity and shear wave velocity over time. Figure 32a shows the linear relationship both field and laboratory maturity data have with time. In the first 24 hours, maturity in the laboratory and field are similar indicating similar strength developments. After the first day, the slab begins maturing faster than the laboratory specimens. This is likely due to a higher ambient temperature for the slab when compared to the specimen environment. The pavement was constructed during the summer when the average daily temperature is about 85°F (30°C) whereas the laboratory was cooler and shaded.

Maturity is the cumulative effect of temperature and this increase in ambient temperature likely caused the slab to cure faster than the specimens.

A similar comparison was performed on shear wave velocity data. Data on laboratory specimens is limited as MIRA is only able to scan beam specimens and there was only one for the HES mixture. Figure 32b shows the shear wave velocity development over time which has two well-defined stages. In the first 24 hours, there is a drastic increase in velocity. After the first day, the increase becomes more gradual before becoming nearly stable around 2400 m/s.

Figure 33 shows MIRA measurements exemplifying shear wave velocity and hydration development over time. At around 3 hours (Figure 33a) after concrete placement, shear wave velocity is extremely low. Concrete is hardening faster at the top of the slab and the ultrasonic signal captures some reflections due to this heterogenous hardening process. Around 2 hours later (Figure 33b), shear wave velocity has increased considerably and the slab/base backwall is now visible but with a weak intensity. After 1 day (Figure 33c), the material completes most of its hardening process, shear wave velocity is established, and the slab/base backwall is clearly marked.

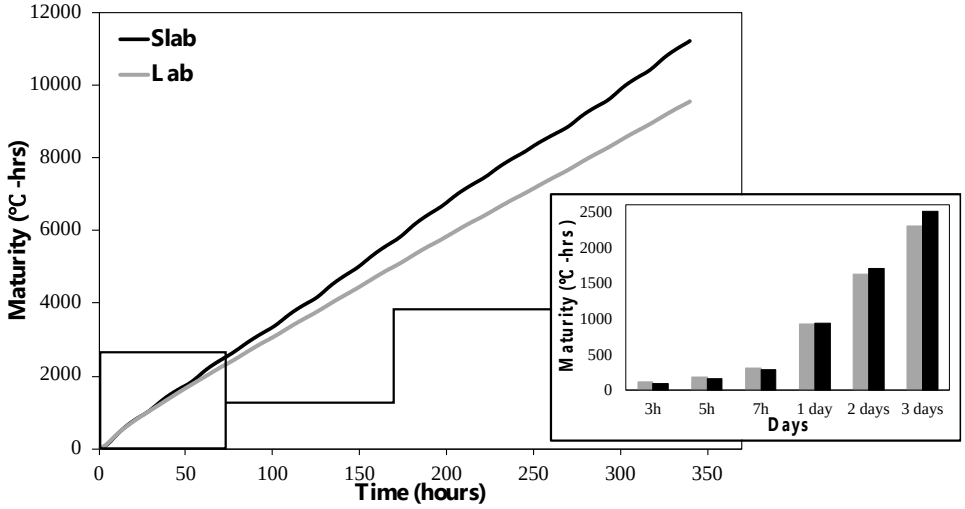

(a)

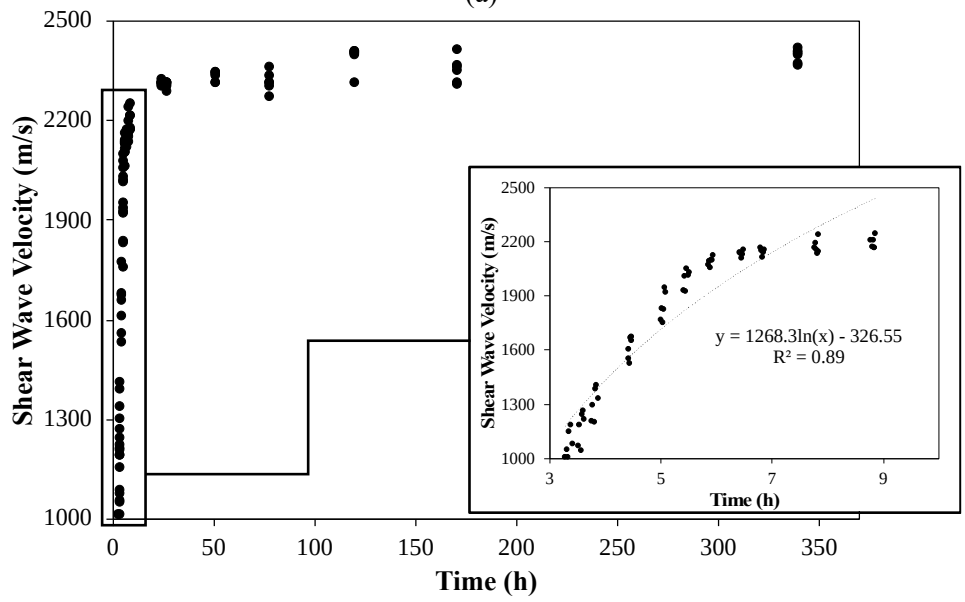

(b)

Figure 32: (a) Slab and laboratory maturity over time and (b) slab shear wave velocity over time

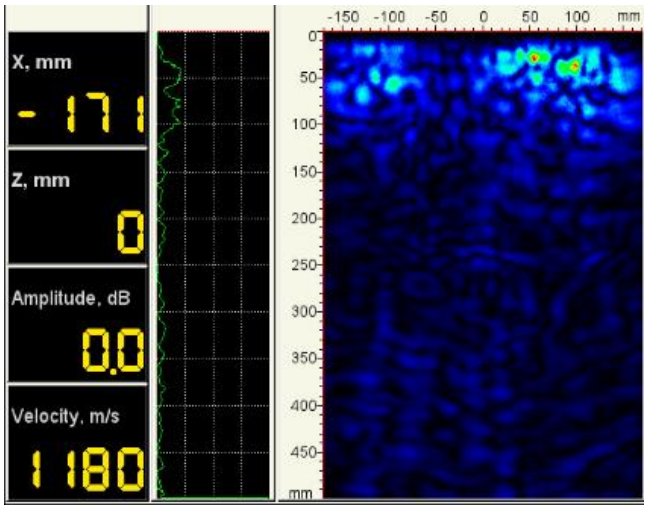

(a) 3.5 hours, no slab/base backwall

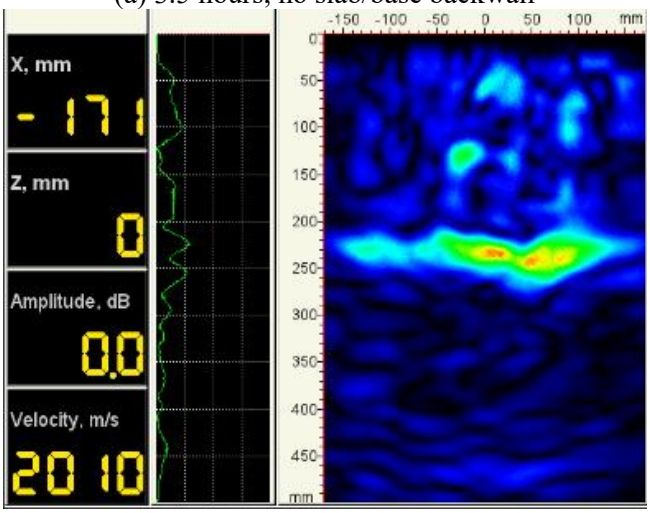

(b) 5.5 hours, weak backwall

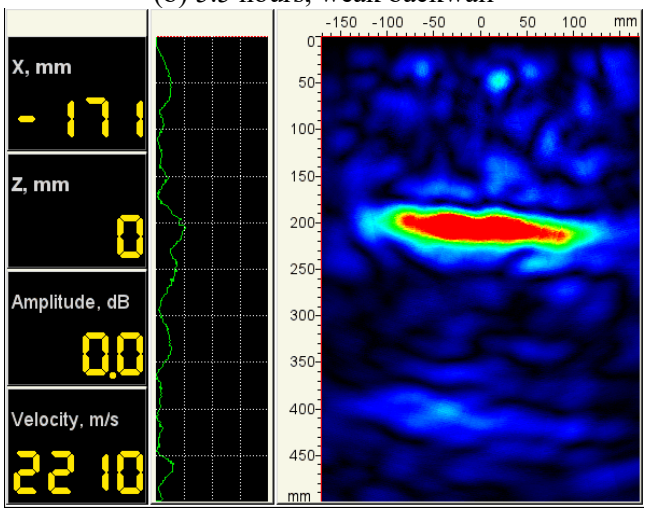

(c) 27 hours, well defined backwall

Figure 33: Development of concrete subsurface and shear wave velocity 27 hours after construction

4.3.1 HES Compressive Strength Development

Strength development was closely monitored for the first 24 hours after construction when most strength is gained for HES mixtures. There were a limited number of beam specimens so compressive strength was used. Slab shear wave velocity was correlated to compressive strength at specific ages when the slab and specimen maturity aligned. Figure 34 presents the relationship between HES compressive strength gain and nondestructive test results for the first 24 hours. Compressive strength correlates well with both tests with shear wave velocity presenting nearly perfect correlation. Maturity tends to underpredict compressive strength in this case study.

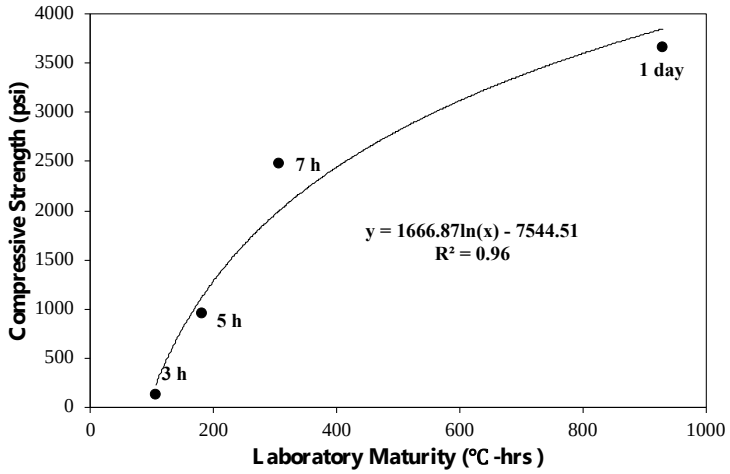

(a)

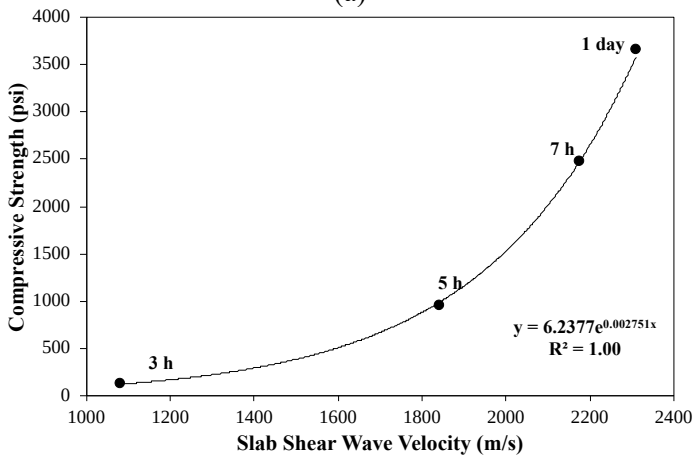

(b)

Figure 34: Relationship between concrete compressive strength and (a) maturity and (b) shear wave velocity

4.3.2 Effect of Variability on HES results

Concrete strength gain is not a uniform process as hydration depends on many varying conditions. This can cause areas of significant strength variation. Significant internal variability can be caused by improper placement or mixing [78]. While improper construction can be avoided, there will still be slight variability simply due to location within the slab or minor environmental effects such as shade. Pavement variability is especially important when considering early opening decisions as the entire structure must be able to support the traffic load.

This study considered two forms of variation: variation at different locations within the same slab and variation between separate slabs. Figure 35a shows shear wave velocity variability in the same slab (HES1) from six different positions. There was substantial variability in shear wave velocity measurements in the first few hours after construction that diminished with time with a maximum difference of 21%. After 24 hours, the variation fell to a maximum of 5%. This small-scale variation could be caused for several reasons like variations in concrete mixture, densification, or curing conditions. The heterogenous qualities of concrete cause strength to develop differently depending on location even within a single slab. These small variations in shear wave velocity can have a significant impact on strength variation.

On a slightly larger scale, three consecutive slabs in the same lane were compared in Figure 35b. Due to limited ultrasonic device access and time, only one HES slab was able to be consistently measured in the first 24 hours. The remaining two HES slabs were regularly monitored after 24 hours for 14 days. The maximum difference in shear wave velocity between slabs was 7%, a similar value to the variation within a single slab after 24 hours. These three slabs were paved using the same concrete and methodology five minutes apart, confirming that concrete strength gain varies in other slabs. Fixed form construction, which was used on this lane, is

especially susceptible to differences in placement and mixing. Small variations in environmental conditions may also play a factor, such as the presence of shade on HES1 that was not significant on the other monitored slabs.

For maturity testing, to detect both variations within a single slab and between other slabs it would be necessary to install a large quantity of sensors in several locations prior to construction. Recording and interpreting temperature data would be needed in a short period of time. Both actions are impractical for most pavement construction projects due to their expensive and time-consuming characteristics.

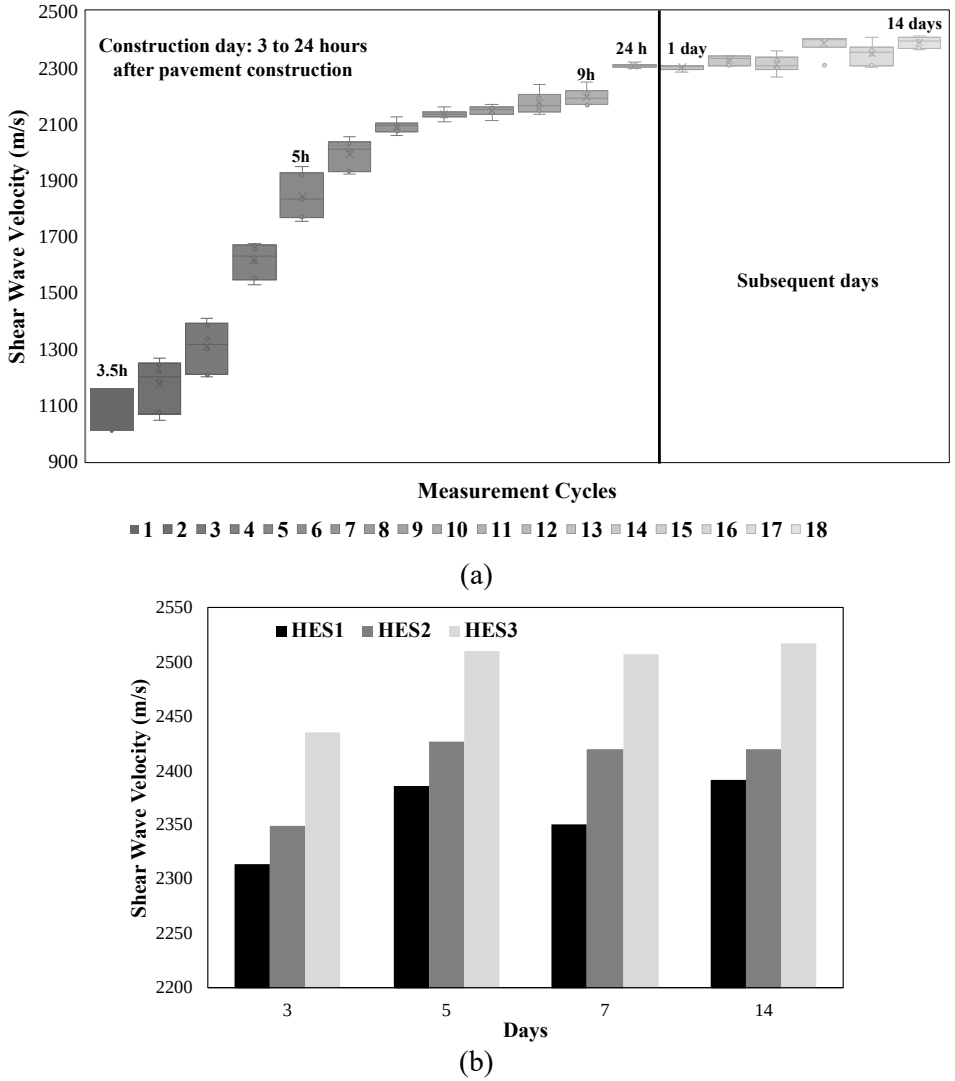

Figure 35: Shear wave velocity variability in (a) different positions within a single slab and (b) different slabs

4.3.3 Effects on Early-Opening for HES

For the HES mixture, the following relationship was found between compressive strength and the nondestructive test results:

$$f'_c = 1666.87 \times ln\big(M(t)\big) - 7544.51, (R^2 = 0.96), (psi) \quad \textbf{(4-1)}$$

$$= 11.493 \times ln\big(M(t)\big) - 52.018, \quad (R^2 = 0.96), (MPa)$$

$$f'_c = 6.2377 \times e^{0.002751 \times V_s}, (R^2 = 1.00), (psi) \quad \textbf{(4-2)}$$

$$= 0.043 \times e^{0.002751 \times V_s}, (R^2 = 1.00), (MPa)$$

where f'_c is concrete compressive strength, psi or MPa; $M(t)$ is maturity, °C-hr; V_s is shear wave velocity, m/s.

Using these relationships, maturity and shear wave velocity compressive strength estimations were compared to laboratory compressive strengths 5 and 8 hours after construction to establish method accuracy compared to traditional destructive testing. Table 12 provides the average measurements at each location of testing as shown in Figure 26. Values highlighted in red are far below the required 3000 psi compressive strength for Pennsylvania. The color changes to yellow then green as the strength gets closer to and eventually surpasses the requirement.

Five hours after construction, compressive strength estimations using maturity and shear wave velocity were similar to each other and the laboratory measured strength. Maturity became conservative six hours and beyond. Shear wave velocity indicated a steep increase in compressive strength between five and six hours and aligned well with laboratory measured compressive strength at 7.85 hours. Using values linearly interpolated between 7 and 8 hours, maturity predicted a compressive strength of 1865 psi while shear wave velocity was closer to laboratory measured values at 2459 psi.

For the HES mixture at an early age, shear wave velocity shows better predictions than maturity. Shear wave velocity was sensitive enough to capture the dramatic increase in compressive strength at 5 hours, common in early ages of HES mixtures. The portability of ultrasonic devices allows multiple areas to be analyzed which better captures the variability of the pavement due to the differing strength gain rates.

Table 12: Hourly predicted compressive strength for maturity and shear wave velocity

Time (hours)	Slab Maturity Based Compressive Strength (psi)	Slab Shear Wave Velocity Based Compressive Strength (psi)	Lab Compressive Strength (psi)
5	NA NA 922 NA 966 NA	1227 1333 971 779 812 958	951 (5.2 hours)
6	NA NA 1175 NA 1222 NA	2157 2014 1986 1804 1880 2014	
7	NA NA 1555 NA 1599 NA	2375 2248 2343 2098 2441 2311	2484 (7.85 hours)
8	NA NA 1896 NA 1936 NA	2960 2311 2615 2217 2441 2375	

4.4 Results and Analysis for Long-Life Concrete

Figure 36 presents long-life concrete pavement (LLCP) compressive and flexural strength verses maturity and shear wave velocity. Both nondestructive tests had strong correlations with strength, but shear wave velocity had the closest correlation. This was mainly due to maturity estimating a significant increase in concrete maturity between 3 and 5 days of about 1200 °C-hrs. However, neither compressive nor flexural laboratory measured strength experienced this rise. Shear wave velocities measured on beam specimens produced similar values between 3 and 5 days that better captured the slower strength development for that time.

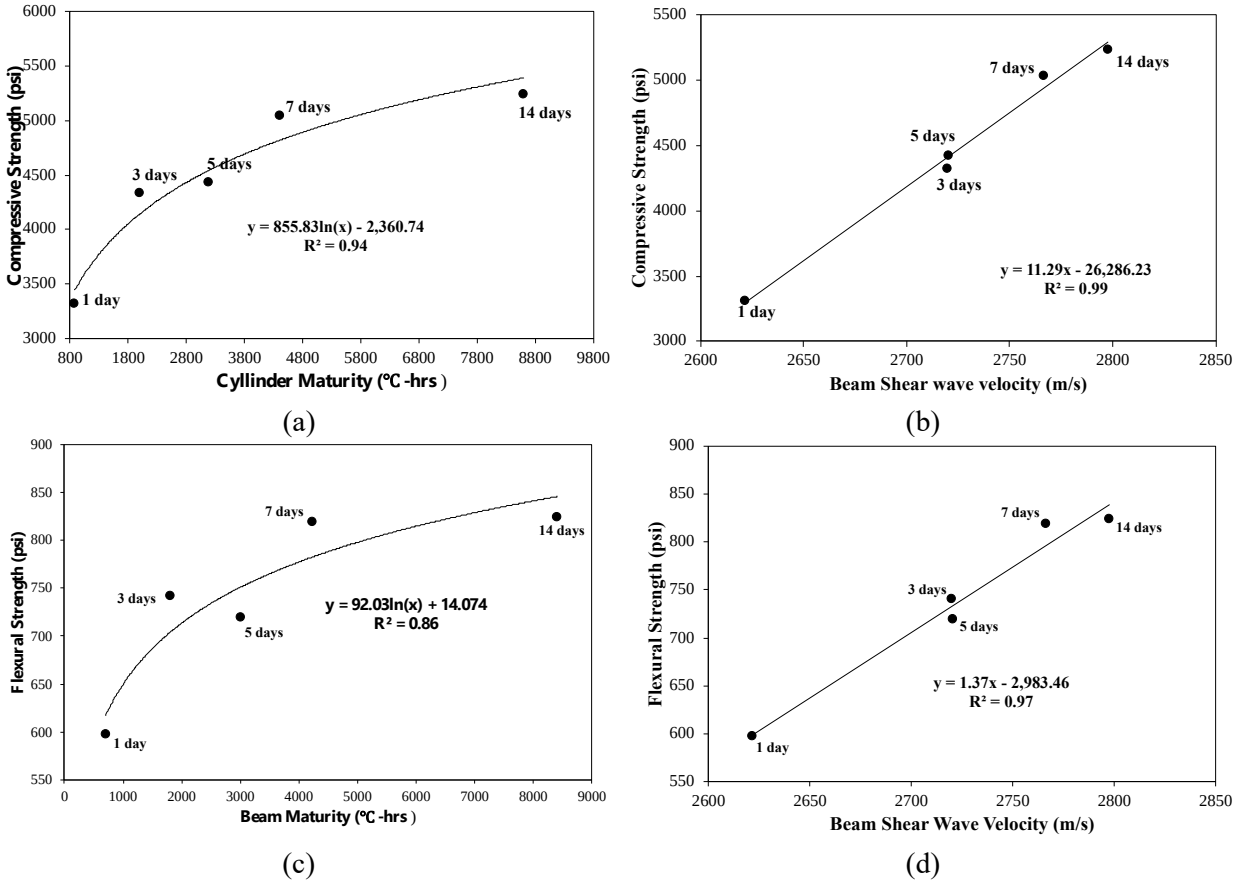

Figure 36: Measured cylinder compressive strength (a and b) and beam flexural strength (c and d) versus maturity and shear wave velocity

Figure 37 presents the average maturity verses shear wave velocity at locations TC and TE on the slab and the beam specimens (Figure 26). This would be a comparison of the exact same concrete for either test minimizing the effect of concrete variability. For the same maturity, wave velocities measured on beam specimens are consistently higher than velocities measured on the concrete slab. This could be due to the MIRA procedure used in this study not being made with smaller beam specimens in mind. The nearby vertical edges or field conditions may affect wave velocity measurements. A solution for this discrepancy will be explored further in this section and potential reasonings will be hypothesized in the next chapter.

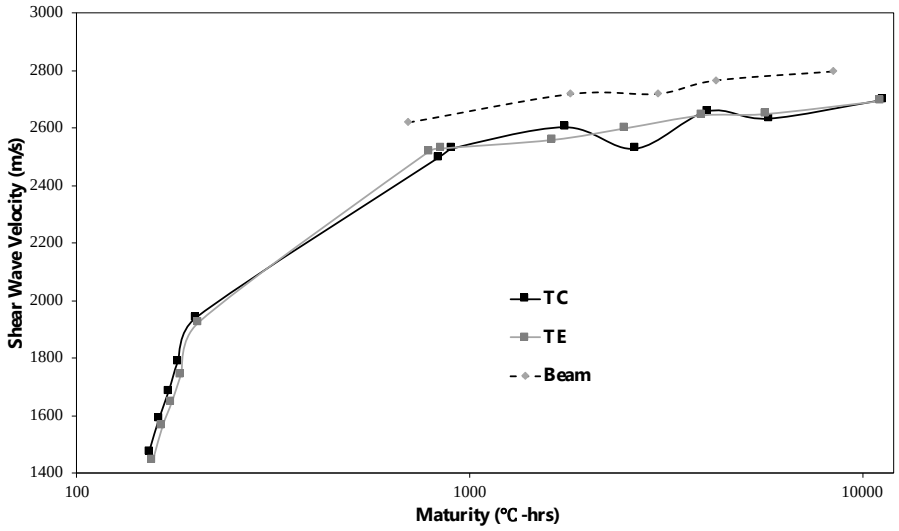

Figure 37: Shear wave velocity vs maturity for concrete slab and beams

4.4.1 Effect of Variability on LLCP Results

Conventional concrete mixtures experience nonuniform strength gain causing varying strengths within the same pavement structure which has a serious effect on traffic opening decisions and other construction operations. Figure 38 shows this variability using the measured shear wave velocity from the LLCP slab (C1.1) at six measurement positions (Figure 26). There

was substantial variability in shear wave velocity that diminished with time as the concrete became more uniform indicating the different strength gain rates of early age concrete.

To consider a larger scale, the three different LLCP lanes were compared using variation in shear wave velocity as shown in Figure 39. LLCP Lanes 2 and 3 were paved approximately 2 and 3 hours after construction of Lane 1 using the same paver and mixture. One would believe that 3 days after construction, all lanes would have similar concrete properties, but this did not occur here. Variation in shear wave velocity did decrease after one day but there was significant variation between the lanes weeks after construction. This indicates that different slabs and lanes have different strength gain rates for a significant amount of time. Lane 3 had greater shear wave velocity variation than the others two, three, and seven days after construction. Although Lanes 1 and 2 still had significant variability. After seven and fourteen days, Lane 3 exhibited significantly lower shear wave velocities than the other lanes.

This indicates the necessity of regular monitoring throughout a project length. Assuming data collected from a single slab or lane is acceptable for an entire project is incorrect. Varying data collection locations is critical to ensuring the entire pavement has met procedure criteria.

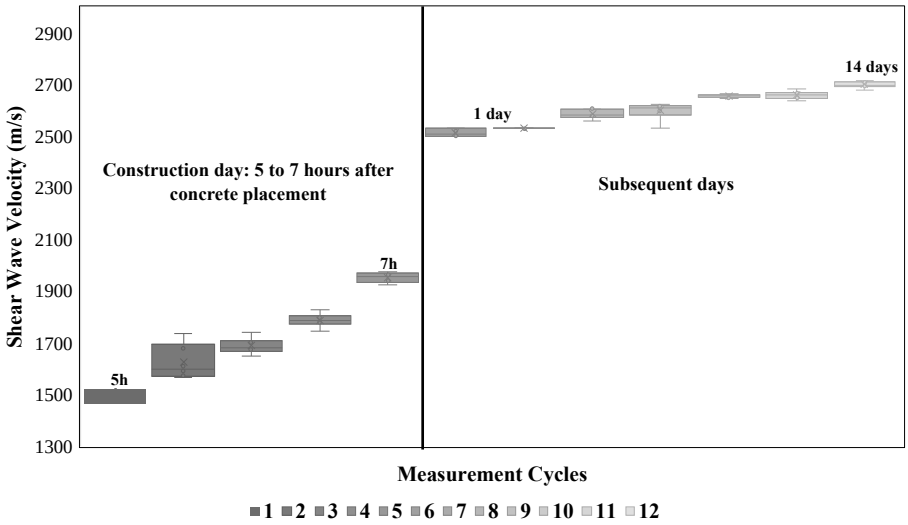

Figure 38: Slab shear wave velocity variation in different positions of the instrumented slab

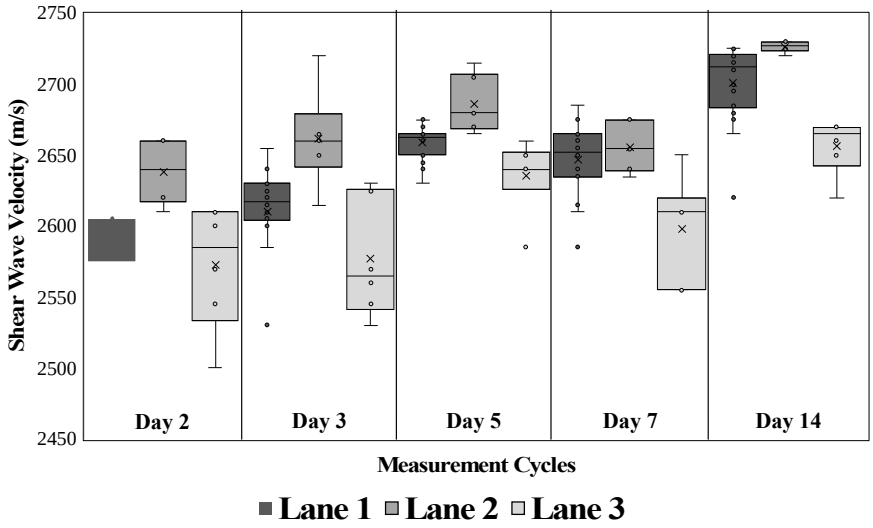

Figure 39: Shear wave velocity variation in different slabs

4.4.2 Effects on Early-Opening for LLCP

For the LLCP conventional concrete mixture, the following relationship was found between laboratory measured concrete strength and nondestructive test results. Equations (4-3) and (4-5) show the relationship between maturity as measured on beam and cylinder specimens and concrete strength. Equation (4-6) shows the relationship between shear wave velocity measured on beam specimens and flexural strength. Shear wave velocity was not computed for cylinders, therefore slab shear wave velocity was correlated to the compressive strength at specific ages when the maturity for the slab and specimen aligned. The corresponding relationship is shown in Equation (4-4).

$$\begin{aligned} f'_c &= 885.83\ ln\big(M(t)\big) - 2{,}360.74\ \ (R^2 = 0.94), (psi) \\ &= 5{,}900\ ln\big(M(t)\big) - 16{,}277\ \ (R^2 = 0.94), (MPa) \\ f'_c &= 11.29\ V_s - 26286.2\ \ (R^2 = 0.99), (psi) \end{aligned} \quad \textbf{(4-3)}$$

$$= 77.81\, V_s - 181{,}237\ (R^2 = 0.99), (MPa) \quad \textbf{(4-4)}$$

$$M_r\ = 92.03\, ln\big(M(t)\big) + 14.074\ \ (R^2 = 0.86), (psi)$$
$$= 634.53\, ln\big(M(t)\big) + 97.035\ \ (R^2 = 0.86), (MPa) \quad \textbf{(4-5)}$$

$$M_r = 1.37\, V_s - 2{,}983.46\ \ (R^2 = 0.97), (psi)$$
$$= 9.421\, V_s - 20{,}570.3\ \ (R^2 = 0.97), (MPa) \quad \textbf{(4-6)}$$

where f'_c is concrete compressive strength, psi or MPa; $M(t)$ is maturity, °C-hr; V_s is shear wave velocity, m/s; M_r is concrete flexural strength (modulus of rupture), psi or MPa.

Using these relationships, maturity and shear wave velocity concrete strength estimations for slabs were compared to laboratory measured strengths two days after construction to establish the accuracy of each method compared to traditional destructive testing. Figure 40 shows the average measurements at each location of testing as shown in Figure 26. This includes two locations over the thermocouples using maturity estimations and six locations using shear wave velocity estimations. Values highlighted in red are below the required 3000 psi compressive strength as determined by Pennsylvania or the required 700 psi flexural strength as based on other state policies. The color becomes lighter as the strength gets closer to the standard. Once these requirements are surpassed, the value is highlighted green which grows darker as the strength continues to increase.

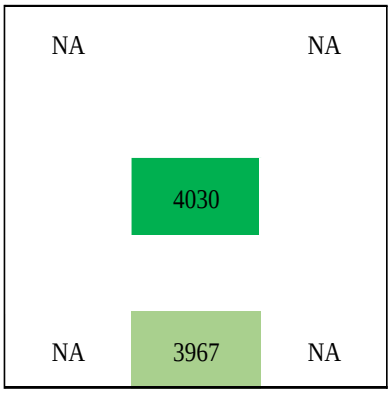

(a) Maturity-based compressive strength estimation (psi)

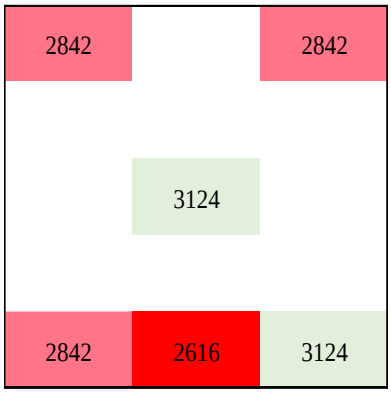

(b) Shear wave velocity-based compressive strength estimation (psi)

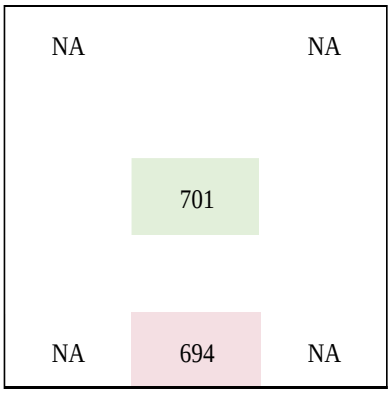

(c) Maturity-based flexural strength estimation (psi)

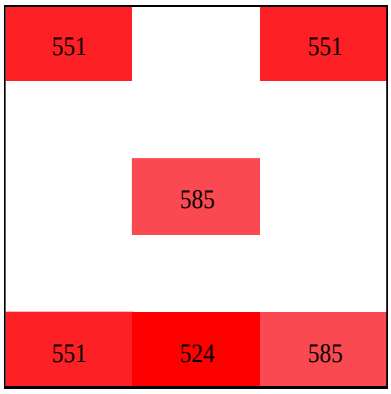

(d) Shear wave velocity-based flexural strength estimation (psi)

Figure 40: Concrete strength estimation for slab C1.1 two days after construction

Shear wave velocity-based analysis resulted in a lower strength level compared with the maturity-based method. As previously discussed, the procedure the linear array ultrasonic device, MIRA, uses to calculate shear wave velocity may not be accurate on beam specimens, possibly due to reflections from vertical edges or laboratory conditions. A simple procedure to adjust the wave velocities was developed based on field maturity data. This issue with specimen size will be further explored in the next chapter.

The simplified solution assumes that the accurate shear wave velocity is measured on the beam and is equal to the shear wave velocity of the slab when the maturities are equal. Equation (4-7) shows the correction factor proposed for this concrete mixture. Figure 41 shows the modified beam velocities and slab measured velocities versus maturity when measured at the same point of the slab (slab center-TC, and slab edge-TE (Figure 26)). Similar relationships for beam- and slab-measured velocities and maturity are observed.

$$V_{s,Field} = 0.9823 * V_{s,Lab} - 72.068 \ (R^2 = 0.90) \quad \textbf{(4-7)}$$

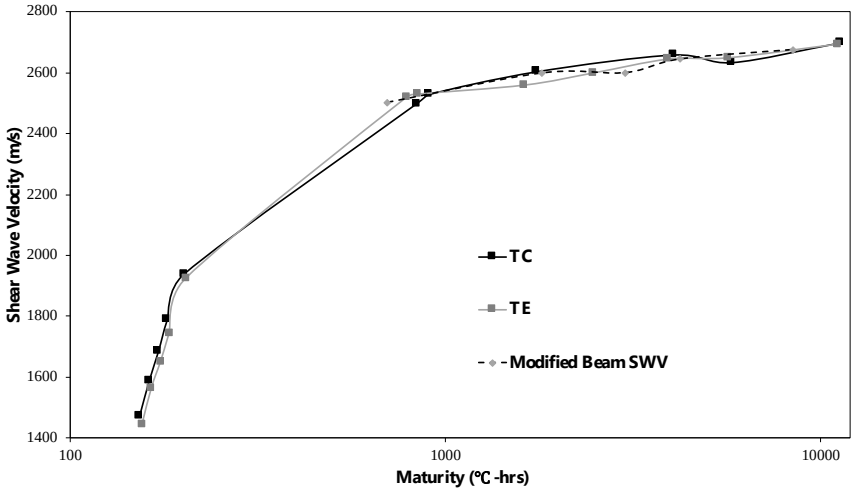

Figure 41: Slab and modified beam shear wave velocity (SWV) versus maturity

The correction factor, Equation (4-7), was combined with the predictive Equations (4-4) and (4-6) resulting in the following model:

$$f'_c = 11.493\, V_s - 25458 \quad \textbf{(4-8)}$$

$$M_r = 1.395\, V_s - 2{,}883 \quad \textbf{(4-9)}$$

Figure 42 shows the concrete strength gain predicted by maturity and the original and adjusted shear wave velocities. Compressive strength is compared in Figure 42a using the modified shear wave velocity described in Equation (4-8) and flexural strength is shown in Figure 42b using the modified shear wave velocity described in Equation (4-9). Using modified shear wave velocity results in a comparable strength gain to maturity results.

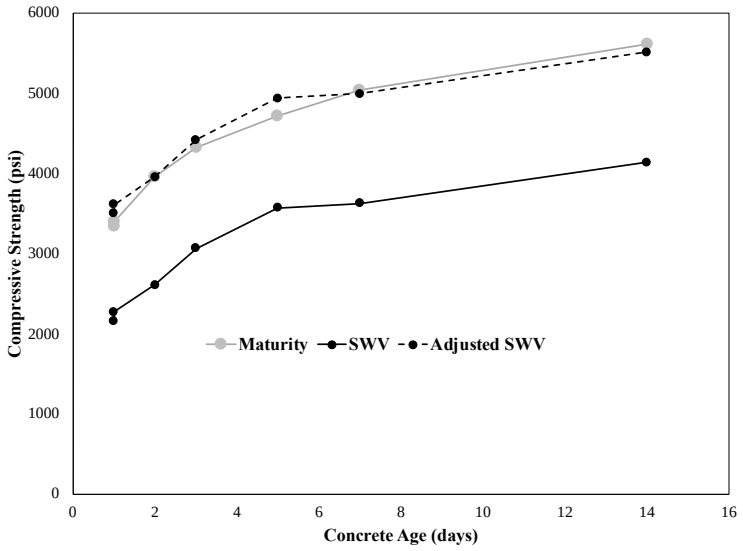

(a)

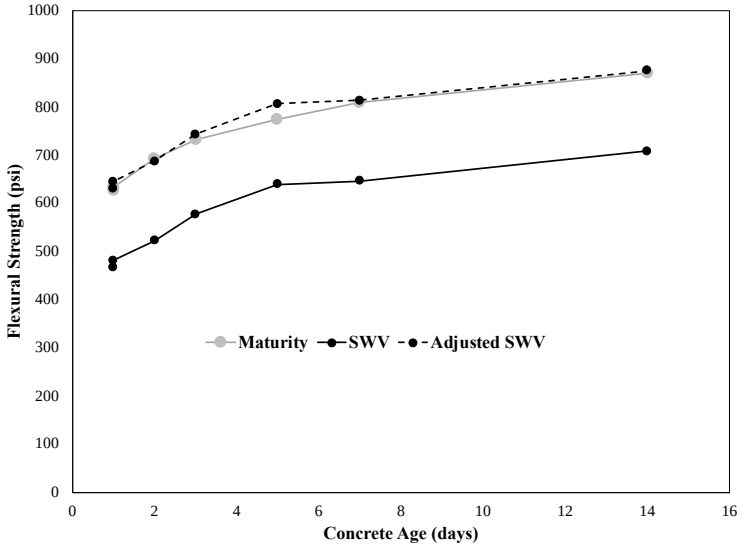

(b)

Figure 42: Concrete strength gain versus maturity and shear wave velocity (SWV)

Using Equations (4-8) and (4-9), maturity and shear wave velocity estimated concrete strength two days after construction for slab C1.1 was updated (Figure 43). The modified estimates provide more reasonable results and indicate the strength requirements for a majority of the slab was met. This is a valid method to adjusting the shear wave velocity on a beam specimen when temperature sensors and maturity is used in tandem.

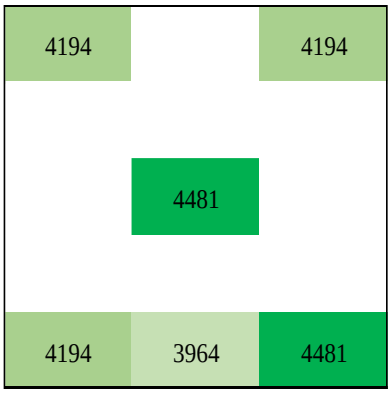

(a) Modified shear wave velocity-based compressive strength estimation (psi)

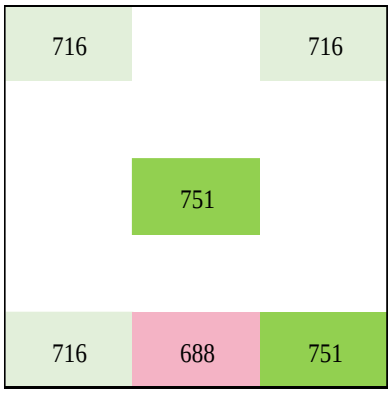

(b) Modified shear wave velocity-based flexural strength estimation

Figure 43: Concrete strength estimation for slab C1.1 two days after construction using modified shear wave velocity

Models developed in this chapter for this mixture are only valid after the pavement cures for one day. Using these models to compute strength in the first few hours after paving might predict unrealistic, negative strength estimations.

4.5 Summary

Maturity and ultrasonic testing were investigated for early age in-situ strength estimations for newly constructed HES and conventional concrete pavements. Both methods estimated concrete strength with accuracy. In this study, maturity had difficulty adjusting to variable strength gain rates leading to under- and overestimations of strength. This inconsistency is especially hazardous in early age construction as there is a higher risk of pavement damage or wasting precious construction time with no reliability or consistency.

Ultrasonic testing predicted early age strength with more accuracy than maturity for both mixtures when compared to traditional destructive testing. The significant concrete strength gain variation common in early age concrete was accurately captured using shear wave velocity. The

ultrasonic device is portable allowing for variability measurements along the pavement or the specific analysis of problem areas. The need for permanent instrumentation when using the maturity method limits the testing area and the ability to test for variability along a pavement.

Ultrasonic testing provides fast, accurate results from any location on the concrete pavement surface which improves information on early stages of concrete development allowing users to improve early age construction efficiency. The predictive potential of maturity is still a major benefit but when used simply for strength at time of testing it is not as efficient or informative as ultrasonic testing. However, at this time, the discrepency of shear wave velocity on beam specimens has not been fully addressed and no such issue is present when using the maturity method.

5.0 Evaluation of Concrete Pavement Strength in the Field by Combined Nondestructive Tests

The purpose of this chapter is to increase the accuracy and efficiency of concrete strength determination in the field by combining maturity and ultrasonic testing. Both nondestructive methods have been explored and tested in previous chapters and their respective advantages and limitations have been identified.

Maturity and ultrasonic testing correlated well to concrete strength and provide reliable strength estimations, but ultrasonic testing was more accurate than maturity at early ages [37,38,79]. The improved accuracy and mobility make ultrasonic testing preferable for early age field use. This would remove the need for numerous permanent sensors along the pavement as required by maturity. Wave velocity only estimates strength at the time of scanning. There are no predictable aspects to ultrasonic testing unlike maturity which utilizes temperature models to predict strength. Ultrasonic testing is also affected by specimen size which changes wave velocity on smaller specimens.

This chapter addresses these limitations and offers corrections. Combining the field use of ultrasonic testing and the predictable strength development from the maturity – strength relationship provides the user with comprehensive knowledge on concrete strength and improves construction efficiency. A procedure to use the nondestructive tests in combination will be outlined. This procedure includes measuring the shear wave velocity of a beam specimen to establish the shear wave velocity – strength relationship and therefore the effect of specimen size on wave velocity will also be investigated and potential reasonings suggested. The dataset collected in the previous chapter were used to calibrate and validate this procedure.

5.1 Combining Nondestructive Procedures

Maturity and ultrasonic testing are both reliable nondestructive methods individually but have unique advantages over each other. Combining methodologies can use both tests to their highest ability and provide the user with thorough information on concrete strength development. This procedure will allow strength estimations from ultrasonic testing to utilize the predictive temperature models through the maturity – strength relationship, accurately providing both current and future field strength estimations. This proposed procedure is outlined below.

To best explain the combined procedure, the conventional concrete dataset collected in Chapter 4 will be used as an example. Table 13 shows a summary of the relevant data to be used in this chapter.

Table 13: Example dataset including maturity and wave velocity

Test Time	Compressive Strength (psi)	Modulus of Rupture (psi)	Cylinder Maturity (°C-hr)	Beam Maturity (°C-hr)	Beam Shear Wave Velocity (m/s)
1 day	3311	597	847	694	2622
3 day	4329	741	2006	1808	2720
5 day	4426	719	3192	3001	2721
7 day	5040	819	4409	4224	2766
14 day	5237	824	8604	8411	2798

Step 1: Performing Laboratory Testing

As with separate maturity and ultrasonic testing procedures, perform laboratory testing using the concrete mixture. Cylinder and beam specimens should be prepared for compressive and flexural strength testing. Several ages should be tested to establish a proper strength gain rate. The final cylinder and beam specimens should be imbedded with thermocouples to monitor

temperature for the entirety of the testing period. Each beam should be scanned with the ultrasonic device before flexural testing.

Step 2: Establishing Maturity – Strength and Wave Velocity – Strength Relationships

Establish the maturity – flexural strength (Equation (2-4)), maturity – compressive strength (Equation (2-5)), and wave velocity – flexural strength (Equation (2-9)) relationships using the procedures outlined in Chapter 2. This will provide calibration coefficients for each of the three models.

Step 3: Determining Wave Velocity – Compressive Strength Relationship

When using linear array ultrasonic devices, compressive strength specimens cannot be scanned for wave velocity. Use the following equation to relate wave velocity to compressive strength through maturity relations:

$$f_c' = f'_{cu} \times \exp\left(-\left(\frac{c_m}{a_m}\right)^{d_m}(-a_s V_s - b_s)^{\frac{d_m}{b_m}}\right) \quad \textbf{(5-1)}$$

The required laboratory work was performed on the dataset to establish the model coefficients described in Steps 1-3 for Equations (2-4), (2-5), (2-9), and (5-1) as shown in Table 14. Visualizations of these models compared to destructive strength testing are shown in Figure 44 and Figure 45.

Table 14: Strength model coefficients

Maturity – Strength Model		Shear Wave Velocity – Strength Model	
a_m	271.35	a_s	0.002
b_m	1.015	b_s	-5.417
c_m	489.50		
d_m	1.021		

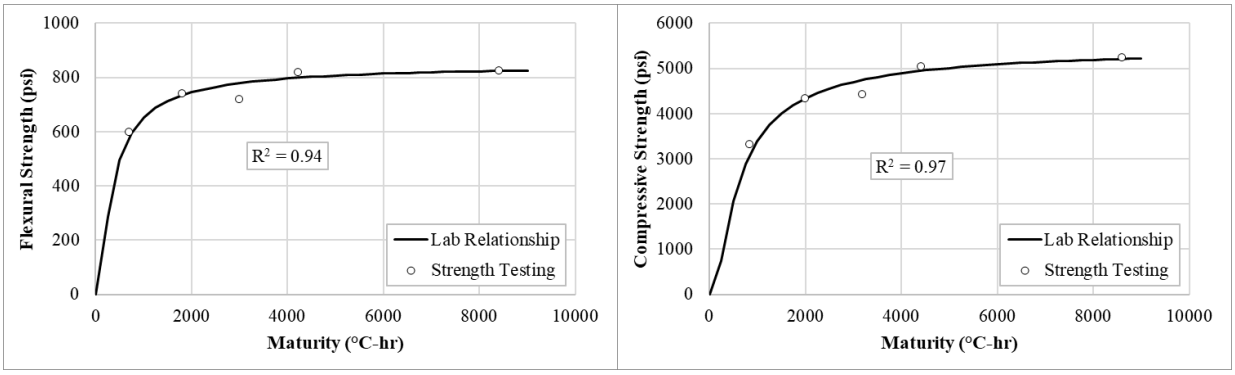

Figure 44: Maturity - strength relationships for the example dataset

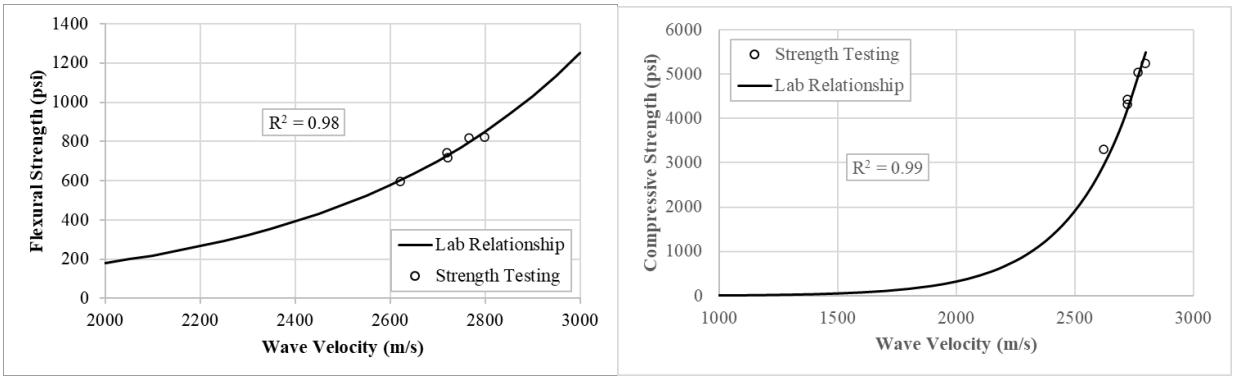

Figure 45: Shear wave velocity – strength relationship for the example dataset

Step 4: Choosing a Strength

Now that all models have been established, select a compressive or flexural strength (f'_{c0} or M_{r0}) to be considered for an early age procedure. This can be any strength the user may want to confirm in the field. The example will use a compressive strength of 3000 psi which is a common strength for opening to traffic.

Step 5: Calculating Relative Shear Wave Velocity

The strength chosen in Step 4 must be converted to shear wave velocity. Equations (2-9) and (5-1) can be rearranged to find the relative wave velocity for the chosen flexural or compressive strength, respectively:

$$V_{s,0} = \frac{1}{\mathrm{a_s}} \ln \frac{M_{r0}}{M_{ru}} - \frac{b_s}{a_s} \quad \textbf{(5-2)}$$

$$V_{s,0} = -\frac{1}{a_s}\left(\left(-ln\frac{f'_{c0}}{f'_{cu}}\right)^{\frac{b_m}{d_m}}\left(\frac{a_m}{c_m}\right)^{b_m}\right) - \frac{b_s}{a_s} \quad \textbf{(5-3)}$$

Using Equation (5-3) and the respective coefficients from Table 14, the relative shear wave velocity at 3000 psi can be calculated to be 2627 m/s.

Step 6: Using Shear Wave Velocity Field Shift Factor

Linear array ultrasonic devices are affected by specimen size causing higher shear wave velocities in beams compared to slabs of the same age and mixture. The discrepancy between laboratory and field measurements has been identified in previous studies [80–82]. The next section will hypothesize why this discrepancy is occurring but for the purpose of this procedure, a simple solution is presented. Chapter 4 used field maturity data to adjust slab velocity measurements to beams of the same maturity. This is a valid method of adjusting beam wave velocity data if temperature sensors are used in the field. However, since field strength can be more reliably estimated with ultrasonic testing in the field, temperature sensors would not necessarily be required so this step introduces an alternative shift factor that does not rely on maturity.

With the datasets in this study, the difference between beam and slab velocities remains relatively consistent. Ages of testing were 1, 3, 5, 7, and 14 days and the difference between slab and beam shear wave velocities were 108, 121, 64, 107, and 99, respectively. This resulted in an average difference of 100 m/s and a standard deviation of 19 m/s. Full data like this would be unavailable at the time this procedure is needed at the beginning of construction.

Using the difference between the first field wave velocity measurement and the laboratory velocity at the same age provides a reasonable shift factor for the remaining data points (Figure 46). Zhang et. al. (2020) also used the first wave velocity field measurement as a shift factor for their beams to create a relationship between wave velocity and temperature [80]. This provided

accurate property predictions for their considered field material. When using the first data point as a shift factor, wave velocity measurements should be taken at the earliest age tested in the laboratory. Determine the difference between the field wave velocity and the laboratory wave velocity at this age. This value can be subtracted from $V_{s,0}$ which provides the user with the velocity to look for as it is read on the device in the field and obtain the corresponding strength.

For the test pavement, the earliest time of testing was 1 day when the average laboratory shear wave velocity measurement was 2622 m/s. In the field, the average shear wave velocity measurement was 2513 m/s. This leads to a difference of 108 m/s to be subtracted from $V_{s,0}$ providing the device velocity. Figure 47 shows how the field shift factor adjusts the field strength gain rate to better correspond to strengths measured in a laboratory. The dashed line represents a 1:1 ratio between beam and slab shear wave velocity and the shifted slab data is clearly closer to representing beam velocities. A compressive strength of 3000 psi is equivalent to a shear wave velocity of 2647 m/s. Applying the field shift factor of 108 m/s, the value to be expected in the field would be 2539 m/s.

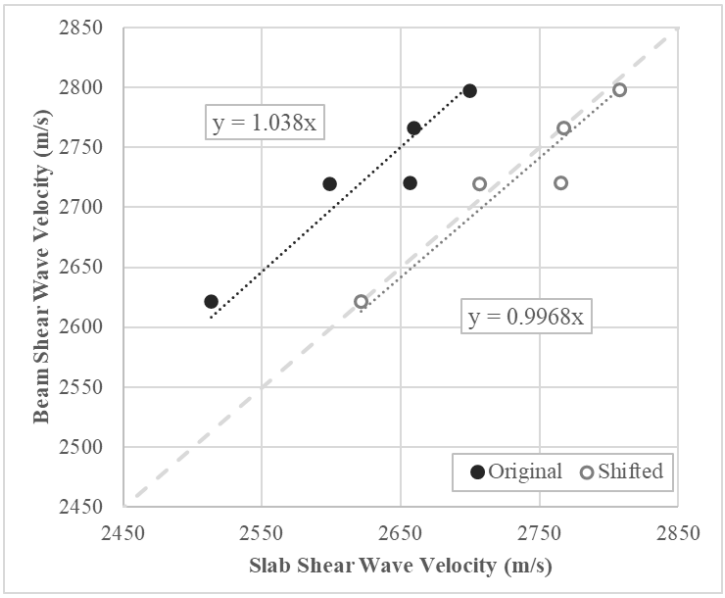

Figure 46: Difference between beam and slab velocities before and after shifting

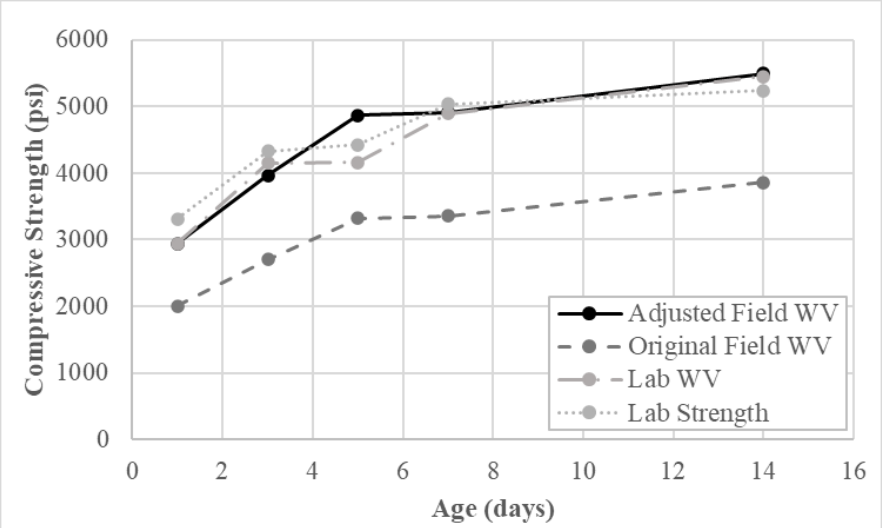

Figure 47: Adjusting the field wave velocity (WV)

Step 7: Calculating Relative Maturity

The strength chosen in Step 4 now can be converted to maturity. Equations (2-4) and (2-5) can be rearranged to find the maturity relative to the chosen flexural or compressive strength, respectively. Using Equation (5-5), the maturity at 3000 psi is calculated to be 800 °C-hr.

$$TTF_0 = \frac{a_m}{\left(\ln\frac{M_{ru}}{M_r}\right)^{\frac{1}{b_m}}} \quad \textbf{(5-4)}$$

$$TTF_0 = \frac{c_m}{\left(\ln\frac{f'_{cu}}{f'_c}\right)^{\frac{1}{d_m}}} \quad \textbf{(5-5)}$$

Step 8: Updating Concrete Strength Development for Specific Strength

Update the predictive maturity – strength relationship to include the concrete strength development after the chosen strength from Step 4 based on the anticipated change in maturity.

$$M_r = M_{ru}e^{-\left(\frac{a_m}{TTF_0 + t*T_{pcc,m}}\right)^{b_m}} \quad \textbf{(5-6)}$$

$$f'_c = f'_{cu}e^{-\left(\frac{c_m}{TTF_0 + t*T_{pcc,m}}\right)^{d_m}} \quad \textbf{(5-7)}$$

where t is the time from specified strength in hours; and T_{pcc} is the mid-depth mean concrete slab temperature depending on the pavement location, concrete slab thickness, and construction month.

The mid-depth mean temperature of the concrete slab can be obtained in several ways. As with a standard maturity procedure, the exact mid-depth temperature can be measured with imbedded sensors. The measured temperature for the test pavement and resulting maturity – strength relationship can be seen in Figure 48. Pavement temperature can also be accurately modeled. After the first few hours of curing, the pavement temperature relies less on heat of hydration and more on ambient temperature. The Mechanistic Empirical Pavement Design Guide uses the Enhanced Integrated Climatic Model (EICM) to estimate the hourly temperature of the pavement layers based on the ambient climate data from local weather stations [83]. The average ambient temperature of Pittsburgh, PA in July 2020 is 23.8°C. This average monthly temperature and resulting relationship can be seen in Figure 48. Despite the different temperatures, the maturity – strength relationships are similar. A temperature model based on ambient temperature, such as EICM, can be used for accurate results without the need for permanent sensor installation.

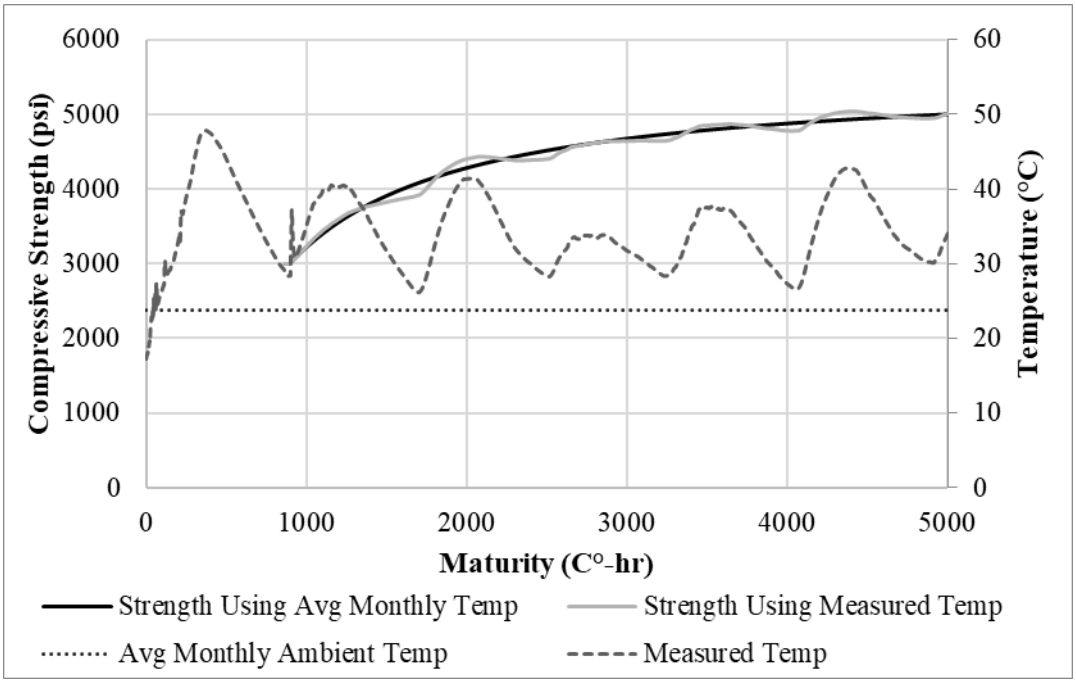

Figure 48: Predicted maturity – strength relationship at the strength of 3000 psi

5.1.1 Benefits of the Procedure

As previously established, shear wave velocity correlated better to strength than maturity. Other studies have observed inconsistencies in the accuracy of strength estimation using maturity with over-estimations [29], under-estimations [34], or both depending on concrete mixture and maturity – strength relationship used [36,84]. In this study, strength estimated using maturity has an average difference from compressive and flexural strength of 8.5% and 7.4%, respectively. Strength estimated using shear wave velocity has an average difference from compressive and flexural strength of 5.7% and 1.9%, respectively. This may seem like a minimal increase in accuracy but when considering early age concrete, accuracy is extremely important. Early age concrete is changing very quickly, gaining substantial strength and stiffness in a relatively short amount of time. It is important to accurately know the concrete strength to properly schedule

construction procedures. Incorrect strengths can accelerate or delay procedures that can reduce the integrity of the pavement when mistimed.

Another advantage is the removal or reduction of permanent equipment installation while increasing the monitored area. Minimal temperature sensors could be used to adjust the discrepancy between the laboratory and field shear wave velocity. No permanent installation is required when predicting pavement temperature using ambient conditions from a temperature model such as EICM. Temperature models are required to determine future strength development.

There is an important distinction between ultrasonic testing and maturity. Ultrasonic testing uses a shear wave velocity measurement at a certain time to determine a single strength. Maturity has a major benefit because it uses temperature models to accurately predict the change in maturity and therefore provide predictive strength estimations. The relationships established in this study allow strengths estimated from ultrasonic testing to adjust the predicted strength development.

Step 8 can be used multiple times to continuously adjust the predicted strength gain rate. Simply shift the strength gain rate as predicted by estimated maturity higher or lower to follow the more accurate strength estimated by shear wave velocity. This allows the user to visualize all aspects of in-situ strength development as it evolves in the pavement based on the shear wave velocity of the pavement.

Figure 49 shows how the strength gain rate was adjusted for this data on days 3 and 5. At this time, the data experienced a reduction in strength gain rate that maturity was unable to identify. The original line shows the strength gain rate from the initial pour according to the maturity – strength relationship. It aligns well with the Day 1 field strength estimated by shear wave velocity. However, on Day 3 when the field strength was again determined, it was found that the prediction was overestimated. The strength gain rate can be adjusted down to the field strength estimated by

shear wave velocity to provide the strength gained from that point. On Day 5, it was found that the prediction underestimated the strength in the field. The strength gain rate can then be adjusted up where it continued to represent the actual field strength well.

When considering a specific strength, the final outcomes from this procedure include the shear wave velocity to watch for in the field and the predicted strength development moving forward in construction. This collaboration of nondestructive tests increases the available concrete strength information for immediate field use and for future construction scheduling.

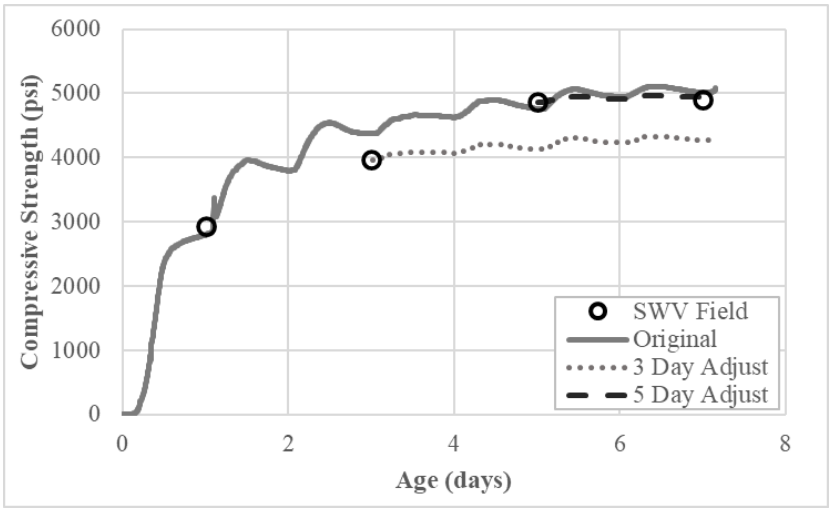

Figure 49: Adjusting the strength gain rate in accordance with field shear wave velocity (SWV)

5.2 Linear Array Ultrasonic Devices on Beam Specimens

Ultrasonic testing is a growing method of estimating concrete strength in the field but there is a reoccuring issue with modern devices and strength correlation. Traditional devices have difficulty with heterogenous materials, such as concrete, because they contain different material properties in the same scan that can affect wave propagation differently and increase variability [19]. Linear array devices contain multiple transducers to reduce variability and increase

repeatability over the traditional single transducer and receiver arrangement [44,58,59]. The linear array ultrasonic device used in this study is an A1040 MIRA from Acoustic Control Systems which contains 48 dry point contact transducers in 12 channels. Each transducer can transmit and receive waves which increases the data points for measuring wave propagation. Shear waves are emitted and received by 66 horizontally spaced transducer pairs allowing for multiple incident angles and consistent analysis of heterogeneous materials.

There is a significant limitation of linear array devices: the manufacturer procedure for calculating wave velocity was designed for large areas and discrepancies occur when used on small specimens. For accurate strength estimation, ultrasonic testing requires laboratory strength correlation on beam specimens. With linear array devices increasing the accuracy of velocity measurements, similar concrete should result in nearly the same wave velocities but those measured on beam specimens are higher than velocities measured on a concrete slab. This section will explore deeper into what specifically in the raw data is different for smaller specimens and why this might be occuring.

5.2.1 Effect of Vertical Edge Proximity

Different laboratory and field conditions may affect measurements and the overall comparison. However, dimension is a markable difference between concrete slabs and beam specimens that needs to be considered. A specimen was made with differing dimensions to directly consider the effect of specimen size because the conditions and concrete mixture between different sides of the same specimen would be as close as possible.

The specimen concrete mixture was designed to meet standards provided by Pennsylvania Department of Transportation (PennDOT) for a conventional concrete mixture design. A summary

of the mixture design is provided in Table 15. The mixture included Type I/II Portland cement. The coarse aggregate was comprised of American Association of State Highway Transportation Officials (AASHTO) #57 limestone and fine aggregate was concrete sand. The ultrasonic device, MIRA, was used to measure wave velocity.

Table 15: Mixture design details (for 1 ft^3 concrete)

Cement, lb	25.9
Coarse Aggregate, lb	62.0
Fine Aggregates, lb	43.2
Total Water, lb	10.5
Admixture	Air Entrainer, Water Reducer, Superplasticizer
w/c by weight	0.4
Slump, inch	2
Air Content	6.5%

The specimen, shown in Figure 50, is a 16 x 11 x 6 inch beam and was cured with wet burlap for 28 days. Lines were marked at the halfway point so the device could easily be aligned at the center using MIRA's laser feature. On the 6 inch sides, the distance between the closest transducer and the boundary was 1.25 inches. On the 11 inch sides, the distance between the closest transducer and the boundary was 3.75 inches. The final raw data provided by MIRA is a combination of the four channels across the device so the exact distance to the edge is not represented in the signal time history, but the general proximity still has an effect.

Ultrasonic testing scans were performed on each side of the beam at ages 1, 3, 7, 14, and 28 days (Figure 51). Three scans were performed on each side at each age and the average was considered the manufacturer velocity for that side.

Figure 50: Size effect specimen

Figure 51: Velocity measurements on a 6-inch side (left) and an 11-inch side (right)

The average manufacturer shear wave velocity of the top, bottom (6 inch), left, and right (11 inch) were compared. All 11-inch scans were nearly identical. There was a slight difference at very early ages between the top and bottom simply due to how the specimen was cast. On day 1 there was a difference of 50 m/s, day 3 was 10 m/s, and on day 7 the 6-inch sides were identical.

Figure 52 shows the comparison between 6-inch and 11-inch shear wave velocity. Every data point is taken from the same specimen therefore velocities should all be nearly identical. However, there is a clear difference proving the effect of specimen size and the dependence on

edge proximity. The original velocity calculation procedure developed by the MIRA manufacturer for larger specimens is unreliable for small specimens.

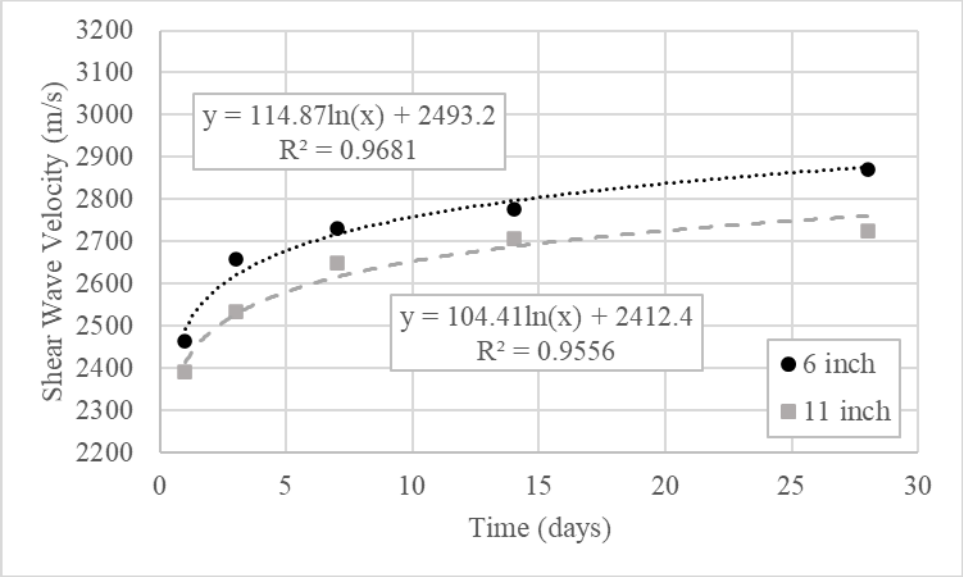

Figure 52: Difference in shear wave velocity for different edge proximities

5.2.2 Raw Linear Array Data Analysis of a Beam Specimen

A deeper comparison of raw beam and slab wave velocity data is necessary to understand the causes of the discrepancy. Data from the conventional concrete mixture explained in Chapter 4 was used in this comparison since the differences between 6-inch beams and slabs are more significant than a 6-inch and 11-inch beam.

Chapter 2.3.3 has a basic overview of how impulse time histories are used to determine the arrival times for different sensor distances and how to calculate the velocity from raw data. The arrival time is the first peak time in the impulse time history (Figure 4). Arrival times and corresponding sensor distances are plotted together (Figure 5) and the trendline slope is the wave velocity for that scan. The ultrasonic device, MIRA, has 66 horizontally spaced measurement pairs, each providing a set sensor distance and measured arrival time. The transducers are spaced 30 mm

apart allowing for sensor distances up to 330 mm. The number of measurements for each sensor distance are listed in Table 16.

Table 16: Number of measurements per sensor distance

Sensor Distance	Number of Measurements
30	11
60	10
90	9
120	8
150	7
180	6
210	5
240	4
270	3
300	2
330	1
Total	66

For slabs and beams, signal time histories from each sensor distance are shown in Figure 53. The farther sensor distances have longer arrival times and smaller intensities when compared to shorter sensor distances. Figure 53a shows the signal time histories for a slab which has clear peaks for each sensor distance. Figure 53b shows the same comparison for a beam specimen of the same age and mixture. Shorter sensor distances are clear, but peaks become less obvious for farther distances as multiple wave arrivals are recorded at higher amplitudes.

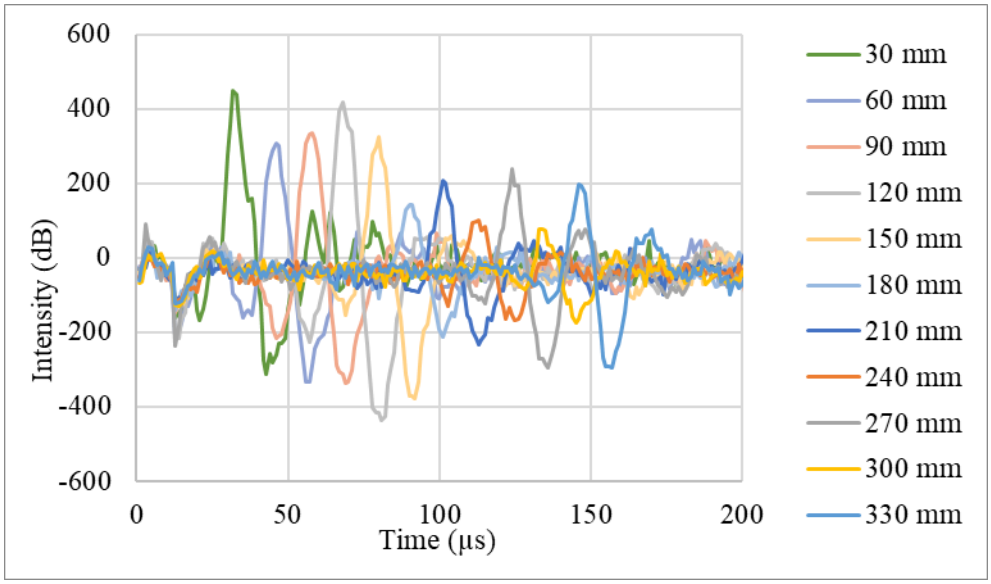

(a)

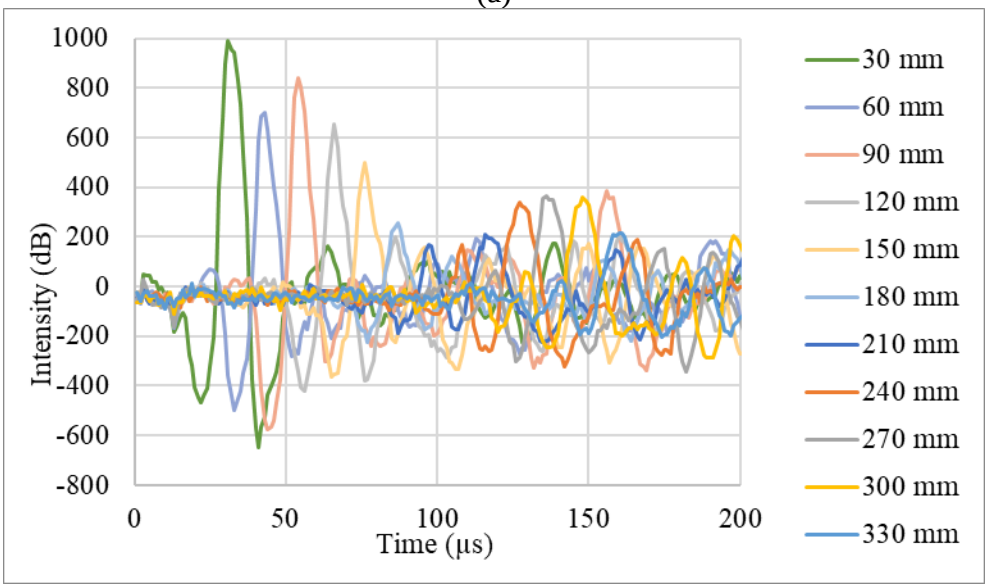

(b)

Figure 53: Signal time histories for each sensor distance for a (a) slab and (b) beam

Figure 54 focuses on three sensor distances. After the initial peak, other secondary peaks of comparable amplitude can be observed for a beam scan. At 180 mm, the direct arrival peak is still significantly different than any later peak. At 210 mm, there is a second peak of approximately the same amplitude. At 240 mm, the second peak amplitude is larger than the direct arrival. Observing farther sensor distances shows this first peak continuing to shrink and eventually, it becomes lost in the general signal noise with the secondary peaks' greater amplitude remaining.

Incorrect direct arrival times could be identified and used in velocity calculation. Sensor distances can be restricted for more accurate beam wave velocity calculation. For this example, after 240 mm the direct arrival peak could not be reliably identified so only sensor distances up to 240 mm were used. This leaves 60 out of 66 data points available to calculate wave velocity.

The maximum peak value cannot be used for calculating beam wave velocity because this does not necessarily represent the direct arrival wave like in slab measurements. When calculating velocity, only the first peak should be used despite the amplitude until it is no longer identifiable from the noise as this is most likely to be the direct arrival of the emitted wave.

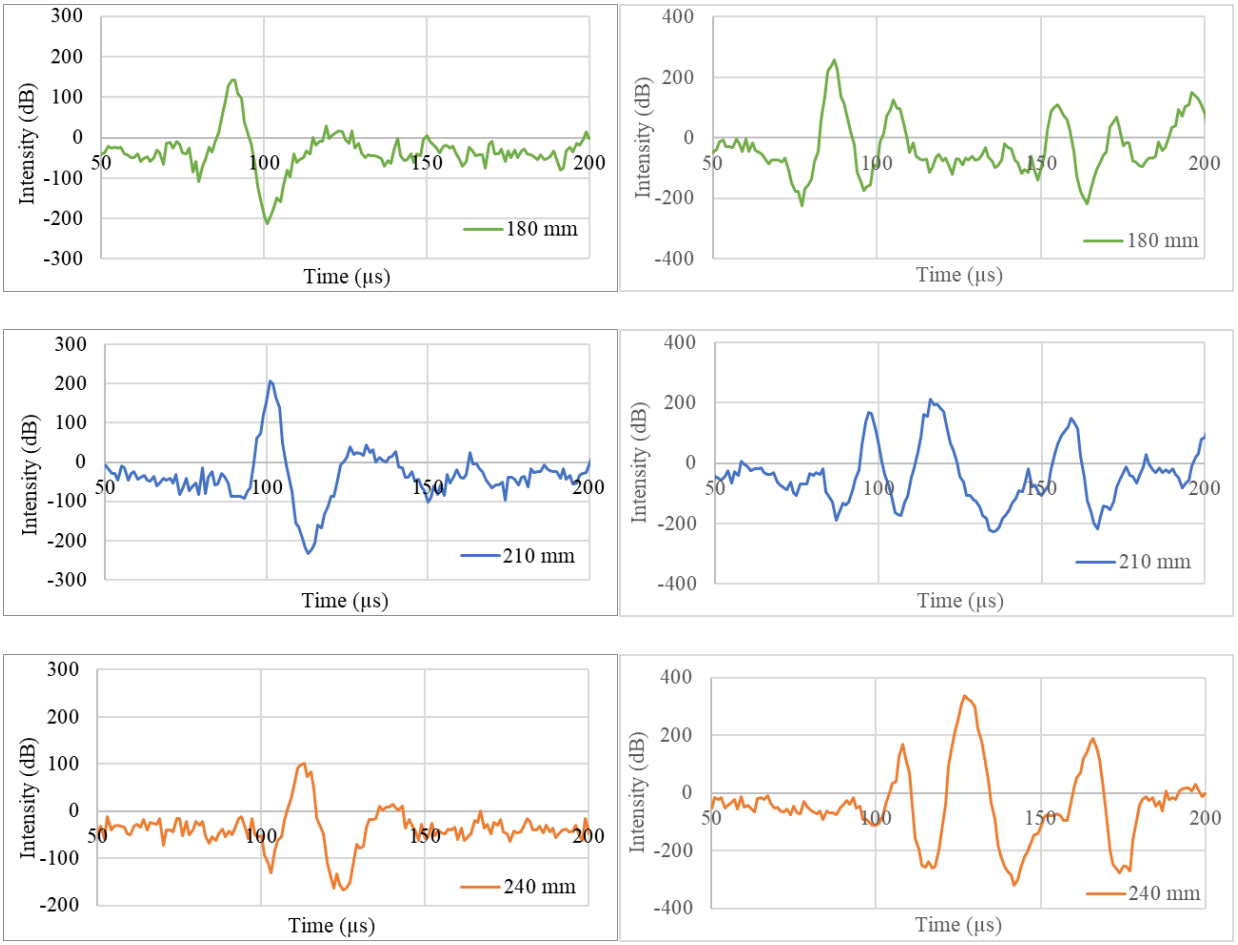

Figure 54: Peak intensities at farther sensor distances for the slab (left column) and beam (right column)

Wave velocity was recalculated for beam and slab data after removing the farthest sensors distances. Since the slab did not have the issue with competing peaks, the direct arrival peak was also the maximum amplitude. Despite this, the calculated wave velocity was lower than the manufacturer velocity. For example, 2670 m/s was measured by the device, but the calculated velocity was 2634 m/s for the same scan of a slab. This is likely due to calculated velocity restricting sensor distance to 240 mm instead of 330 mm. Using every sensor distance changes the calculated wave velocity to 2652 m/s which is closer to the manufacturer value. Restricting sensor distances reduces the calculated wave velocity.

The clarification between the direct arrival peak and maximum peak is important when calculating wave velocity of a beam, however, it does not solve the discrepancy between slab and beam data of the same age and mixture. The arrival time on a beam specimen is earlier than a slab measurement (Figure 55).

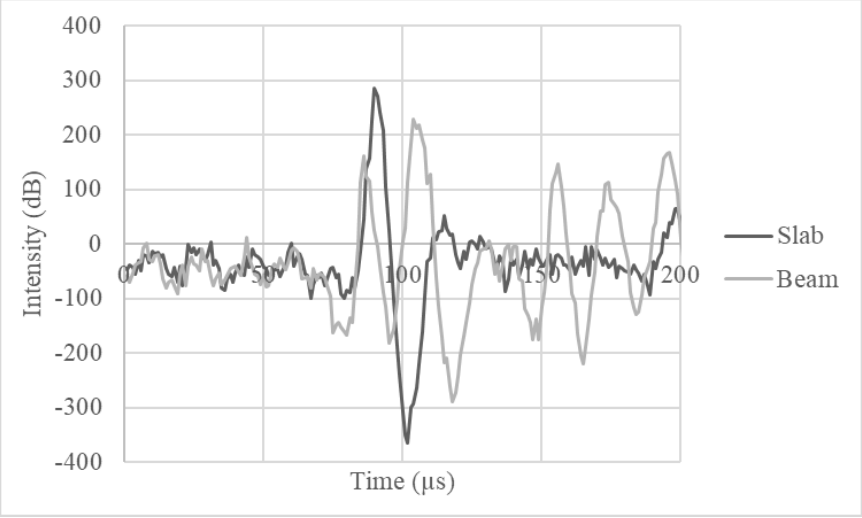

Figure 55: Comparing signal time histories between slab and beam at 180 mm sensor distance

To adjust the arrival time, the beam velocity was shifted later until it aligned with the direct arrival peaks. This small shift in time resulted in beam velocities significantly closer to the slab. Figure 56 shows the time signal analysis of the calculated beam and slab velocities and the effect

of the shift. For this example, the calculated beam, calculated slab, and shifted beam velocities are 2758, 2636, and 2570 m/s, respectively. The shifted velocity is significantly closer to the slab value.

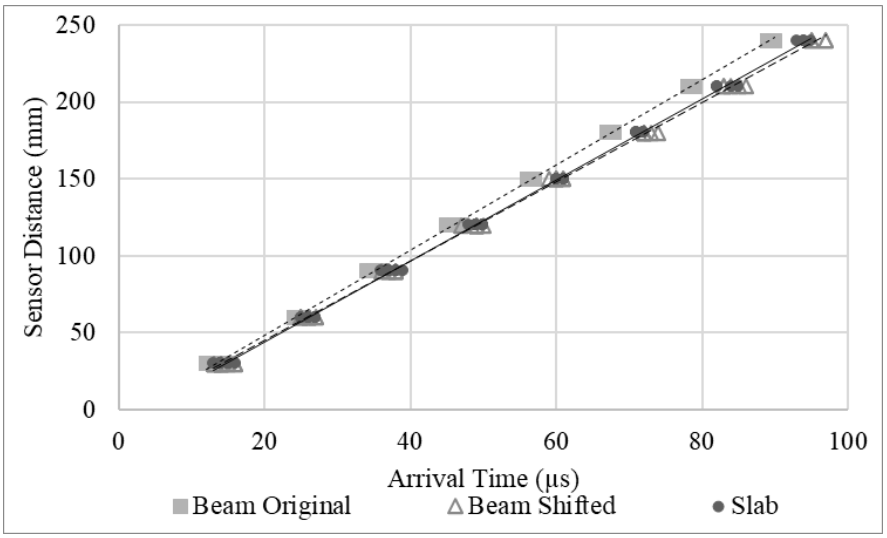

Figure 56: Comparison of beam to slab velocities before and after shift

It can be observed that the shift begins to underestimate velocity with farther sensor distances. Restricting the sensor distance to 150 mm instead of 240 mm leaves 45 out of 66 data points available to calculate wave velocity and results in nearly identical wave velocities between slab and beam. Now the wave velocities of the beam, slab, and shifted beam shown in Figure 56 are 2741, 2606, and 2600 m/s, respectively. The shift and sensor distance restriction are visualized on average beam data over time in Figure 57. This indicates the primary issues causing the difference between field and laboratory shear wave velocities are competing peaks and higher wave velocity in a beam specimen as now that this has been adjusted, field and specimen data are similar.

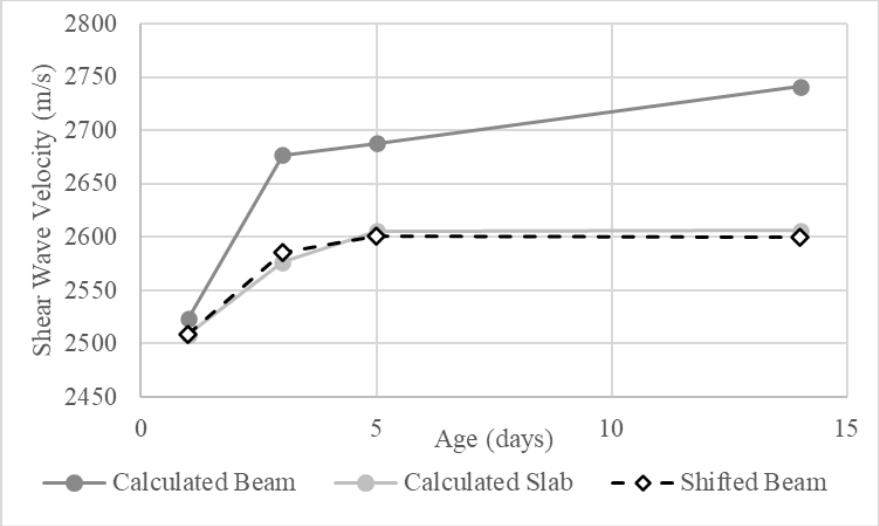

Figure 57: Effect of shifting beam arrival time for early concrete ages

The same analysis was performed on the size effect specimen. As Figure 58 shows, the shifted 6-inch shear wave velocity is close or a little under the calculated 11-inch velocity. The underprediction is due to a significant difference in amplitudes between the 6- and 11-inch sides causing a slight overestimation of the shift. Recall the manufacturer velocity will be higher than the calculated values since restricted sensor distances were used in calculation. The 11-inch data is subject to the same issues with beam specimens as the 6-inch data, so the shift is not as significant as when shifting to a slab which is infinite in comparison. However, the shift still resulted in the 6-inch side wave velocity aligning well with the 11-inch side.

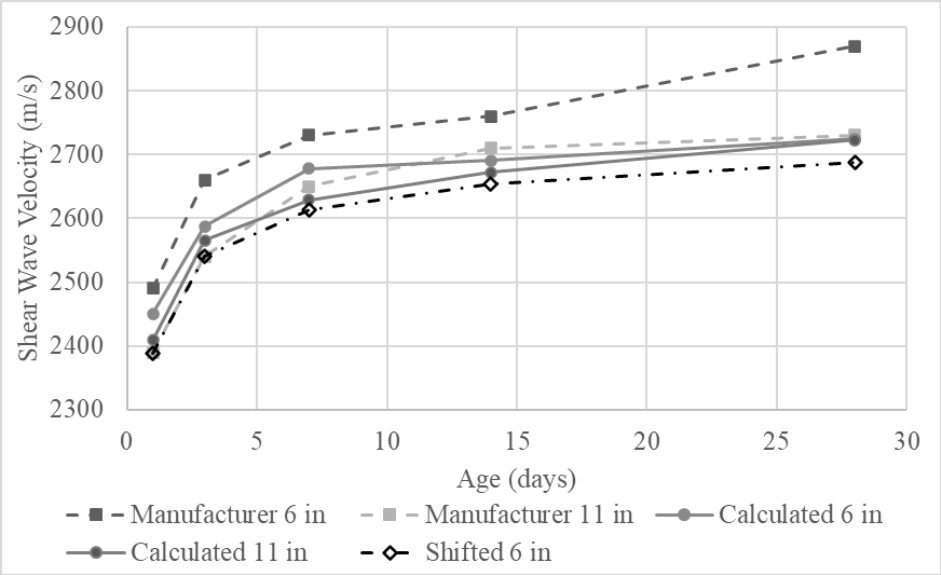

Figure 58: Effect of shifting frequencies on size effect specimen

From this experiment and analysis, the following could be observed:

- Wave arrivals in a small specimen are indistinct at farther sensor distances,
- Maximum amplitude is not necessarily direct arrival,
- Waves in a beam have a greater velocity, and
- Removing farther sensor distances reduces calculated wave velocity.

5.2.3 Device Comparison for Different Transducer Amounts

To confirm the effect is due to the use of a linear array device, a second device was used on the specimen with differing dimensions. This device is the UK1401 Surfer from Acoustic Control Systems which consists of two ultrasonic transducers (one transmitting and the other receiving) that measure the propagation of pressure waves. As previously mentioned, the relative speed between shear and pressure waves depends on the Poisson's ratio of the concrete. Assuming a Poisson's ratio of 0.2, the relationship between shear and pressure waves is the following:

$$V_s = 0.61V_p \quad (5\text{-}8)$$

where V_s is the shear wave velocity and V_p is the pressure wave velocity.

Three scans were taken on each side of the specimen concurrently with each device: linear array and 2-point. Pressure wave velocity was converted to shear wave velocity and the comparative results are shown in Figure 59.

The wave velocity on the 6 inch sides is significantly higher than the 11 inch sides when measuring with the linear array device as previously identified. On the top, left, and right sides (6, 11, and 11 inch), there is no discernable difference in wave velocity when using the 2-point device. There is a small increase in wave velocity on the bottom side (6 inch) identified by both devices. This shows the effect of vertical edge proximity on beam specimens is unique to linear array devices.

The simplest solution to this problem is to use a 2-point device or a smaller linear array device for both beam and field analysis. This would remove the discrepancy and allow for strength correlations to be made. However, this also comes with an increase in wave velocity measurement variability as exemplified in Figure 59. The procedures developed in this study could also be used to shift beam data however both methods require field data to determine the degree of shift required. An alternative solution would be to develop a procedure that adjusts wave velocity measured with linear array devices on standard 6 inch beam specimens. This would increase the complexity of the data analysis but retain the reduction in wave velocity variability that accompanies linear array devices and remove the reliance on field data required by the other linear array adjustments introduced in this study. More detailed analysis of what is happening to the propagating waves in a small beam specimen is required to develop this procedure and to understand the root cause of the discrepancy. Until this procedure can be developed, the two

methods of correcting beam wave velocity developed in this paper, maturity correction and shift factor, provide a reasonable correction when slab data is also available.

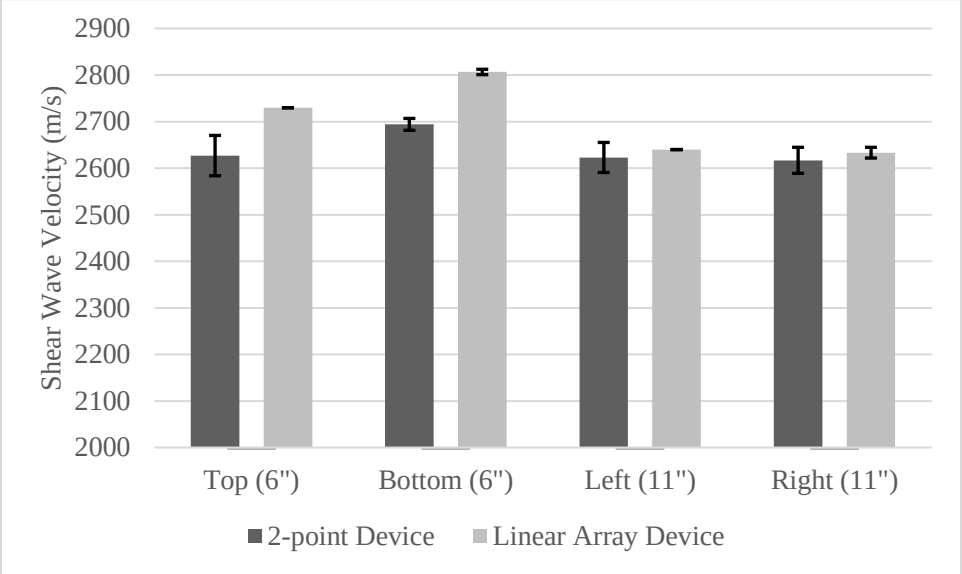

Figure 59: Wave velocity comparison between a linear array device and 2-point device

5.2.4 Factors Affecting Beam Wave Velocity Measurement

The experiment determined differing environmental conditions were not causing the discrepancy, but specimen size did have an effect. The analysis of beam time signals found two significant factors affecting beam specimens: the wave experiences reflections which reduces the accuracy of direct arrival time identification and the wave travels slightly faster causing an earlier arrival time.

Boundary conditions are the clear difference between beam and slab specimens. The close proximity of vertical edges on a standard beam specimen to the device transducers may be affecting results. In a slab, the edges are far enough away that a slab can be considered infinite in comparison to a beam. Additionally on a slab, the vertical edge boundaries are often met with more concrete or soil. On a beam specimen, the boundaries are significantly closer with only air beyond.

All mechanical waves have boundary interactions. When an incident wave is moving through a material and encounters a boundary, there are two resulting waves: a trasmission wave that continues through the second material and a reflection wave that interacts with the boundary and redirects into the first material (Figure 60). The trasmitted wave will have a different amplitude than the incident wave depending on the properties of the second material. The reflected wave will be the opposite phase, or negative amplitude, of the incident wave.

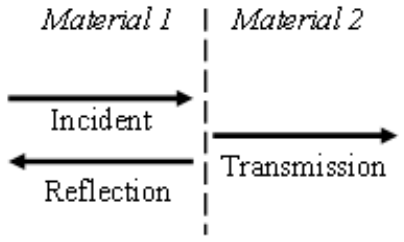

Figure 60: A mechanical wave hitting a boundary normally

Conservation of energy must be maintained therefore the energy of the incident wave will be distributed between the transmitted and reflected wave [85,86]. The distribution depends on the difference in material properties, specifically acoustic impedance or density. A greater difference causes higher reflection and lower transmission energy. The reflectivity of an mechanical wave interacting normally at a boundary is shown in Equation (5-9) [40,62,87].

$$\sigma_{reflected} = \sigma_{incident} \times \frac{Z_2 - Z_1}{Z_2 + Z_1} \quad \textbf{(5-9)}$$

where $\sigma_{reflected}$ is the stress associated with the reflected mechanical wave; $\sigma_{incident}$ is the stress associated with the incident mechanical wave; $Z_{1,2}$ is the acoustic impedance of materials 1 and 2.

If acoustic impendence of the second material is lower than the first ($Z_2 < Z_1$), the reflected stress will be much larger than what is transmitted. In the case of beam specimens, the interface is between concrete and air. There is a large difference in acoustic impedance between these

materials with concrete and air having values of 7 to $10x10^6$ and 0.4 kg/m^2s, respectively [40,62,87]. The device used in this study, MIRA, uses shear waves to determine velocity but shear waves are unable to travel through air and therefore even more energy is converted to reflection. In a slab specimen, the second material is often another solid like soil, which can have a closer acoustic impedance to the original concrete at 0.3 to $4x10^6$ kg/m^2s [62]. This would cause less of a reflection because more energy goes into transmission.

The reflected wave amplitude also depends on the angle of incidence with the maximum at 90°. As the angle changes, the amplitude decreases but there is also a point, depending on the Poisson's ratio of the material, where both shear and pressure waves will propogate from a single incident wave (Figure 61) [85]. This occurance is called mode conversion. In regards to the device used in this project, MIRA, the incident shear waves interact with a boundary above a certain angle and create both a shear and pressure wave reflections. Fundamentally, pressure waves are faster and contain more energy than shear waves.

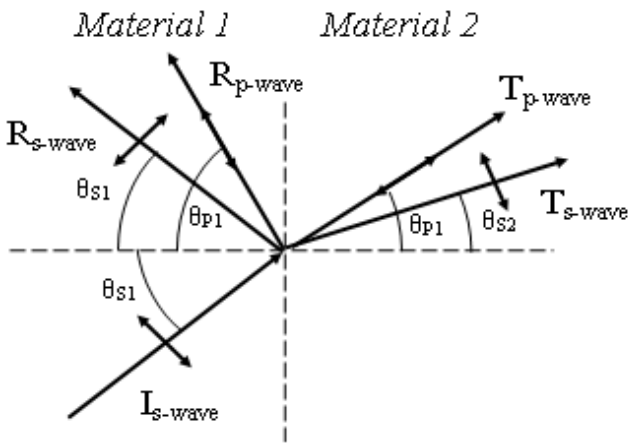

Figure 61: Wave boundary interactions at an angle between two solids with mode conversion

Scanning a beam specimen could result in numerous waves since a single scan emits multiple incident waves, depending on the number of transducers in the device, with each having

potential to reflect at least one wave, depending on the angle. This large number of waves reflecting in the specimen can cause wave interactions including superimposition, increasing the amplitude.

In the beam specimens explored in this study, an increase in secondary wave amplitudes and faster signal arrival was observed, which the mechanics of wave reflections from boundary interactions could explain. Superimposed waves could be increasing secondary peak amplitudes causing direct wave arrival misidentification. Mode conversion could also be occuring so that the first peak may not be the direct shear wave arrival, but the significantly faster reflection of a converted pressure wave.

A consistent observation in beam specimens is how issues seem to magnify at farther sensor distances. It has already been noted that amplitudes of secondary waves begin interfering with direct arrival at a certain sensor distance but there is also a descrease in first wave arrival time at farther distances. Figure 62 compares the difference in arrival time time shift between first beam scan peak to the first slab scan peak of the same age and mixture. There is a clear trend indicating that at farther sensor distances, discrepencies between wave velocity in a beam and wave velocity in a slab are higher. These issues may be due to farther sensor distances receiving noise from multiple reflections or receiving a faster pressure wave from mode conversion.

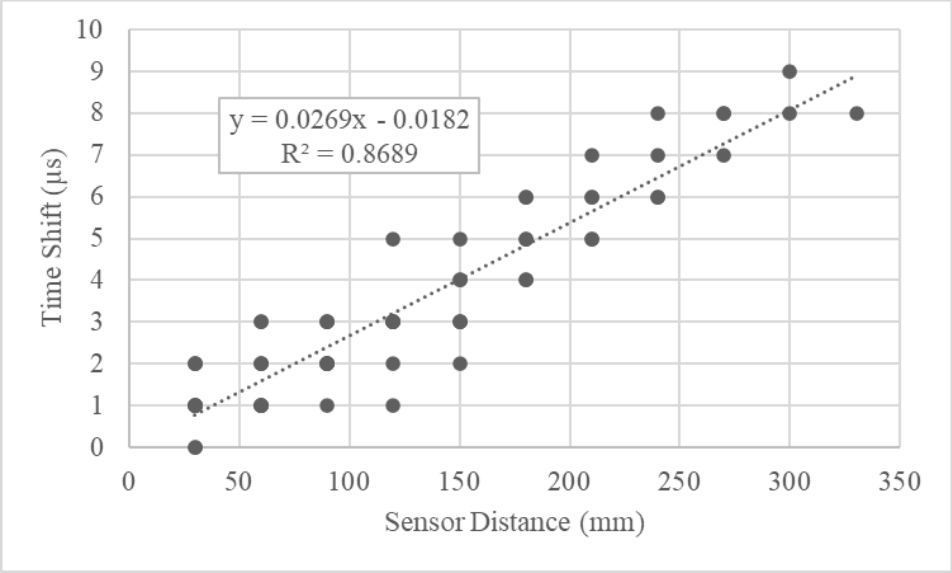

Figure 62: Time shift dependence on sensor distance

It is evident there is some degree of boundary and wave interaction occurring in beam specimens that affect the measurement of direct arrival time. Further study is necessary to test these hypotheses and determine any trends relating vertical edge proximity to direct arrival time and sensor distance. If trends are consistent for different beam specimen sizes, a generalized procedure could be developed to accurately determine the wave velocity of a beam specimen without the need for slab comparisons.

5.3 Summary

The aim of this chapter was to enhance the accuracy and efficiency of determining concrete strength in the field by combining nondestructive tests. Both maturity and ultrasonic testing offer unique advantages in the field that can overcome limitations when performed individually. A procedure was developed to integrate the predictive maturity-strength relationship with the versatility and accuracy of ultrasonic testing. Given that early age concrete is a rapidly changing

and nonuniform material, the added speed and accuracy of ultrasonic testing provide significant benefits for construction applications.

Early age strength is a critical concrete property for pavement engineers who rely on accurate strength information to schedule time sensitive construction procedures. Any additional data gathered quickly and reliably allows them to make more informed decisions on construction scheduling. Combining nondestructive testing is recommended to improve available strength data. The process outlined combines two popular techniques, each with unique advantages. After applying the procedure, the nondestructive tests can be utilized together to determine strength estimations and development for more comprehensive results in the field. This combination also allows the predicted strength development to be modified in the field to best represent the in-situ strength as measured by ultrasonic testing.

The benefits of this procedure are most evident during construction because of the flexibility in testing. Ultrasonic testing can be used quickly and often at any point of concern on the pavement to determine strength and strength variability throughout construction. Temperature modeling can then be used to determine future strength development to estimate when construction procedures like opening to traffic or joint cutting can be performed. It is recommended to perform this procedure on rehabilitation projects or projects that require fast construction because it encourages efficient construction that reduces time without increasing costs or changing common practices.

In this dissertation and numerous other projects, a discrepancy between beam- and slab-measured shear wave velocities has been identified. To identify the root cause, a small laboratory experiment was conducted. A specimen with varying side dimensions was created to directly confirm that the discrepancy is based on boundary conditions. The results showed a clear

difference in measured shear wave velocities, with the smaller dimension consistently exhibiting higher measured velocities, similar to what was observed between beam specimens and slabs. Comparison of raw impulse time histories revealed challenges in identifying direct arrival times due to competing secondary waves and eventual disappearance of the direct arrival wave into general noise. It was also observed that signal arrival in a beam specimen occurs earlier than in a slab specimen of the same mixture and age. Further observations indicated that the direct arrival may not necessarily correspond to the maximum amplitude, and removal of far sensor distances can reduce the shear wave velocity. Potential wave mechanics were explored to explain the changes in amplitudes and arrival times, and boundary and wave interactions were considered as possible causes. However, additional experiments and analysis would be necessary to test these hypotheses and establish generalized relationships.

Ultrasonic testing plays a crucial role in understanding heterogeneous materials, but the identified discrepancy between wave velocities measured in large slabs and small beam specimens poses challenges in establishing accurate strength correlations. This study has confirmed that the discrepancy is due to the proximity of vertical edges, but further experiments and analysis are needed to develop generalized relationships and confirm the proposed hypotheses on the root causes of this issue. Currently, the best recommendation for establishing strength correlations is to use a smaller linear array or 2-point device. Future research could focus on developing methods to adjust linear array wave velocities of a specimen without the need for accompanying slab data, or exploring the use of ultrasonic devices with fewer transducers. These advancements would enable the more reliable linear array devices to be used for accurate strength correlations of heterogeneous materials.

6.0 Mechanistic-Based Early Opening Damage Analysis

The purpose of this chapter is to create a new method of evaluating stress in a pavement using the knowledge gained in field experiments. The finite element model from Chapter 3 showed the importance of including axle weights, wheel path, temperature gradients, and concrete strength at the time of loading in an early age concrete model. Chapters 4 and 5 focused on improving methods of strength estimation at the time of loading. Improving efficiency of traffic opening is still restricted by the current criteria. A flexible criteria based on stress occurring in the individual pavements must be used to maximize the efficiency of traffic opening without risking pavement performance. This chapter shows the development of a method to evaluate critical stresses. The newly established stresses and strengths are then combined to determine the effect of early loading on pavement reliability.

As previously established, the same level of traffic can have varying effects on pavement performance depending on environmental, loading, and structure conditions. Restricting early loading to lightweight vehicles or only loading under a small or negative temperature gradient can control the critical conditions and reduce the risk of damage. However, changeable traffic levels and environmental effects are difficult to model. To address this challenge, a probabilistic approach was applied to evaluate critical stresses for each vehicle pass applied before design strength and assess the risk of early opening.

This model includes the effects of strength gain rate, traffic, climate, and pavement structure which have been shown to be critical in early age pavement performance. The user provides the initial strength of the pavement when it is expected to be opened to traffic, the number of expected vehicles until concrete strength reaches the design value, and the axle spectrum

frequency. The model considers each vehicle individually, predicting critical stresses caused by a single loading and comparing it to the corresponding strength based on concrete mixture strength development. To compute stresses, the procedure selects the following parameters for each simulated vehicle pass:

- Axle weights and types randomly selected from the provided axle spectrum frequency.
- Axle wheel path assuming the normal distribution with the given wheel path and standard deviation.
- Effective temperature gradient selected based on effective temperature difference frequency for the location and construction month.

Using the strength development found in laboratory work, a strength is calculated based on a random time between when the pavement is opened and when the design strength is met. If the calculated critical stress is greater than the corresponding strength at the same age, then the vehicle load may cause damage and is considered a failure. Each vehicle simulation failure is totaled and divided by the number of vehicles loaded before the design strength. This provides the probability of failure for a single traffic opening simulation. This analysis is repeated multiple times, the average probability of failure from all simulations is computed, and the pavement reliability to carry the early loading is determined.

Two types of common but serious damage were included in this analysis: transverse cracking and dowel damage. Both have similar procedures to determine critical stress levels and performance reliability. Cracking and dowel bar performance reliability will be combined to assess the optimal opening strength for the pavement. The resulting reliability allows the user to make an educated decision on when to open to traffic fully understanding the risk of damage. The

mechanistic-based early opening damage analysis is detailed below. The datasets collected in the previous chapters were used to calibrate and validate this procedure.

6.1 Concrete Property Estimation

Accurate concrete property estimations at any time between opening strength and design strength are needed for the following damage analyses:

- Flexural strength for transverse cracking damage analysis,
- Compressive strength for dowel damage analysis,
- Modulus of elasticity for both damage analyses,
- Spatial variability of concrete strength for both damage analyses.

6.1.1 Concrete Strength Prediction

The concrete strength must be obtainable at any time between when the pavement is opened and when the design strength is met. The maturity – strength relationship allows this prediction based on opening strength. Generally, prediction of concrete maturity is quite complicated and demands extensive details on ambient conditions. However, an analysis of maturity data collected at MnROAD showed that after concrete solidifies, the maturity development can be estimated from maturity based on the mean monthly concrete temperature. In this study, the following simplified procedure was proposed:

$$TTF(t) = TTF_0 + T_{PCC,m}(t - t_0) \quad \textbf{(6-1)}$$

where TTF_0 is the concrete maturity at the time of opening to traffic, $T_{PCC,m}$ is the estimated mean monthly concrete slab mid-depth temperature, and $t - t_0$ is the time from opening to traffic, hours.

The mean monthly concrete slab mid-depth temperature was collected in databases for national and regional use described in the next section.

The user is expected to provide the maturity – strength relationship coefficients. There are many potential relationships between strength and maturity. Equations (6-2) and (6-3) are examples utilized in this study. Figure 63 shows a comparison of the two maturity models using conventional mixture strength and temperature data outlined in Chapter 4. The second maturity model (Equation (6-3)) is more representative of the measured strengths. However, both models have accurate representations and are applicable in this damage analysis procedure.

$$M_r = a_m \ln TTF - b_m \quad \textbf{(6-2)}$$

$$M_r = M_{ru} e^{-\left(\frac{a_m}{TTF}\right)^{bm}} \quad \textbf{(6-3)}$$

where M_r is the flexural strength (modulus of rupture), psi; M_{ru} is the ultimate expected flexural strength, psi; TTF is the maturity index; and a_m and b_m are calibration coefficients.

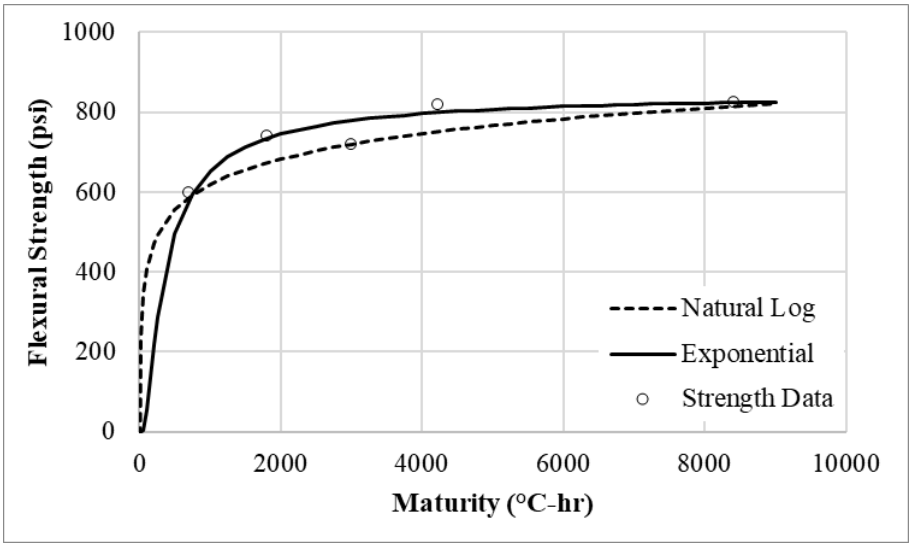

Figure 63: Comparison of two common maturity models

6.1.2 Concrete Modulus of Elasticity Estimation

The concrete modulus of elasticity can be estimated using the ACI equation:

$$E_c = 57{,}000\sqrt{f_c'} \quad \textbf{(6-4)}$$

6.1.3 Concrete Properties Variability Predictions

The spatial variability at an early age is much higher for newly poured concrete than for mature concrete. Since this damage analysis is specifically considering early age concrete, the spatial variability of concrete strength must be considered. A young concrete will have a high variability, typically about 25%, but as concrete matures, the variability reduces to around 6% [23]. The following model was adapted to evaluate the strength coefficient of variation, COV_R:

$$COV_R = C\ Exp(-D\ \times TTF) + E \quad \textbf{(6-5)}$$

where *C, D, E* are calibration coefficients with default values of 0.25, 0.001, and 0.075, respectively.

To account for the strength spatial variability, the following expression for the damage analysis strength is adopted:

$$R_C = R_M(1 - c\ COV_R) \quad \textbf{(6-6)}$$

where R_M is the maturity-estimated strength (flexural or compressive), R_c is the damage analysis strength (flexural or compressive), and *c* is a coefficient with a default of 1.

6.2 Traffic Characterization

Traffic characteristics, such as axle weight and wheel path, are critical when determining the appropriate loading strength required of a concrete pavement. The expected traffic conditions for each pavement must be considered separately to encompass all possible loadings. This reduces the risk the pavement will be overloaded while maintaining an efficient use of construction time.

To characterize traffic, the user defines the daily truck traffic per lane and the type of roadway. Mean wheel path and traffic wander are assumed to be 18 and 10 inches, respectively. Traffic spectrum characterization was adapted from Pavement Designer, a program developed by the American Concrete Pavements Association. This program is similar to the generally accepted and used method from the Mechanistic Empirical Pavement Design Guide (MEPDG) but is simplified to be less computationally expensive. This will populate the axle spectrum with single, tandem, and tridem axle loads as well as the axles per 1000 trucks for each axle type. If the number of axles is less than 1000, then that axle type is ignored in this analysis.

6.3 Transverse Cracking Performance

Transverse cracking is a major concrete pavement distress that can lead to serviceability loss and structural failure. This distress is a result of excessive mid-slab edge stress from axle loading and temperature curling/warping. If the combined total stress is greater than concrete flexural strength, transverse cracking will initiate.

Only bottom-up fatigue damage is considered in this study. To compute axle load stress independently from temperature curling stress, it is assumed that an early age pavement does not significantly separate from the subgrade. This also means that the dynamic coefficient of subgrade reaction can be used for the moving axle load stress calculation and the static coefficient of subgrade reaction can be used for the curling analysis. The static coefficient of subgrade reaction was assumed to be half the dynamic coefficient of subgrade reaction.

When a restrained slab shrinks or a slab contains temperature or moisture gradients that cause curling or warping, stresses will form in the slab. The relaxation of this stress creates a strain called tensile creep. Creep mainly occurs in very early age concrete at a high creep rate that will decrease and stabilize with age [88–91]. The inclusion of creep is important in predicting early age cracking due to its impact on shrinkage and thermal stresses [91]. Creep depends on age and rate of loading, aggregate content, water to cement ratio, and shrinkage or thermal stress [88,90,92,93] and can significantly reduce environmental stresses in a slab [94,95]. This reduction certainly impacts cracking prediction at an early age; however, creep is difficult to control, measure, and model [88]. To reduce the transverse cracking model complexity, tensile creep was neglected so that the environmental stresses were considered at their fullest potential.

The total stress considered for transverse cracking is the combination of longitudinal stresses caused by axle loads and temperature curling stresses. The longitudinal stresses at the

bottom of the slab were computed using an adapted neural network developed under the NCHRP 1-37A project [96]. The temperature curling stresses and thermal load characterization is further explained below [97].

6.3.1 Thermal Load Characterization

Thermal stresses are primarily affected by temperature gradients present in the pavement at the time of loading. A temperature gradient can cause curling or warping in a slab, where the slab edges or center may attempt to lift off the ground causing critical stress points. Temperature gradients are comprised of three strain types: constant, linear, and nonlinear (Figure 64).

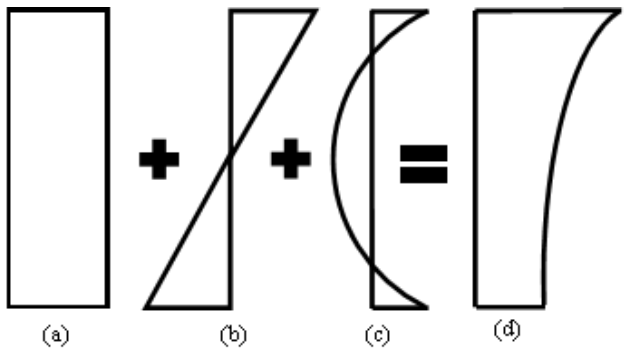

Figure 64: Temperature profile in a slab is the combination of (a) constant, (b) linear, and (c) nonlinear gradients to determine the final profile (d)

The effect of temperature gradients can be characterized through effective temperature gradient distributions [98]. Predicting temperature distributions is typically a complex procedure that requires sophisticated modeling. This project will adopt a simplified procedure previously developed [99–102]. The basic concept is if two slabs have the same plane-view geometry, flexural stiffness, self-weight, boundary conditions, and applied pressure, and rest on the same foundation, then they have the same deflections and bending moment distribution if the throughout-the-thickness temperature distributions satisfy the condition shown in Equation (6-7). This study will

adapt a procedure, shown in Figure 65, for thermal stresses in an unbonded concrete overlay developed elsewhere [103,104].

$$\int_{h_a} E_a(z)\alpha_a(z)\big(T_a(z) - T_{0,a}\big)zdz = \int_{h_b} E_b(z)\alpha_b(z)\big(T_b(z) - T_{0,b}\big)zdz \qquad \textbf{(6-7)}$$

where *a*, *b* are the subscripts denoting two slabs; *z* is the distance from the neutral axis; $T_{0,}$ is the temperatures at which theses slabs are assumed to be flat; α is the coefficient of thermal expansion; *E* is the modulus of elasticity; *h* is the slab thickness.

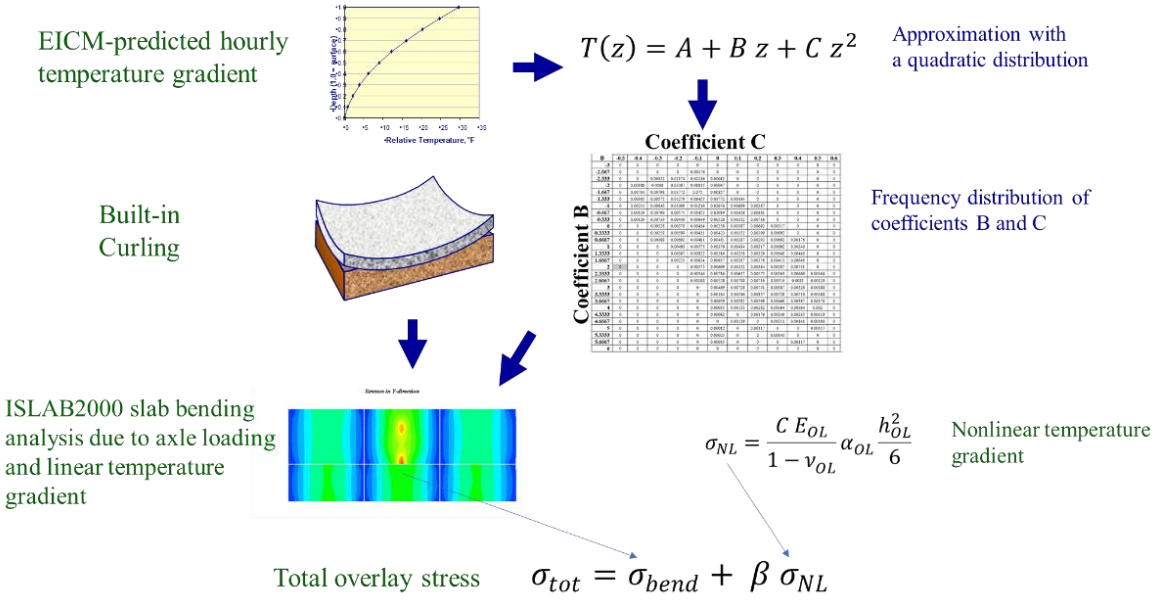

Figure 65: Accounting for temperature load in the proposed procedure

This procedure begins by using the Enhanced Integrated Climatic Model (EICM) module of AASHTO M-E Design software to generate thermal profiles through the concrete slab thickness for every hour of pavement life [103,104]. Then, each hourly temperature profile is approximated by a quadratic temperature distribution:

$$T(z) = A + B\,z + C\,z^2 \qquad \textbf{(6-8)}$$

where *z* is the distance from mid-depth (inches).

The gradients can be used to compute the temperature difference between the top and bottom overlay surfaces that are used to compute overlay bending stresses. The procedure for calculating the overlay critical bending stress due to combined action of linear temperature gradients and axle load is discussed in more detail in the literature [105]. The quadratic term, *C*, is used to compute self-equilibrating top and bottom overlay surface stresses, σ_{NL}, using the following equation:

$$\sigma_{NL} = \frac{C\ E_{OL}}{1 - v_{OL}} \alpha_{OL} \frac{h_{OL}^2}{6} \quad \textbf{(6-9)}$$

where α_{OL} is the overlay coefficient of thermal expansion; h_{OL} is the overlay thickness; E_{OL} is the overlay modulus of elasticity; v_{OL} is the overlay Poisson's ratio.

The total stress for the combination of nonlinear temperature distribution and axle load is calculated as follows:

$$\sigma_{tot} = \sigma_{bend} + \sigma_{NL} \quad \textbf{(6-10)}$$

where σ_{bend} is the bending stress due to linear component of the temperature distribution and axle load.

To account for the effect of climate, the procedure requires the mean monthly concrete temperatures at mid-depth and frequency of linear temperature gradients, which depend on pavement location, construction month, and concrete strength. To simplify this step, databases were made to predict mean monthly concrete temperatures, assuming standard concrete thermal properties as described in the MEPDG, and concrete slab thicknesses, ranging 6 to 12 inches [83]. Two databases were made: one for national use which includes forty major cities across the United States (Figure 66) and a second for regional use which includes five locations in Pennsylvania. The state was divided into regions with similar climates centralized around Pennsylvania Department of Transportation (PennDOT) districts (Figure 67). The only exception is Erie County

whose severe climate due to the Great Lakes requires its own region. The EICM, incorporated into the AASHTOWare Pavement ME Design software, was then used to predict a generalized mean monthly concrete temperature for each location.

In the databases, after the hourly temperature profile is approximated using Equation (6-8), the frequency distribution of linear and quadratic coefficients is created. In this study, the increment of the linear term B was selected to ensure 2 °F for the linear temperature difference between the top and bottom concrete surfaces. The frequency distribution for the quadratic term, C, is in increments of 0.1 °F/in^2. Table 17 presents an example of the frequency distribution for a 9-in thick concrete pavement located in Pittsburgh, PA. For this example, the probability of the temperature profile with the coefficients B and C equal to 2 and 0.3, respectively, is equal to 0.00898. This simulation would be applied with the corresponding equivalent temperature difference and non-linear temperature stress.

Figure 66: Forty locations used in the national climate database

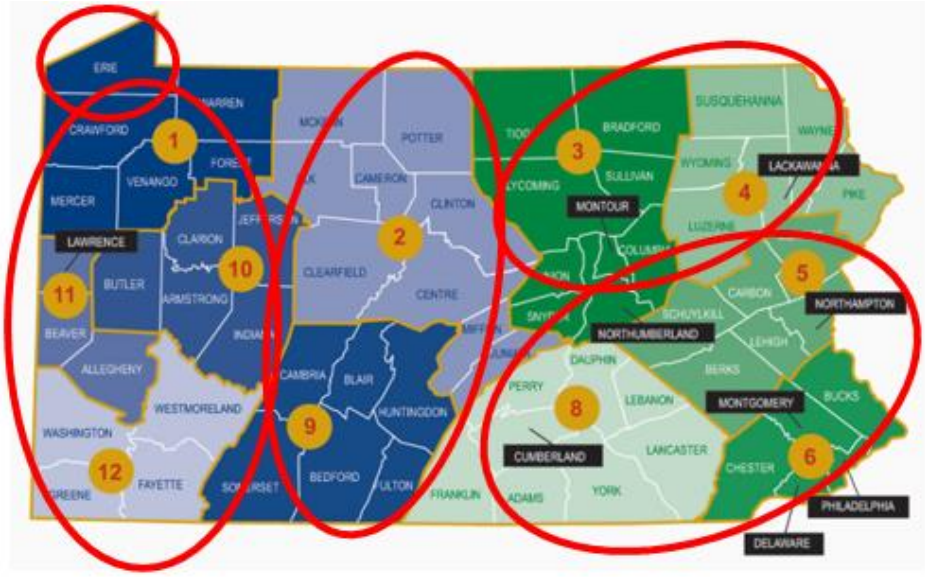

Figure 67: The grouping of PennDOT regional offices with similar climate conditions [106]

Table 17: Frequency distribution probability of a given combination of B and C

	Coefficient C										
Coefficient B	-0.400	-0.3	-0.2	-0.1	0	0.1	0.2	0.3	0.4	0.5	0.6
	-2.667	0	0	0	0	0	0	0	0	0	0
	-2.444	0	0	0.00037	0.00018	0	0	0	0	0	0
	-2.222	0	0	0.00079	0.00061	0	0	0	0	0	0
	-2.000	0	0.00006	0.00202	0.00318	0	0	0	0	0	0
	-1.778	0	0.00006	0.0033	0.00733	0	0	0	0	0	0
	-1.556	0	0.00012	0.00593	0.0245	0.00055	0	0	0	0	0
	-1.333	0	0.00024	0.01002	0.04484	0.00116	0.00018	0	0	0	0
	-1.111	0	0.00037	0.01332	0.05682	0.0044	0.00049	0	0	0	0
	-0.889	0	0.00055	0.01375	0.06397	0.01167	0.0025	0	0	0	0
	-0.667	0	0.00067	0.0102	0.05444	0.01918	0.00403	0	0	0	0
	-0.444	0	0.00043	0.008	0.04099	0.0176	0.00556	0.00006	0	0	0
	-0.222	0	0.00055	0.00672	0.02285	0.00965	0.00764	0.00098	0	0	0
	0.000	0	0.00055	0.00544	0.01558	0.00379	0.01191	0.00336	0	0	0
	0.222	0	0.00018	0.00348	0.01246	0.00464	0.01375	0.00446	0	0	0
	0.444	0	0	0.00098	0.01191	0.00916	0.01234	0.00611	0	0	0
	0.667	0	0	0.00092	0.00965	0.01185	0.01381	0.00495	0.00018	0	0
	0.889	0	0	0.00043	0.00703	0.01533	0.01527	0.00849	0.00098	0	0
	1.111	0	0	0.00049	0.00385	0.01656	0.01735	0.01033	0.00275	0	0
	1.333	0	0	0	0.00299	0.01411	0.02004	0.01057	0.00379	0	0
	1.556	0	0	0	0.00147	0.00935	0.01851	0.01136	0.00287	0	0
	1.778	0	0	0	0.00073	0.00672	0.01741	0.01087	0.00373	0	0
	2.000	0	0	0	0.00024	0.00477	0.01112	0.00898	0.0047	0.00006	0
	2.2222	0	0	0	0.00006	0.00196	0.00806	0.00861	0.00513	0.00031	0
	2.4444	0	0	0	0	0.00177	0.00629	0.00672	0.0044	0.00018	0
	2.6667	0	0	0	0	0.00043	0.00452	0.00599	0.00434	0.00055	0
	2.8889	0	0	0	0	0.00018	0.00293	0.00544	0.00385	0.00043	0
	3.1111	0	0	0	0	0	0.00104	0.00409	0.00354	0.00055	0
	3.3333	0	0	0	0	0	0.00037	0.0025	0.00299	0.00031	0
	3.5556	0	0	0	0	0	0.00018	0.00086	0.0011	0.00031	0
	3.7778	0	0	0	0	0	0	0.00037	0.00086	0.00037	0
	4	0	0	0	0	0	0	0.00006	0.00073	0	0
	4.2222	0	0	0	0	0	0	0	0.00006	0	0
	4.4444	0	0	0	0	0	0	0	0	0	0

6.3.2 Transverse Cracking Reliability

At this point, methods of calculating flexural strength, modulus of elasticity, axle stress, and thermal stress at early ages have been established. The probabilistic approach can now begin by analyzing a randomly selected time for each vehicle pass to determine the concrete modulus of elasticity and flexural strength using the following procedures:

a) Estimate concrete maturity using Equations (6-2) and (6-3);

b) Determine concrete flexural and compressive strength using corresponding strength-maturity relationships;

c) Adjust strengths to account for spatial variability using Equation (6-6); and

d) Determine the concrete modulus of elasticity using Equation (6-4).

The user must define the location and construction month to determine potential thermal gradients from environmental conditions using the created climate databases. The traffic and environmental inputs are then randomly selected through axle weight, traffic wander, and temperature gradients to simulate many possibilities. Using these inputs and variable ranges, the longitudinal and thermal stresses at the bottom of the slab are computed for time of loading. If the combined stresses from that axle weight and thermal loading are greater than the flexural strength at the time of loading, the run counts as a failure.

The number of failures is totaled for each expected vehicle and is used to compute the probability of failure for each simulation. It is recommended to conduct multiple simulations (between 100-800 simulations) and average the probability of cracking failure between all simulations. The reliability that cracking will not occur is calculated using the following equation:

$$CrRel = 100\% \times \left(1 - \frac{1}{N_{simulations}} \sum_{i=1}^{N_{sim}} \frac{N_{failures,i}}{n_{vehicles}}\right) \quad \textbf{(6-11)}$$

where $CrRel$ is the cracking resistance reliability, $N_{failures}$ is the total number of failures for simulation i, $n_{vehicles}$ is the total number of vehicles in one simulation, and N_{sim} is the total number of simulations.

6.4 Dowel Bar Performance

In a jointed plain concrete pavement (JPCP), dowel bars are a key structural component for distributing traffic loads from one slab to the next. Heavy axle loads in combination with lower concrete strength can lead to excessive bearing stress acting beneath the dowels causing micro or macro cracking in the concrete. If damage occurs to dowels and the surrounding concrete, it will reduce joint performance and increase differential deflections between the slabs. This reduces dowel effectiveness and compromises long-term performance.

Dowel-concrete interaction is complex to model. MEPDG developed rapid solutions to determine deflections needed to compute bearing stress for a two-layered pavement which is implemented in this study [98]. This section outlines this procedure and how it is incorporated into calculating dowel bar performance reliability.

6.4.1 Differential Deflection and Bearing Stress Calculations

Tabatabae and Barenberg (1980) [107] proposed modeling dowel bars as beam elements based on the classical solution for a beam on Winkler foundation shown in Figure 68. This solution relates the shear force transmitted by the dowel with the concrete bearing stresses as shown in Figure 69.

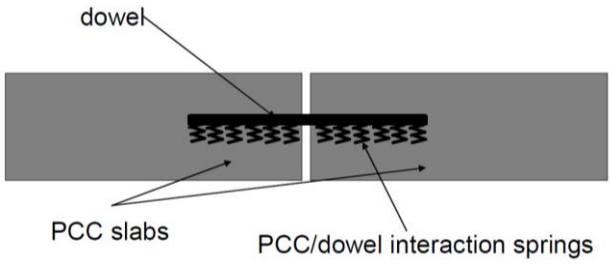

Figure 68: Tabatabae and Barenberg model of doweled joints of concrete

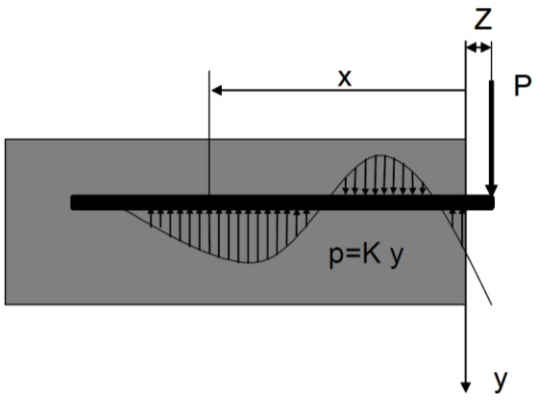

Figure 69: Dowel bearing stress distribution

The maximum bearing stress can be obtained using the following equation:

$$\sigma_{c,max} = \frac{K_d\, P_d(2+\beta\, Z)}{4\,\beta^3\, E_d\, I_d} J_d\, \Delta_{1,r} \quad \textbf{(6-12)}$$

$$\beta = \sqrt[4]{\frac{K_d}{4\, E_d\, I_d}} \quad \textbf{(6-13)}$$

where σ_c is the maximum concrete bearing stress, P_d is the shear load transferred by the dowel, β is the relative stiffness of a dowel bar embedded in concrete, E_d is the modulus of elasticity of dowel. For a steel dowel E_d = 29,000,000 psi. K_d is the modulus of dowel support, psi/in, I_d is the moment of inertia of the dowel bar cross section (0.9 times the moment of inertia for a solid circular cross section), d is the dowel diameter, in, and Z is the joint opening.

The shear force transferred by a single dowel is related to the joint deflections of the leave and approach slab at the dowel location:

$$P_d = J_d\,(w_a - w_l) \quad \textbf{(6-14)}$$

where w_a is the deflection of the approach side of the joint at the dowel location, w_l is the deflection of the leave side of the joint at the dowel location, and J_d is the dowel-concrete slab connection shear stiffness computed as:

$$J_d = \frac{1}{Z^3 \frac{1+\Phi}{12\,E_d\,I_d} + \frac{2+\beta\,Z}{2\,\beta^3\,E_d\,I_d}} \quad \textbf{(6-15)}$$

$$\Phi = \frac{24(1+\mu_d)}{A_d\,Z^2} \quad \textbf{(6-16)}$$

where μ_d is Poisson's ratio of the dowel material and A_d is the dowel cross-sectional area effective in shear.

Deflections are needed for the leave and approach side of the joint to determine dowel bearing stress. This is typically achieved through finite element analysis but for the sake of this project and simplicity, a rapid solution was developed [98]. This solution uses the principle of similarity to reduce the number of possible cases. It generalizes the pavement structure and traffic loading by determining critical deflections due to a single and tandem axle loading for three dowels in the right wheel path. The similar structure concept permits the computation of deflections in a multi-layer system (a concrete slab with a base on a subgrade) from those in a similar system. This concept has been used in the MEPDG for both JPCP and continuously reinforced concrete pavement (CRCP) cracking models [98]. The two systems can be considered equivalent provided their deflection basins are scalable, meaning that:

$$w_I(x_1, y_1) = \lambda_{def} w_{II}(x_2, y_2), \quad \textbf{(6-17)}$$

where *w* are deflections, *x* and *y* are horizontal coordinates, λ_{def} is the scaling factor for deflections (dependent only on properties of the pavement structure), and the subscripts I and II denote pavement systems I and II, respectively.

A past finite element analysis that considered the combined effects of axle and thermal loading on deflections showed the presence of a temperature gradient does not significantly affect differential deflections between the leave and approach slab. This is especially evident if there is no significant separation between the concrete slab and base. As this damage analysis only

considers early age concrete when the joint is closed and the slab remains in full contact with the base, the effect of slab curling can be ignored in dowel bearing stress calculation.

In the absence of temperature gradients, the following sufficient conditions for slab similarities were identified [98]:

- Two pavement systems have same in-plane geometry.
- The load footprint geometries and load positions are the same for both systems.
- The corresponding slab joints have the same load transfer efficiency.
- The radii of relative stiffness, ℓ_I and ℓ_{II}, are equal. The radius of relative stiffness for a slab-on-grade system is defined as following:

$$\ell = \sqrt[4]{\frac{D}{k}} \tag{6-18}$$

where *k* is the coefficient of subgrade reaction and *D* is the flexural stiffness of the slab-on grade.

For a single layer slab, the flexural stiffness is defined as:

$$D = \frac{E\ h^3}{12(1 - \mu^2)} \tag{6-19}$$

where *h*, *E*, and μ are the slab thickness, modulus of elasticity, and Poisson's ratio, respectively.

For a two-layered slab consisting of a concrete layer and a base with an unbonded interface between the layers, the flexural stiffness is defined as a sum of the flexural stiffnesses of the individual layers. The deflections scaling factor has the following form:

$$\lambda_{def} = \frac{P_1 k_1}{P_2\ k_2} \tag{6-20}$$

where subscripts *1* and *2* denote the slab systems.

For deflection calculation rapid solution, the following ISLAB2000 finite element model of a six-slab system was adopted [98]. The width for the slab modeling the effect of shoulder was set to 8 ft for a shoulder and the width for the slabs modeling traffic lanes was set to 12 ft. The transverse joint spacing was set to 15 ft. Two types of loading were considered: 18-kip single axle loading (Figure 70) and 34-kip tandem axle loading (Figure 71). The tire width and pressure were assumed to be equal to 8 in and 120 psi, respectively.

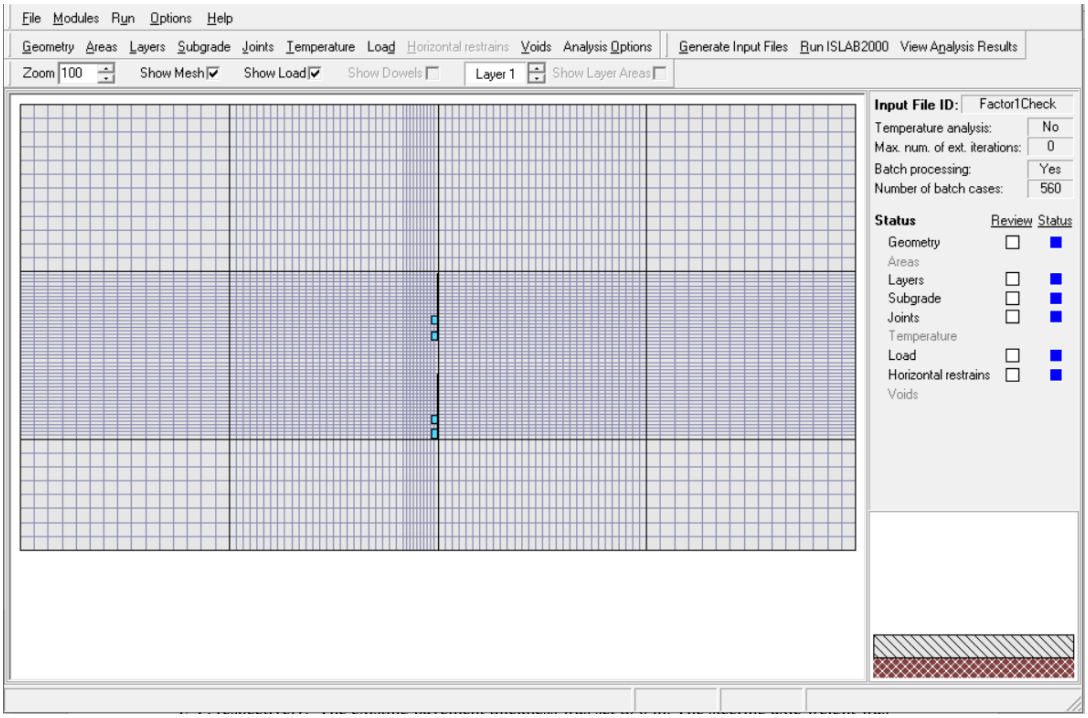

Figure 70: ISLAB2000 model for determination of transverse joint deflections due to single axle loading

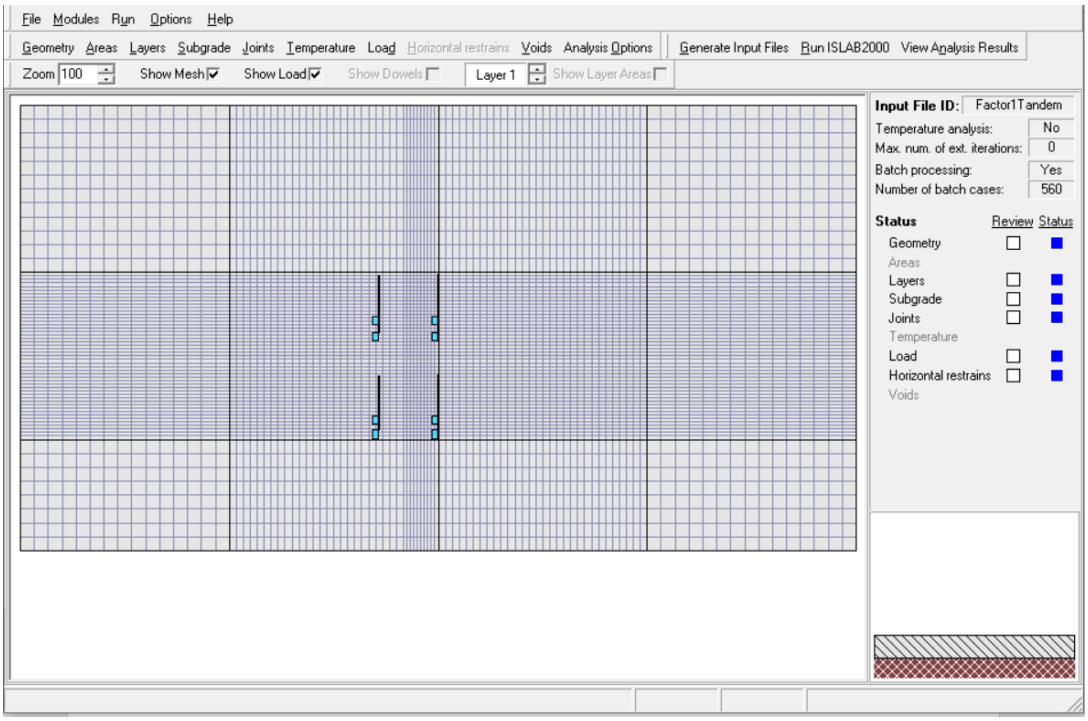

Figure 71: ISLAB2000 model for determination of transverse joint deflections due to tandem axle loading

A single layer slab system with the following parameters was considered:

- Slab thickness: 6 in
- Slab modulus of elasticity and Poisson's ratio: 4×10^6 psi and 0.15
- Longitudinal joint deflection load transfer efficiency, LTE: 70%
- Lane/shoulder LTE: 20%
- Transverse joint LTE: varied between 20 and 95%
- Distance between the axle load and the slab/shoulder joint varied from 0 to 36 in
- Coefficient of subgrade reaction varied between 3.125 psi/in and 1600 psi/in. It should be noted that this unrealistic range of this parameter permits solutions for pavement systems with the radii of relative stiffness ranging from 15 to 69 in.

The deflection at the loaded and unloaded side of the transverse joints 6, 18, and 30 in from the slab/shoulder joints were determined for each ISLAB2000 run and the rapid solutions were developed using modified MS-HARP neural network architecture [108,109]. The following procedure was used to calculate the deflections for this location for a two-layered pavement:

Step 1: Determine the flexural stiffness, D_e, for a two-layered pavement:

$$D_e = \frac{E_{pcc}\, h_{pcc}^3}{12(1-\mu_{pcc}^2)} + \frac{E_{base}\, h_{base}^3}{12(1-\mu_{base}^2)} \quad \textbf{(6-21)}$$

Step 2: Calculate the radius of relative stiffness:

$$\ell_1 = \sqrt[4]{\frac{D}{k_1}} \quad \textbf{(6-22)}$$

Step 3: Calculate the coefficient of subgrade reaction for the similar system using the condition $\ell_1 = \ell_2$:

$$k_2 = \frac{D_e}{\ell_1^4} \quad \textbf{(6-23)}$$

Step 4: Using the rapid solutions, determine the differences between deflections at the loaded and unloaded sides of the joints 6, 18, and 30 in away from the slab/shoulder joint.

Step 5: Compute difference between deflections at the same location in the original two-layered system:

$$\Delta_{1,r} = \frac{P_1 k_1}{P_{ref}\, k_2} \Delta_{NN,r} \quad \textbf{(6-24)}$$

where $\Delta_{NN,r}$ is the difference between deflections of the loaded and unloaded sides of the joint at distance *r* from the longitudinal edge, P_{ref} is the axle load used to generate the training data for the Neural Networks (17,000 lb for a single axle loading and 34,000 lb for the tandem axle loading), and P_1 is the axle load for the two-layered system.

Using these deflections, the maximum bearing stress for dowels at this location can be determined using the following equation:

$$\sigma_{c,max} = \frac{K_d\,(2+\beta\, Z)}{4\,\beta^3\, E_d\, I_d} J_d\, \Delta_{1,r} \quad \textbf{(6-25)}$$

The modulus of dowel support, K_d, is estimated using the following equation:

$$K_d = 0.7651\, E_{PCC} \quad \textbf{(6-26)}$$

where E_{PCC} is measured in psi and K_d is measured in psi/in.

6.4.2 Dowel Bar Performance Reliability

When axle loading causes maximum bearing stress greater than allowable bearing stress, damage will occur and performance will decrease. Dowel bearing stress has been established considering a standard legal truck having a 12-kip single axle load and two 34-kip tandem axles. The allowable bearing stress is a function of concrete compressive strength at the time of loading which was determined earlier using strength development and spatial variability models. In this analysis, the allowable concrete bearing stresses, f_b, is defined as:

$$f_b = f_c' \frac{4 - d}{3} \quad \textbf{(6-27)}$$

where f_c' is concrete compressive strength at the time of traffic loading and *d* is the dowel diameter.

At this point, methods of calculating compressive strength, modulus of elasticity, dowel bearing stress, and allowable bearing stress at early ages have been established. As with the transverse cracking procedure, the probabilistic approach can now begin by analyzing a randomly selected time for each vehicle pass to determine the concrete modulus of elasticity and compressive strength, including spatial variation adjustment. After opening to traffic, concrete strength, modulus of elasticity, and allowable bearing stress will continue to increase with time. The increase in modulus of elasticity will also increase the dowel bearing stress under the same loading but at a slower pace than the allowable concrete bearing stress.

The maximum bearing stress is calculated and compared to the allowable bearing stress for the randomized time. If the maximum bearing stress is greater than the allowable, the run counts

as a failure. The number of failures is totaled for each expected vehicle and is used to compute the probability of failure for each simulation. It is recommended to conduct multiple simulations (between 100-800 simulations) and average the probability of dowel bar failure between all simulations. The reliability that dowel bar damage will not occur is calculated using the following equation similar to that from transverse cracking reliability:

$$DowelRel = 100\% \times \left(1 - \frac{1}{N_{simulations}} \sum_{i=1}^{N_{sim}} \frac{N^{d}_{failures,i}}{n_{vehicles}}\right) \quad \textbf{(6-28)}$$

where $DowelRel$ is the dowel performance reliability, $N^{d}{}_{failures}$ is the total number failures, i.e. bearing stresses exceed the bearing strength, for simulation i, $n_{vehicles}$ is the total number of vehicles in one simulation, and N_{sim} is the total number of simulations.

6.5 Summary

The experience obtained from Chapter 3 was used to develop a mechanistic-based model to determine the risk of damage from early loading. This model accounts for the rate of concrete strength gain, traffic volume, load characteristics, and pavement structure properties which have been shown to be critical in early age pavement performance. This damage model permits the user to determine the optimal strength of early opening that minimizes unnecessary risk to short- or long-term performance.

To consider changing traffic levels and environments, a probabilistic approach was chosen that individually considers vehicles expected to travel over the pavement between the time the pavement is opened to when the design strength is met. The model requires the user to choose an opening strength, expected number of vehicles until design strength is met, and the axle spectrum

frequency. Then certain parameters are randomly chosen for each vehicle. These parameters are used to calculate critical stress in the slab. This is compared to estimated strength at the randomized time of vehicle loading. If stress is greater than strength, it is considered a failure. This is repeated numerous times and provides the probability of failure for a single opening to traffic simulation. Simulations performed with this model compared well to data gathered at MnROAD.

This procedure was repeated for two types of damage: transverse cracking and dowel bar damage. There are separate methods of calculating the specific stresses but the method of determining the reliability remains the same.

7.0 Web Tools for General Use

To implement the general use of the mechanistic-based early opening damage analysis and maturity – shear wave velocity relationship developed in this study, web tools were developed for both national and regional use. As this study was focused on Pennsylvania, separate, specified software was developed for the different regions of the state. The national web tool was generalized to best represent the practices of all states.

Both web tools can be found on the Pitt Pavements Software Hub (https://software.pavements.pitt.edu/). The computation models were implemented into a Fortran code while the web-based interface written in C#.NET permits the user to provide the input information for the analysis and displays the results.

There are a few distinct differences between the web tools including:

- Climate database
- Nondestructive tests
- Maturity models

The regional tool uses a database of mean monthly concrete temperatures and frequency of linear temperature gradients developed for five Pennsylvania locations. The national tool generates thermal profiles based on general environmental conditions centralized around forty major cities.

The use and models for nondestructive tests also differs between web tools. The national web tool focuses on the maturity method while the regional web tool includes both maturity and shear wave velocity. Maturity is a generally accepted method used across the country. Ultrasonic testing is still an emerging technology for concrete strength estimation. Pennsylvania is taking

strides toward utilizing shear wave velocity on sites, therefore it is also included in the regional web tool alongside the combined nondestructive test procedure described in Chapter 5.1. The websites also use two different maturity – strength relationship forms which are further detailed in this chapter.

Outlines of both tools are described below along with several example simulations depicting the effect of changing inputs.

7.1 National Web Tool

The Early Opening to Traffic Analysis webpage for national use opening screen is shown in Figure 72 (https://software.pavements.pitt.edu/EOP-National). There are three distinct areas providing different information or input sections: Section A contains the required user inputs that will represent the pavement in question; Section B contains the axle spectrum; and Section C contains additional, optional settings including model coefficients.

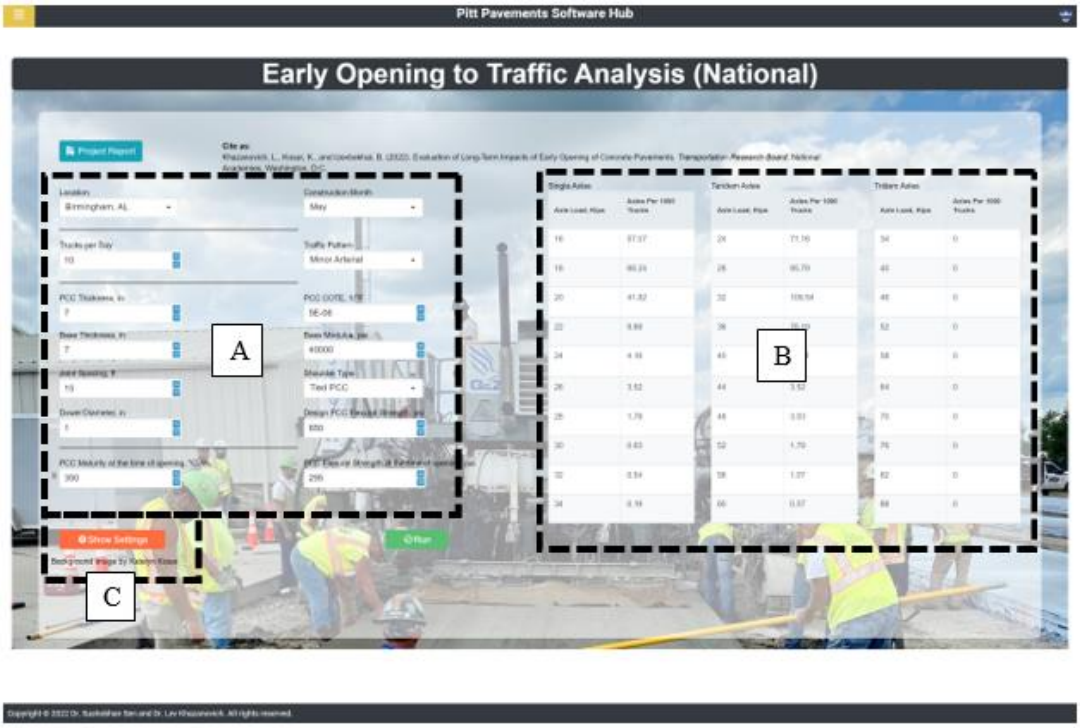

Figure 72: Starting screen on the national use web tool

Section A is magnified in Figure 73. The first inputs represent environmental conditions for the pavement through location and construction month. Location can be chosen from forty locations across the United States that represent the regions' general weather conditions. The next inputs focus on traffic properties the pavement will be exposed to using the inputs trucks per day and traffic pattern, which can be chosen from a drop down menu between minor arterial, residential, interstate, or custom. Choosing a traffic pattern automatically fills in the axle spectrum shown in Figure 74 (Section B in Figure 72). If custom is chosen, the user can fill in their own values directly into the table.

The next inputs focus on the material properties and design of the concrete pavement. The user must input concrete thickness, concrete coefficient of thermal expansion, base thickness, base modulus, joint spacing, shoulder type, dowel diameter and the design concrete flexural strength. For the remaining inputs, the user must choose either maturity or flexural strength for traffic

opening. The program will automatically fill in the other based on the maturity – strength relationship provided.

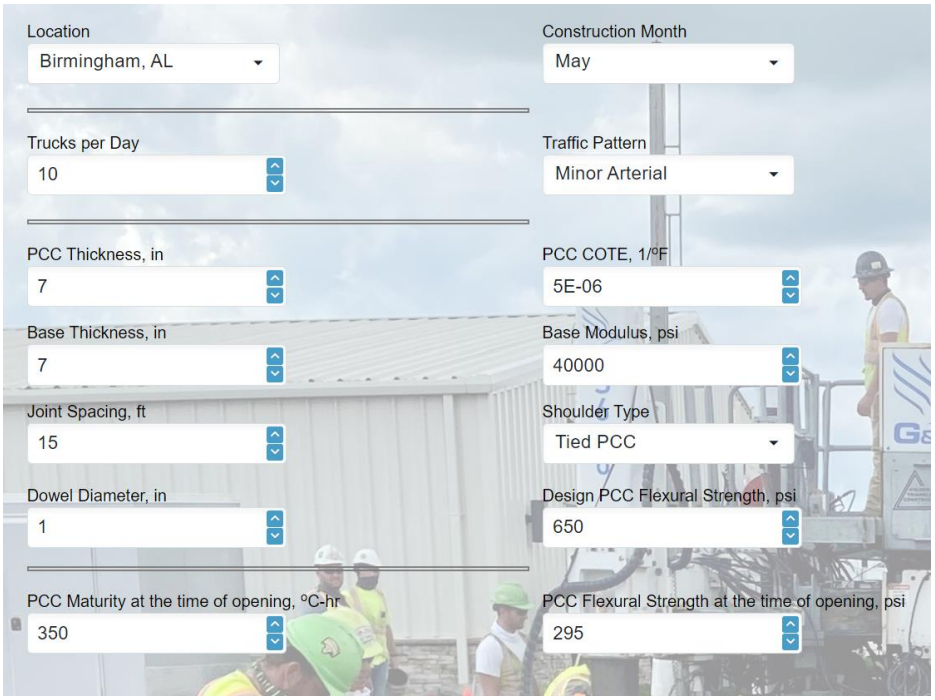

Figure 73: Traffic, location, and pavement structure settings for web-based damage analysis tool

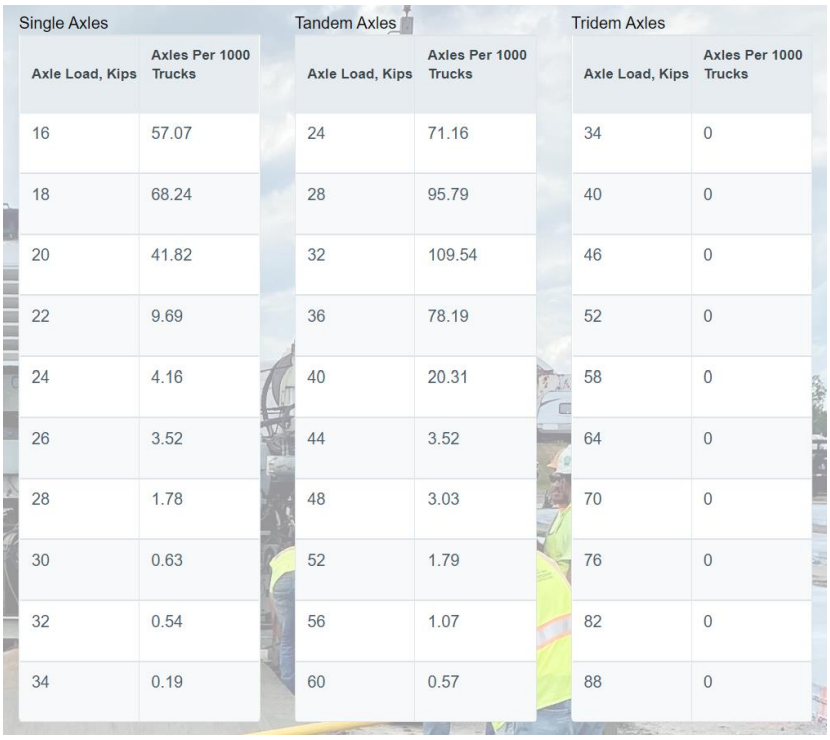

Single Axles

Axle Load, Kips	Axles Per 1000 Trucks
16	57.07
18	68.24
20	41.82
22	9.69
24	4.16
26	3.52
28	1.78
30	0.63
32	0.54
34	0.19

Tandem Axles

Axle Load, Kips	Axles Per 1000 Trucks
24	71.16
28	95.79
32	109.54
36	78.19
40	20.31
44	3.52
48	3.03
52	1.79
56	1.07
60	0.57

Tridem Axles

Axle Load, Kips	Axles Per 1000 Trucks
34	0
40	0
46	0
52	0
58	0
64	0
70	0
76	0
82	0
88	0

Figure 74: Start up axle spectrum for the National Website

Section C includes the additional settings, shown opened in Figure 75. The national website uses the maturity – strength relationship as defined in Equations (2-2) and (2-3).

The user can input model coefficients for their specific mixture in additional settings. The procedure to use this model and acquire the necessary coefficients for the specific mixture has been described in previous chapters. Other advanced settings can be accessed that allow the user to alter simulation number, built-in curl, and dynamic k-value as well as alter the variability characteristics. These settings' default values are standard but can be altered as the project requires.

The key input in this section is the minimum concrete flexural and compressive strength tested. This is the lowest strength measured in the lab which restricts the program from recommending any opening strengths lower than this value. This removes extrapolation from early age strength prediction and ensures the recommended strength has been confirmed in a laboratory setting. It is encouraged to perform laboratory strength testing as early as possible to obtain the

lowest minimum strength available. Further information on the additional settings can be opened using the model definitions link. This page is shown in Appendix D.

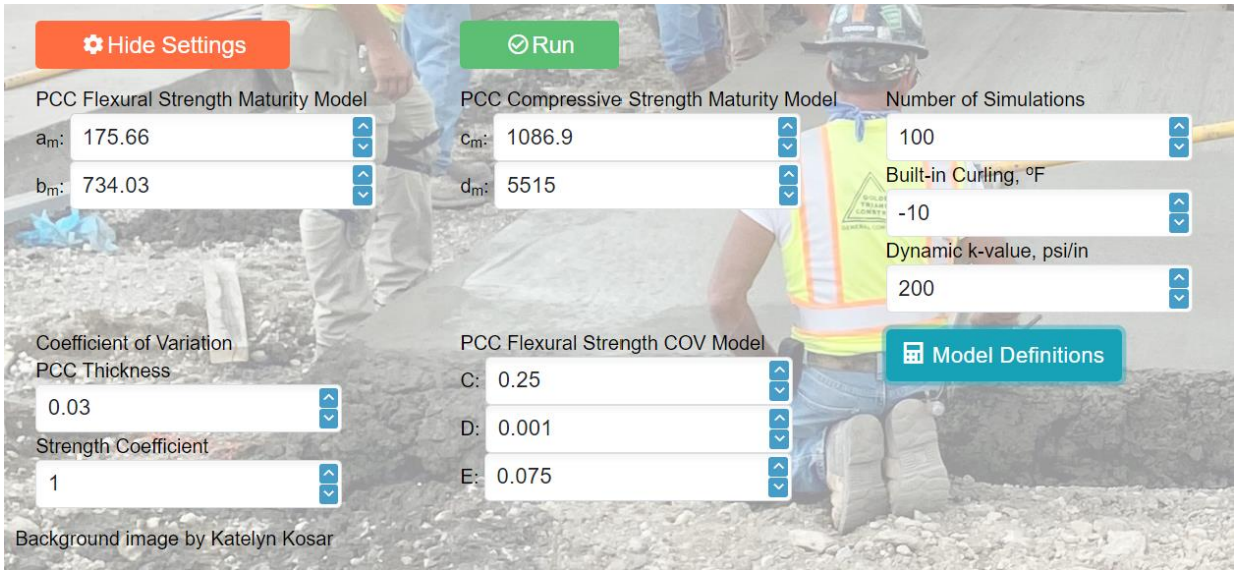

Figure 75: Additional settings to adjust the models

The tool uses the mechanistic-based early opening damage analysis to evaluate the project and outputs the cracking and dowel bar performance reliability, the ESAL repetitions to design strength, and future strength development. The ESAL repetitions represent the number of single axles that will travel the roadway until the design strength specified by the user is reached. Reliability for the opening strength chosen is portrayed as numerical values and separate graphs display additional pavement and reliability information from when the pavement is opened to when the design strength is met. The first two graphs show how reliability changes if the opening time is delayed. The ESAL repetition to design strength is also displayed as a numerical value for the chosen time to open and as a graph for delayed values. The final graph shows the predicted strength gain over time.

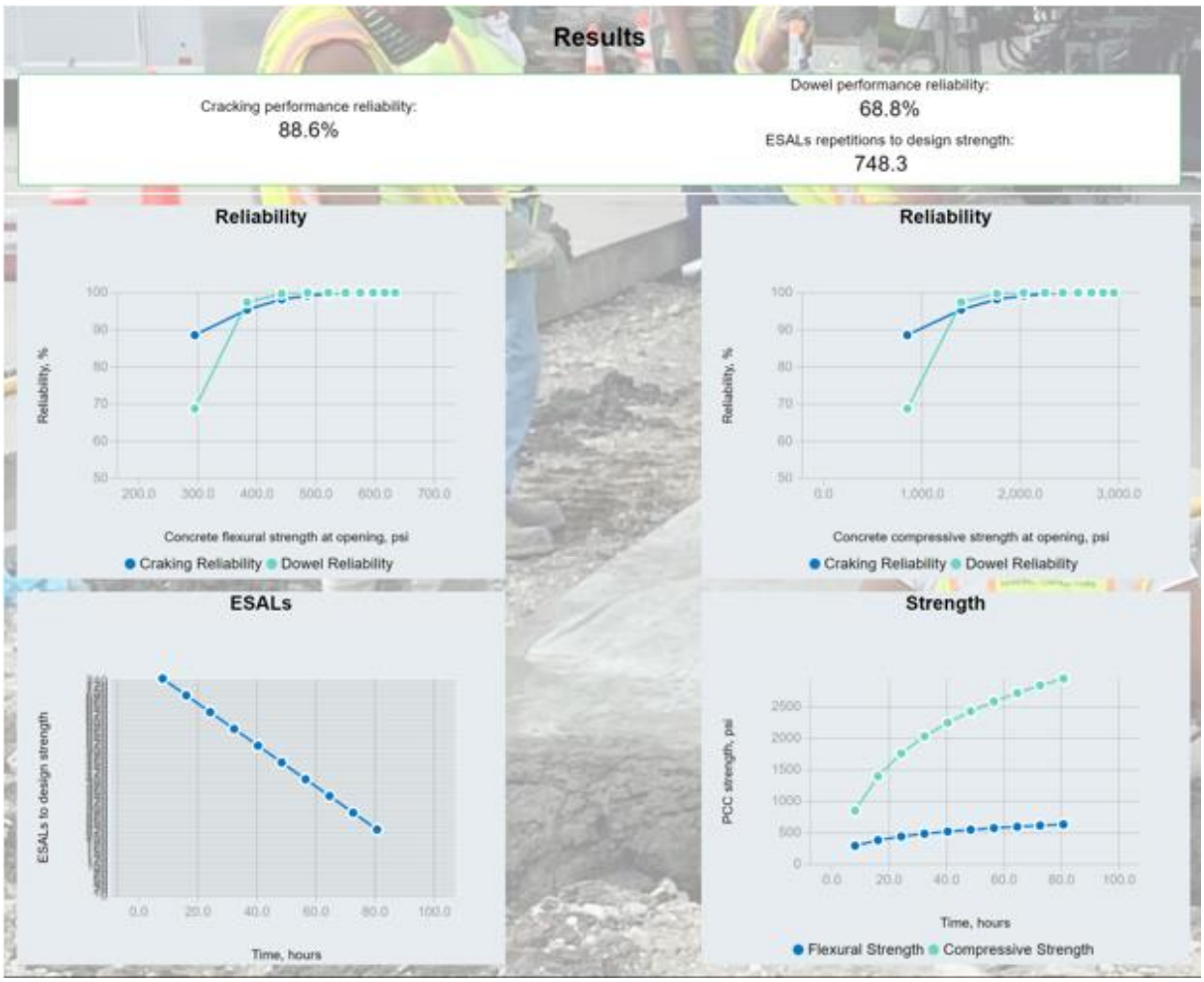

Figure 76: Results using the national web tool

The results shown in Figure 76 is the output using the default values and the following changes:

- Location: Columbus, OH
- Construction Month: July
- Trucks per Day: 200
- Concrete and Base Thickness: 6 inches each

The cracking and dowel bar performance were calculated to be 88.6% and 68.8%, respectively. The pavement is expected to receive 748.3 ESALs after it is opened to traffic at the maturity of 350 °C-hr or flexural strength of 295 psi until it reaches the design flexural strength of

650 psi. Using the results graphs, the reliability improvement can be estimated. If the traffic opening is delayed by 8 hours, the concrete flexural strength at time of opening would reach 383 psi and the cracking and dowel bar performance reliability would increase to 96.2% and 97.6%, respectively. To confirm the values predicted in the graph, it is recommended to rerun the simulation with the new opening strength.

7.1.1 Example Simulations

To demonstrate the effect of varying location, construction month, concrete thickness, and traffic level on the predicted opening time the following examples were simulated using the national web tool. The remaining settings remain constant as used in the previous example which provided the results for Figure 76, the design concrete flexural strength is 650 psi, the maturity at time of opening is assumed to be 350 °C-hr, and the opening flexural strength was found to be 295 psi.

- Case 1: Miami, FL; paved in July; 6-inch concrete thickness; 200 trucks/day
- Case 2: Columbus, OH; paved in October; 6-inch concrete thickness; 200 trucks/day
- Case 3: Columbus, OH; paved in July; 9-inch concrete thickness; 200 trucks/day
- Case 4: Columbus, OH; paved in July; 6-inch concrete thickness; 400 trucks/day

Case 1: Changing Location

A database of temperature data for forty locations within the U.S. was created. Case 1 investigates the effect of changing this location from Columbus, OH to Miami, FL. In this simulation, the cracking and dowel bar performance reliability rises to 96.0% and 72.6%, respectively. Since Miami has a higher anticipated mean monthly concrete temperature than

Columbus, the concrete would gain strength faster. The pavement will receive only 662 ESALs until the design strength is reached.

Case 2: Changing Construction Month

Cases 2 shows the effect of changing the construction month, in this case from July to October. Especially in Ohio, October is much colder than July which significantly slows the heat of hydration in the concrete, reducing the strength gain. In this simulation, cracking reliability has a minimal increase with a value of 90.2%, however, dowel bar performance reliability falls significantly to 34.2% at the opening flexural strength of 295 psi. If the user were to delay opening until the flexural strength reached 380 psi, the cracking and dowel bar reliability rises above 94%. This pavement will receive 1471 ESALs before design strength is reached as compared to 748 ESALs in the initial example due to the slower strength gain rate.

Case 3: Changing Concrete Thickness

Case 3 changes the concrete thickness from 6 inches to 9 inches with all other settings remaining the same as the initial example. Since the concrete is thicker and therefore stronger, the cracking performance reliability and dowel performance reliability are both 99.9%. This case also sees a slightly higher number of ESALs, 766, before design strength is reached.

Case 4: Changing Number of Trucks

Case 4 changes the traffic level from 200 to 400 trucks/day, both keeping a minor arterial traffic spectrum. All other settings remain the same as the initial example. When there are more expected truck loads, the cracking performance reliability falls to 78.3%, dowel performance reliability falls to 44.1%, and ESAL repetitions to design strength increases to 1505.1 ESALs. This simulation could benefit from restricting traffic to smaller axle weights (changing the traffic spectrum) or to essential traffic only (lowering the number of trucks). If only essential trucks are

allowed, lowering the trucks/day to 100, the cracking and dowel bar performance reliabilities raise to 96.6% and 81.4%, respectively.

Cases when the opening strength is 295 psi are summarized in Table 18.

Table 18: Example cases for national website

	Example	Case 1	Case 2	Case 3	Case 4a	Case 4b
Location	Columbus, OH	Miami, FL	Columbus, OH	Columbus, OH	Columbus, OH	Columbus, OH
Construction Month	July	July	October	July	July	July
Concrete Thickness	6 in	6 in	6 in	9 in	6 in	6 in
Number of Trucks/day	200	200	200	200	400	100
Cracking Reliability	88.6%	96.0%	90.2%	99.9%	78.3%	96.6%
Dowel Bar Reliability	68.8%	72.6%	34.2%	99.9%	44.1%	81.4%
ESALs to design strength	748.3	662.3	1470.7	765.5	1505.1	378.4

7.2 Regional Web Tool

The Early Opening to Traffic Analysis webpage for regional use is very similar to use as the national version. The opening screen is shown in Figure 77. Like the national web tool, there are three distinct areas providing different information or input sections: the required user inputs that will represent the pavement in question, the axle spectrum, and additional settings including model coefficients.

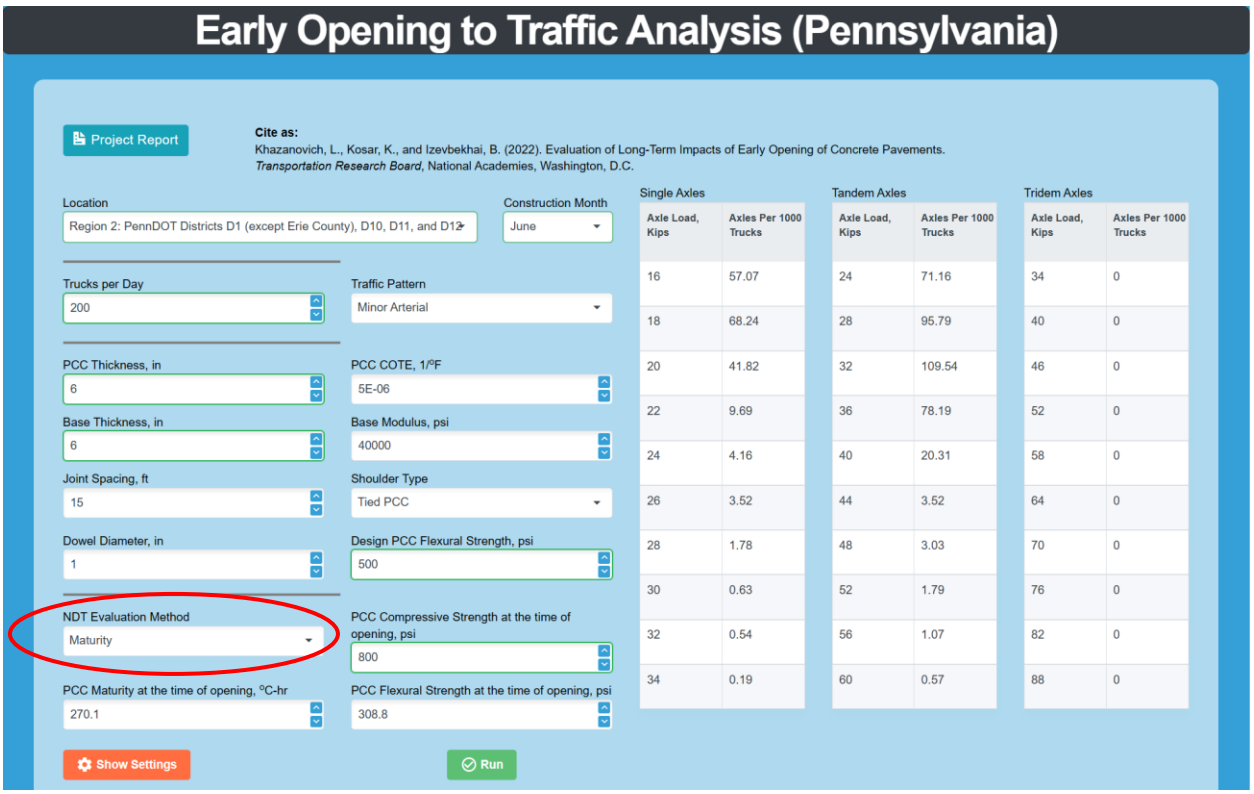

Figure 77: Starting screen on the regional use web tool

The user inputs remain largely the same as the national web tool as the inputs for environmental conditions; traffic properties, material properties, and structural design are the same. The primary difference is in the inputs at the time of traffic opening as this web tool incorporates combined nondestructive procedures (circled). The nondestructive test used on the project must be selected between maturity and shear wave velocity. The model will change depending on which is chosen. Both models require the desired concrete maturity or shear wave velocity at the time of opening. The application then calculates the concrete flexural and compressive strength at the time of opening using the respective models. The coefficients can be changed based on the strength-maturity relationship developed in the laboratory that corresponded to the mixture used. The shear wave velocity model has similar equations to solve for flexural and

compressive strength. There is also the additional equation to relate shear wave velocity to maturity so that strength gain can be predicted forward.

Additional settings are again similar to the national web tool (Figure 78). The regional website uses the maturity – strength relationships shown in Equations (2-4) and (2-5) in combination with the wave velocity – strength relationships shown in Equations (2-9) and (5-1). For a full procedure on how to utilize these models and determine the coefficients, refer to Chapters 2 and 5.

Advanced settings can be accessed that allow the user to alter simulation number, built-in curl, dynamic k-value, variability characteristics, and minimum tested concrete strength. These settings' default values are standard but can be altered as the project requires. Again, it is encouraged to perform laboratory strength testing as early as possible to obtain the lowest minimum strength available. Further information on the additional settings can be opened using the model definitions link. This page is shown in Appendix E.

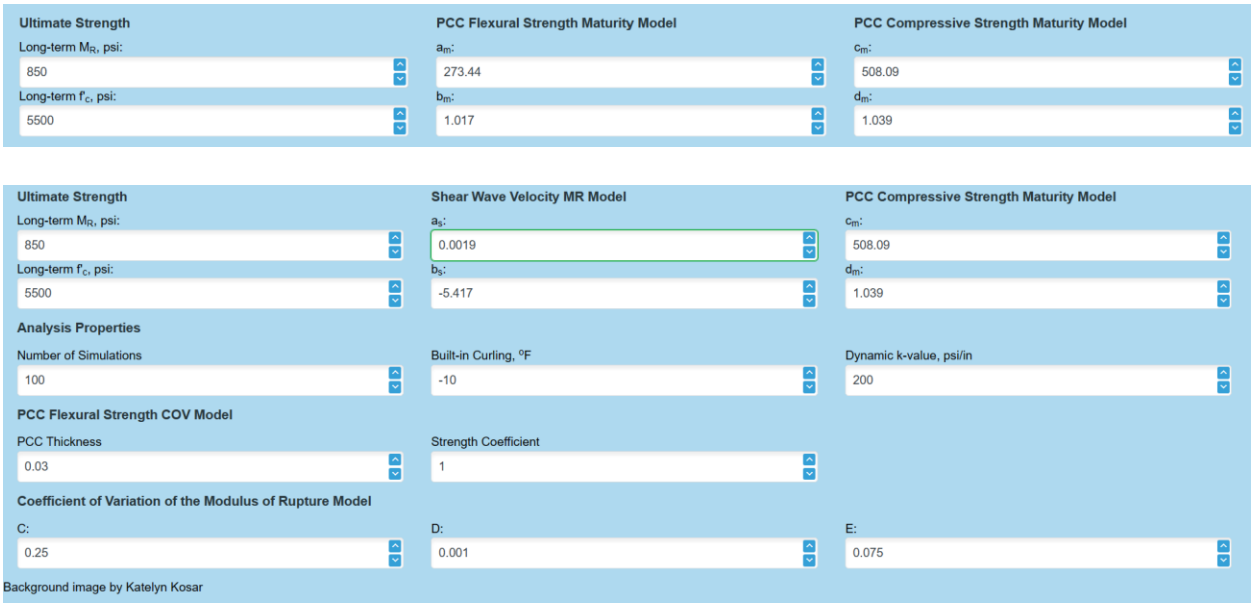

Figure 78: Additional settings to adjust the models

After the inputs are added, the user can run the simulation and the tool will use the mechanistic-based early opening damage analysis to evaluate the project. The tool will output the cracking and dowel bar performance reliability, the ESAL repetitions to design strength, and future strength development. Reliability is portrayed as numerical values at the top of the results. This is the value for the time to opening strength chosen in the inputs. The first two graphs show how reliability changes if the opening time is delayed. The ESAL repetitions to design strength is also displayed as a numerical value for the chosen time to open and as a graph for delayed values. The final graph shows the predicted strength gain over time.

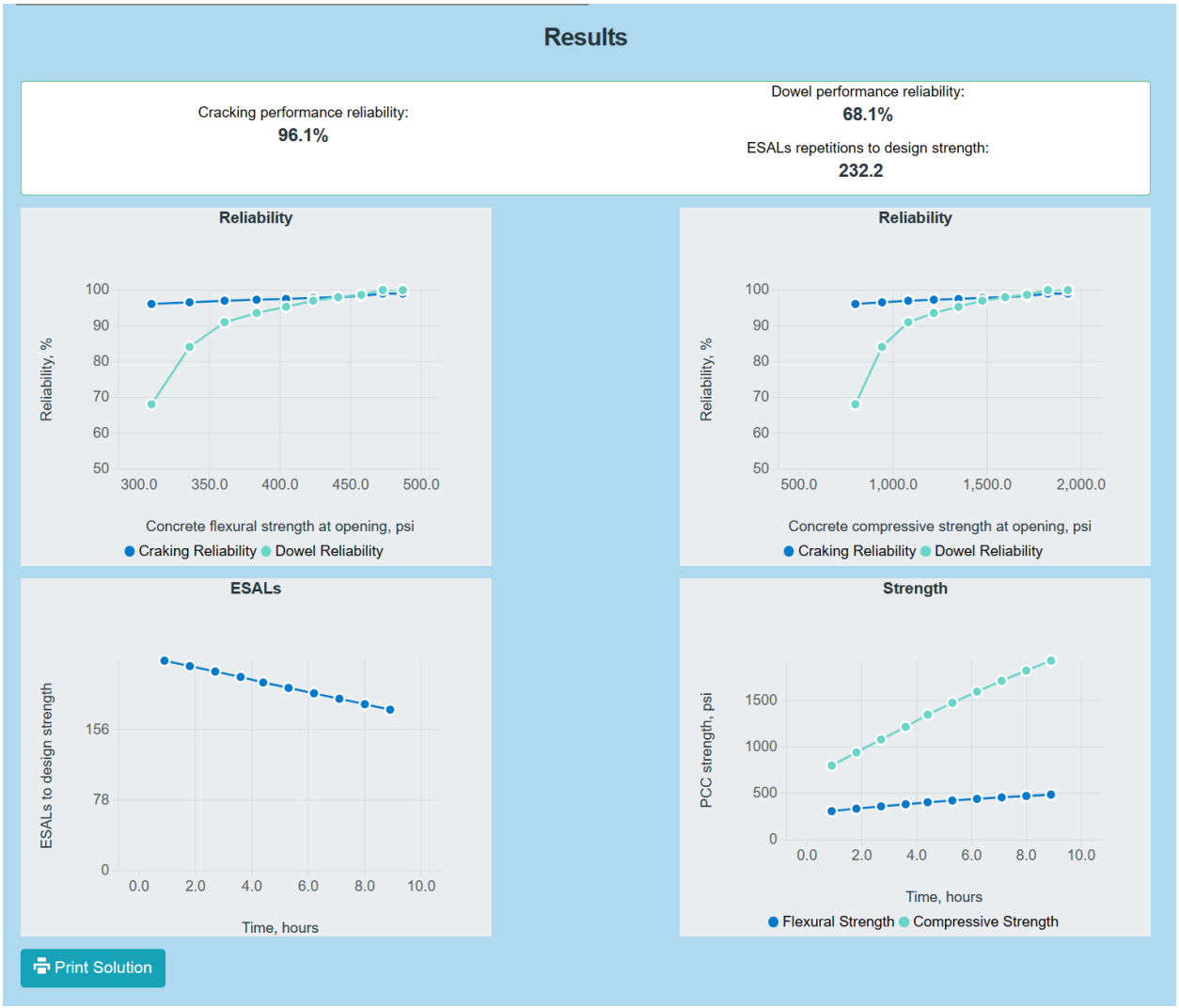

Figure 79: Results using the regional web tool

The original example for cracking and dowel bar performance were calculated to be 96.3% and 68.1%, respectively. The pavement is expected to receive 232 ESALs after it is opened to traffic at the maturity of 270 °C-hr or flexural strength of 309 psi until it reaches the design flexural strength of 500 psi. Using the results graphs, the reliability improvement can be estimated. If the traffic opening is delayed by 4.4 hours, the concrete flexural strength at time of opening would reach 404 psi and the cracking and dowel bar performance reliability would increase to 97.5% and 95.3%, respectively. To confirm the values predicted in the graph, it is recommended to rerun the simulation with the new opening strengths.

The exact same simulation can be performed using shear wave velocity. A flexural strength of 309 psi would correspond to a shear wave velocity of 2277 m/s. This will provide identical simulations and results.

7.2.1 Example Simulations

To demonstrate the effect of varying location, construction month, and traffic pattern, the following examples were simulated using the web tool. The other settings remain at the values shown in the previous example. The maturity model will be used for each case with concrete maturity at the time of opening of 270 °C-hr and the calculated concrete flexural strength at the time of opening of 309 psi. If the shear wave velocity were to be used as the evaluation method, the velocity at the time of opening would be 2277 m/s.

- Case 1: Region 4, paved in June, Minor Arterial
- Case 2: Region 2, paved in October, Minor Arterial
- Case 3: Region 2, paved in June, Residential
- Case 4: Region 2, paved in June, Interstate

Case 1: Changing Location

For this web tool, Pennsylvania was divided into regions that group the regional offices of PennDOT with others with similar climates. Case 1 investigates the change of location from Region 2 (Districts 1, 10, 11, and 12) to Region 4 (Districts 3 and 4). In this simulation, the cracking and dowel bar performance change only slightly to 95.3% and 65.8%, respectively. ESALs repetitions also increases slightly to 240.8 due to the differing climates causing a difference in rate of strength gain.

Case 2: Changing Construction Month

Case 2 shows the effect of changing the construction month, in this case from June to October. On average, October is a colder month than June which can significantly slow the heat of hydration in concrete, reducing the rate of strength gain. In this simulation, cracking and dowel bar performance reliability and ESAL repetitions are 95.8%, 40.1%, and 309.6, respectively. There is a significant difference for each of these values when compared to the same pavement constructed in June. The cracking performance is similar accounting for the increase in stiffness due to the colder weather while the dowel bar performance reliability decreases and ESAL repetitions increase to account for the slow rate of strength gain.

Case 3: Changing Traffic Pattern to Residential

Case 3 shows the effect of changing the traffic pattern, in this case from Minor Arterial to Residential. This input controls the amount and size of vehicles traveling on the pavement. A decrease in traffic to 97.7 ESALs is caused by the user changing the traffic pattern from Minor Arterial to Residential. In this simulation, cracking and dowel bar performance reliability are 100% and 99.9%, respectively. The large increase from the original example shows that allowing lighter weight traffic early is beneficial to lower congestion while maintaining pavement performance

reliability. Changing the allowable traffic to achieve this reliability is a viable method for reducing the user cost of any road type including interstates and minor arterials.

Case 4: Changing Traffic Pattern to Interstate

Case 4 shows the effect of changing the traffic pattern, in this case from Minor Arterial to Interstate. An increase in traffic to 436.8 ESALs is caused by this change. In this simulation, cracking and dowel bar performance reliability fall to 95.2% and 33.8%, respectively. This shows the significant impact of a premature traffic opening.

Table 19 shows a comparison of each case.

Table 19: Example cases for regional website

	Example	Case 1	Case 2	Case 3	Case 4
Location	Region 2	Region 4	Region 2	Region 2	Region 2
Construction Month	June	June	October	June	June
Traffic Pattern	Minor Arterial	Minor Arterial	Minor Arterial	Residential	Interstate
Cracking Reliability	96.1%	95.3%	95.8%	100%	95.2%
Dowel Bar Reliability	68.1%	65.8%	40.1%	99.9%	33.8%
ESALs to design strength	232.2	240.8	309.6	97.7	436.8

7.3 Summary

Two web tools were developed for easy use of the mechanistic-based early opening damage analysis. The National Web Tool incorporates the damage analysis with the maturity method for nationwide use with forty representative climate databases. The Regional Web Tool focuses on practices in Pennsylvania by specifying climate data, changing the maturity – strength relationship, and including the combined nondestructive tests procedure.

Both web tools provide the user with the reliability that transverse cracking and dowel bar damage will not occur and the expected number of vehicles that will traverse the pavement before the design strength is met. Additional information is provided through four graphs that show how reliability, expected trucks, and strength gain will change as opening strength is increased.

8.0 Conclusions

This project aimed to develop rational traffic opening criteria for concrete pavements that improves the efficiency of construction without jeopardizing pavement performance. This was done by improving the methods of determining concrete strength in the field and improving opening criteria using computed critical stresses due to the specific environmental and traffic loading conditions of individual pavements.

A large-scale test at MnROAD demonstrated that simply because a pavement is loaded at a very low strength, it does not necessarily cause performance loss or failure. An extensive examination of the test pavement resulted in no damage being connected to early loading. To understand the lack of damage, a finite element analysis was performed to change loading and environmental conditions and determine the effect on critical stresses. In varying simulation conditions, stresses changed to be equivalent or greater than the strength at the time of loading meaning that unfavorable conditions could have certainly failed the test pavement even under the same vehicle load. Including the loading and environmental conditions in critical stress calculations is necessary to accurately represent the concrete condition. This shows that the current criteria for traffic opening is overly conservative and modern concrete pavements can safely open to traffic earlier than currently allowed.

Maturity and ultrasonic testing are nondestructive methods that were thoroughly explored in this study for their use in the field on early age, modern concrete mixtures. Destructive testing is fundamentally slow and insufficient for field use. To better determine in-situ concrete strength, these nondestructive tests have accurate correlations to strength for both high early strength and modern conventional concrete mixtures. Maturity tended to be more conservative than ultrasonic

testing and had difficulty adjusting to varying strength gain rates common in young concrete. This led to under- and overestimations of strength also found in other studies. The lack of consistency is concerning as this could cause mistiming in early age procedures. Ultrasonic testing was able to track the variability in strength gain more accurately. Maturity requires permanent instrumentation, and many sensors would be needed to monitor a length of pavement. Ultrasonic devices are handheld, external, and require no surface preparation so measurements could be taken at any point along the pavement to assess concrete strength variability or critical areas. Strength determination in the field can be performed efficiently and accurately using nondestructive methods, especially ultrasonic testing.

It was concluded that ultrasonic testing is preferable for field use; however, maturity provides more information on the strength gain rate through predictive temperature models. A procedure was created that allowed ultrasonic testing and maturity to be used congruently. This benefits the user as they can obtain the shear wave velocity, and therefore strength, in the field quickly and at any location of their choosing and still utilize the predictive strength relationship to understand how that area of the pavement will continue to gain strength. This is highly beneficial when scheduling early age concrete procedures.

The combined nondestructive test procedure depends on laboratory correlations. However, the linear array ultrasonic device, MIRA, was not designed for beam specimens and was affected by proximity of vertical edges. Shear wave velocities for beams and slabs reported by this linear array system were different at the same age and maturity level. A small laboratory experiment was conducted to confirm the effect to edge proximity and raw time signal histories were evaluated to find the causes of the discrepancy. It was found that identifying the direct arrival time for farther sensor distances could be difficult due to competing secondary peaks and that wave velocity is

faster in a beam specimen than in a slab. When signal time histories were shifted and the farthest sensor distances removed, there was a higher correspondence between the calculated slab and beam velocities. Wave interactions with boundaries and other waves were considered for potential explanations for the observations; however, more experiments are necessary for a definitive conclusion.

The combined nondestructive test procedure can increase the efficiency and accuracy of strength determination, remove the dependency on destructive testing in the field, and provide users with considerable information on concrete strength development. This addresses the first concern of this project and begins to increase construction efficiency; however, efficiency is limited by the conservative opening requirements decided by each state.

The second aspect of this project was to determine a flexible opening to traffic procedure that developed the risk of damage at different opening strengths depending on the characteristics of individual projects. Using the experience obtained from the MnROAD field test and the respective finite element model, a mechanistic-based early opening damage analysis was created. The analysis includes effects of loading, structural, and environmental conditions on short- and long-term pavement performance to calculate the risk of damage due to early loading, specifically transverse cracking and joint performance. By providing basic information about the pavement and choosing an opening strength, the analysis provides the pavement reliability and additional information on how the pavement will develop in the crucial period after opening until the design strength is met.

The combined nondestructive test procedure and the mechanistic-based early opening damage analysis were used together in simple web tools for public use. These tools allow the user

to choose the optimal opening strength for their specific pavement and understand the risks of premature failure or loss of long-term performance.

8.1 Recommendations for Future Research

This dissertation aimed to improve understanding of early age concrete and the efficiency of construction procedures occurring in this critical time. It is built upon previous research by adding flexibility to criteria and accounting for many conditions affecting pavement performance. However, early age concrete pavement is sensitive to many more factors beyond those explored in this dissertation. Improved models for pavement response under traffic and environmental loads could be implemented to increase accuracy. Dowel-concrete interaction and bearing stresses are difficult to model. This project utilized well established but older, simplified models. Modern models could better represent and predict the interaction and corresponding effect on joint performance. Modifying the dowel bar performance calculation to include new models could improve the accuracy of dowel bar performance reliability. Tensile creep is a material property of concrete that affects early age concrete but was excluded in this dissertation model. Creep is a complex property to measure and model and it can reduce environmental stress experienced by a slab. To improve curling and warping stress predictions, creep could be included in future versions of the transverse cracking model to better represent actual pavement response to environmental stress.

This dissertation briefly explored the discrepancy between beam and slab shear wave velocities at comparable ages and mixtures. The effect of vertical edges was confirmed and differences in the raw time histories were identified. An extensive analysis would be required to

determine the reason behind the discrepancy, although a few hypotheses were explored here. Future research could determine a relationship between sensor distance and direct arrival time shift. If a relationship exists, it would be possible to adjust beam shear wave velocities without scanning a slab.

Appendix A State Opening Criteria

Table A. 1: State opening criteria

State	Opening to Traffic			
	Traffic Level	Age	Compressive	Flexural
Alabama	construction traffic all traffic	72 hours 7 days	3000 4000	
Alaska	all traffic	7 days	70% or 100% of strength	
Arizona	all traffic	7 days	3000	
Arkansas	all traffic	7 days	3000	
California	all traffic	10 days		650
Colorado	all traffic		3000	
Connecticut	all traffic		3500	
Delaware	all traffic		3500	
Florida	all traffic	14 days	2200	
Georgia	all traffic	14 days	2500	
Idaho	all traffic		3500	
Illinois	all traffic	14 days	3500	650
Indiana	construction traffic all traffic	10 days 14 days		550 550
Iowa	all traffic	14 days		400 - 500
Kansas	all traffic	10 days		450
Kentucky	all traffic		3000	
Louisiana	all traffic	14 days	3000	550
Maryland	all traffic		3000	
Massachusetts	all traffic	7 days		550
Michigan	all traffic	72 hours		300
Minnesota	all traffic	7 days	3000	350 - 500
Missouri	construction traffic all traffic		2500 3000	
Montana	all traffic		2500	350
Nebraska	construction traffic all traffic	14 days -	3000 3500	
Nevada	all traffic	10 days		550
New Jersey	all traffic	10 days	3000	
New Mexico	all traffic	3 days	3000	
New York	construction traffic all traffic	10 days 15 days	2500 3000	
North Carolina	all traffic	7 days		
North Dakota	all traffic		3000	450
Ohio	all traffic	7 days		600

Oklahoma	all traffic	14 days		
Oregon	all traffic		70% of strength	
Pennsylvania	all traffic		2000 - 3600	250 - 540
Rhode Island	all traffic			525
South Carolina	all traffic	14 days		
South Dakota	all traffic		4000	
Tennessee	all traffic	14 days	3000	
Texas	construction traffic all traffic	48 hours 7 days	- 3200	- 450
Utah	all traffic		4000	
Virginia	all traffic	14 days		600
Washington	all traffic		2500	
West Virginia	all traffic		3000	500
Wisconsin	all traffic	4 - 7 days	3000	

Appendix B Shear Wave Velocity for Slabs

Appendix B presents the average shear wave velocity (SWV) collected in slabs HES1 and C1.1 during the experiment.

Table A. 2: Shear Wave Velocity of slab C1.1 (Day 1)

Date	Time	Time from construction (h)	Section	Position	Avg. SWV (m/s)	Cycle
7/13/20	15:27	5.13	C-1.1	TE	1445	1
7/13/20	15:28	5.14	C-1.1	TC	1475	1
7/13/20	15:30	5.17	C-1.1	CRS	1520	1
7/13/20	15:31	5.18	C-1.1	CRN	1505	1
7/13/20	15:31	5.19	C-1.1	CLS	1495	1
7/13/20	15:32	5.20	C-1.1	CLN	1520	1
7/13/20	15:45	5.42	C-1.1	TE	1565	2
7/13/20	15:46	5.43	C-1.1	TC	1590	2
7/13/20	15:47	5.45	C-1.1	CLS	1575	2
7/13/20	15:48	5.48	C-1.1	CRS	1610	2
7/13/20	15:49	5.48	C-1.1	CLN	1680	2
7/13/20	15:50	5.50	C-1.1	CRN	1735	2
7/13/20	15:59	5.66	C-1.1	TE	1650	3
7/13/20	16:00	5.68	C-1.1	TC	1685	3
7/13/20	16:01	5.68	C-1.1	CLS	1675	3
7/13/20	16:02	5.70	C-1.1	CRS	1680	3
7/13/20	16:03	5.72	C-1.1	CLN	1700	3
7/13/20	16:04	5.73	C-1.1	CRN	1740	3
7/13/20	16:15	5.92	C-1.1	TE	1745	4
7/13/20	16:15	5.92	C-1.1	TC	1790	4
7/13/20	16:17	5.95	C-1.1	CLS	1785	4
7/13/20	16:18	5.97	C-1.1	CRS	1780	4
7/13/20	16:19	5.98	C-1.1	CLN	1800	4
7/13/20	16:19	5.99	C-1.1	CRN	1830	4
7/13/20	16:44	6.40	C-1.1	TE	1925	5
7/13/20	16:44	6.41	C-1.1	TC	1940	5
7/13/20	16:45	6.42	C-1.1	CLS	1950	5
7/13/20	16:45	6.42	C-1.1	CRS	1965	5
7/13/20	16:47	6.46	C-1.1	CLN	1970	5
7/13/20	16:48	6.47	C-1.1	CRN	1975	5

Table A. 3: Shear Wave Velocity of slab C1.1 (Subsequent days)

Date	Time	Time from construction (h)	Section	Position	Avg. SWV (m/s)	Cycle
7/14/20	8:32	22.21	C-1.1	TE	2520	6
7/14/20	8:35	22.25	C-1.1	TC	2500	6
7/14/20	8:36	22.28	C-1.1	CRS	2500	6
7/14/20	8:37	22.29	C-1.1	CLS	2530	6
7/14/20	8:38	22.31	C-1.1	CRN	2500	6
7/14/20	8:39	22.33	C-1.1	CLN	2530	6
7/14/20	10:50	24.50	C-1.1	TE	2530	7
7/14/20	10:51	24.52	C-1.1	TC	2530	7
7/14/20	10:52	24.53	C-1.1	CLS	2530	7
7/14/20	10:53	24.55	C-1.1	CLN	2530	7
7/14/20	10:53	24.56	C-1.1	CRN	2530	7
7/14/20	10:54	24.57	C-1.1	CRS	2530	7
7/15/20	10:37	48.29	C-1.1	TE	2560	8
7/15/20	10:38	48.30	C-1.1	TC	2605	8
7/15/20	10:39	48.32	C-1.1	CLS	2580	8
7/15/20	10:39	48.33	C-1.1	CLN	2580	8
7/15/20	10:40	48.33	C-1.1	CRN	2580	8
7/15/20	10:41	48.35	C-1.1	CRS	2605	8
7/16/20	12:26	74.11	C-1.1	TE	2600	9
7/16/20	12:27	74.13	C-1.1	TC	2530	9
7/16/20	12:28	74.14	C-1.1	CLS	2615	9
7/16/20	12:29	74.15	C-1.1	CLN	2610	9
7/16/20	12:30	74.17	C-1.1	CRN	2625	9
7/16/20	12:31	74.18	C-1.1	CRS	2610	9
7/18/20	8:06	117.77	C-1.1	TE	2645	10
7/18/20	8:06	117.77	C-1.1	TC	2660	10
7/18/20	8:07	117.78	C-1.1	CRN	2665	10
7/18/20	8:07	117.79	C-1.1	CRS	2650	10
7/18/20	8:08	117.80	C-1.1	CLS	2660	10
7/18/20	8:08	117.81	C-1.1	CNS	2660	10

Table A. 4: Shear Wave Velocity of slab C1.1 (Subsequent days) Part II

Date	Time	Time from construction (h)	Section	Position	Avg. SWV (m/s)	Cycle
7/20/20	10:43	168.38	C-1.1	TE	2650	11
7/20/20	10:44	168.40	C-1.1	TC	2635	11
7/20/20	10:44	168.41	C-1.1	CRS	2655	11
7/20/20	10:45	168.43	C-1.1	CLS	2665	11
7/20/20	10:46	168.44	C-1.1	CRN	2685	11
7/20/20	10:47	168.45	C-1.1	CLN	2665	11
7/27/20	11:46	337.43	C-1.1	TE	2695	12
7/27/20	11:47	337.45	C-1.1	TC	2700	12
7/27/20	11:47	337.46	C-1.1	CRN	2715	12

7/27/20	11:48	337.48	C-1.1	CRS	2695	12
7/27/20	11:49	337.48	C-1.1	CLS	2710	12
7/27/20	11:49	337.49	C-1.1	CLN	2680	12

Table A. 5: Shear Wave Velocity of slab HES1 (Day 1)

Date	Time	Time from construction (h)	Section	Position	Avg. SWV (m/s)	Cycle
7/13/20	10:22	2.78	HES-1.1	TE	3537	1
7/13/20	10:25	2.84	HES-1.1	TC	3930	1
7/13/20	10:29	2.91	HES-1.1	CRS	3387	1
7/13/20	10:30	2.92	HES-1.1	CLS	1997	1
7/13/20	10:32	2.95	HES-1.1	CLN	2453	1
7/13/20	10:34	2.98	HES-1.1	CRN	2657	1
7/13/20	10:37	3.03	HES-1.1	TE	3230	2
7/13/20	10:39	3.07	HES-1.1	TC	1010	2
7/13/20	10:41	3.11	HES-1.1	CRS	2980	2
7/13/20	10:42	3.13	HES-1.1	CLS	1010	2
7/13/20	10:44	3.16	HES-1.1	CLN	1010	2
7/13/20	10:45	3.18	HES-1.1	CRN	1010	2
7/13/20	10:51	3.28	HES-1.1	TE	1010	3
7/13/20	10:53	3.31	HES-1.1	TC	1050	3
7/13/20	10:54	3.33	HES-1.1	CRS	1010	3
7/13/20	10:56	3.35	HES-1.1	CLS	1153	3
7/13/20	10:58	3.38	HES-1.1	CLN	1190	3
7/13/20	10:59	3.41	HES-1.1	CRN	1083	3

Table A. 6: Shear Wave Velocity of slab HES1 (Day 1) Part II

Date	Time	Time from construction (h)	Section	Position	Avg. SWV (m/s)	Cycle
7/13/20	11:05	3.51	HES-1.1	TE	1073	4
7/13/20	11:07	3.53	HES-1.1	TC	1187	4
7/13/20	11:08	3.56	HES-1.1	CRS	1047	4
7/13/20	11:10	3.58	HES-1.1	CLS	1243	4
7/13/20	11:11	3.61	HES-1.1	CLN	1267	4
7/13/20	11:12	3.62	HES-1.1	CRN	1220	4
7/13/20	11:20	3.76	HES-1.1	TE	1210	5
7/13/20	11:21	3.78	HES-1.1	TC	1300	5
7/13/20	11:23	3.80	HES-1.1	CRS	1203	5
7/13/20	11:24	3.82	HES-1.1	CLS	1387	5
7/13/20	11:25	3.84	HES-1.1	CLN	1410	5
7/13/20	11:27	3.87	HES-1.1	CRN	1337	5
7/13/20	12:00	4.42	HES-1.1	TE	1555	7
7/13/20	12:00	4.43	HES-1.1	TC	1610	7
7/13/20	12:01	4.43	HES-1.1	CRS	1530	7

7/13/20	12:02	4.45	HES-1.1	CLS	1670	7
7/13/20	12:03	4.47	HES-1.1	CLN	1675	7
7/13/20	12:03	4.48	HES-1.1	CRN	1655	7
7/13/20	12:34	4.99	HES-1.1	TE	1770	8
7/13/20	12:36	5.03	HES-1.1	TC	1835	8
7/13/20	12:37	5.04	HES-1.1	CRS	1755	8
7/13/20	12:38	5.06	HES-1.1	CLS	1830	8
7/13/20	12:39	5.08	HES-1.1	CLN	1950	8
7/13/20	12:40	5.09	HES-1.1	CRN	1920	8
7/13/20	13:00	5.42	HES-1.1	TE	1935	9
7/13/20	13:01	5.43	HES-1.1	TC	2010	9
7/13/20	13:02	5.45	HES-1.1	CRS	1925	9
7/13/20	13:03	5.47	HES-1.1	CLS	2055	9
7/13/20	13:04	5.49	HES-1.1	CLN	2015	9
7/13/20	13:05	5.51	HES-1.1	CRN	2030	9

Table A. 7: Shear Wave Velocity of slab HES1 (Day 1) Part III

Date	Time	Time from construction (h)	Section	Position	Avg. SWV (m/s)	Cycle
7/13/20	13:26	5.86	HES-1.1	TE	2075	10
7/13/20	13:27	5.88	HES-1.1	TC	2095	10
7/13/20	13:28	5.89	HES-1.1	CRS	2060	10
7/13/20	13:29	5.91	HES-1.1	CLS	2100	10
7/13/20	13:30	5.93	HES-1.1	CLN	2100	10
7/13/20	13:31	5.93	HES-1.1	CRN	2125	10
7/13/20	14:00	6.42	HES-1.1	TE	2140	11
7/13/20	14:00	6.43	HES-1.1	TC	2135	11
7/13/20	14:01	6.44	HES-1.1	CRS	2110	11
7/13/20	14:02	6.45	HES-1.1	CLS	2135	11
7/13/20	14:03	6.47	HES-1.1	CLN	2130	11
7/13/20	14:04	6.48	HES-1.1	CRN	2160	11
7/13/20	14:22	6.78	HES-1.1	TE	2170	12
7/13/20	14:23	6.81	HES-1.1	TC	2155	12
7/13/20	14:24	6.83	HES-1.1	CRS	2115	12
7/13/20	14:25	6.83	HES-1.1	CLS	2150	12
7/13/20	14:26	6.85	HES-1.1	CLN	2140	12
7/13/20	14:27	6.87	HES-1.1	CRN	2160	12
7/13/20	15:21	7.77	HES-1.1	TE	2170	13
7/13/20	15:22	7.78	HES-1.1	TC	2195	13
7/13/20	15:23	7.80	HES-1.1	CLS	2160	13
7/13/20	15:23	7.81	HES-1.1	CRS	2135	13
7/13/20	15:24	7.83	HES-1.1	CLN	2150	13
7/13/20	15:25	7.83	HES-1.1	CRN	2240	13
7/13/20	16:21	8.78	HES-1.1	TE	2210	14
7/13/20	16:23	8.80	HES-1.1	TC	2175	14
7/13/20	16:24	8.82	HES-1.1	CLS	2210	14
7/13/20	16:25	8.83	HES-1.1	CRS	2170	14
7/13/20	16:25	8.83	HES-1.1	CLN	2170	14

7/13/20	16:26	8.86	HES-1.1	CRN	2250	14

Table A. 8: Shear Wave Velocity of slab HES1 (Subsequent Days)

Date	Time	Time from construction (h)	Section	Position	Avg. SWV (m/s)	Cycle
7/14/20	8:16	24.69	HES-1.1	TE	2310	15
7/14/20	8:17	24.71	HES-1.1	TC	2300	15
7/14/20	8:19	24.73	HES-1.1	CRS	2310	15
7/14/20	8:20	24.75	HES-1.1	CRN	2320	15
7/14/20	8:21	24.77	HES-1.1	CLN	2310	15
7/14/20	8:22	24.79	HES-1.1	CLS	2305	15
7/14/20	10:45	27.17	HES-1.1	TE	2305	16
7/14/20	10:45	27.18	HES-1.1	TC	2310	16
7/14/20	10:46	27.19	HES-1.1	CRS	2285	16
7/14/20	10:47	27.20	HES-1.1	CLS	2300	16
7/14/20	10:48	27.22	HES-1.1	CLN	2310	16
7/14/20	10:49	27.23	HES-1.1	CRN	2310	16
7/15/20	10:32	50.96	HES-1.1	TE	2335	17
7/15/20	10:33	50.98	HES-1.1	TC	2310	17
7/15/20	10:34	50.98	HES-1.1	CLS	2340	17
7/15/20	10:35	51.00	HES-1.1	CRS	2310	17
7/15/20	10:36	51.02	HES-1.1	CRN	2345	17
7/15/20	10:36	51.03	HES-1.1	CLN	2330	17
7/16/20	13:04	77.49	HES-1.1	TE	2330	18
7/16/20	13:05	77.50	HES-1.1	TC	2300	18
7/16/20	13:06	77.53	HES-1.1	CLN	2360	18
7/16/20	13:07	77.54	HES-1.1	CRN	2310	18
7/16/20	13:08	77.56	HES-1.1	CRS	2270	18
7/16/20	13:09	77.58	HES-1.1	CLS	2310	18
7/18/20	7:49	120.23	HES-1.1	TE	2405	19
7/18/20	7:50	120.25	HES-1.1	TC	2310	19
7/18/20	7:51	120.27	HES-1.1	CRN	2405	19
7/18/20	7:52	120.28	HES-1.1	CRS	2395	19
7/18/20	7:53	120.30	HES-1.1	CLS	2400	19
7/18/20	7:54	120.32	HES-1.1	CLN	2400	19

Table A. 9: Shear Wave Velocity of slab HES1 (Subsequent Days) Part II

Date	Time	Time from construction (h)	Section	Position	Avg. SWV (m/s)	Cycle
7/20/20	10:36	171.02	HES-1.1	TE	2310	20
7/20/20	10:37	171.04	HES-1.1	TC	2305	20
7/20/20	10:39	171.07	HES-1.1	CRS	2360	20
7/20/20	10:40	171.08	HES-1.1	CLS	2365	20
7/20/20	10:41	171.10	HES-1.1	CRN	2410	20

7/20/20	10:42	171.12	HES-1.1	CLN	2350	20
7/27/20	11:34	339.98	HES-1.1	TE	2405	21
7/27/20	11:35	340.00	HES-1.1	TC	2365	21
7/27/20	11:36	340.03	HES-1.1	CRN	2415	21
7/27/20	11:37	340.03	HES-1.1	CRS	2400	21
7/27/20	11:37	340.04	HES-1.1	CLS	2370	21
7/27/20	11:38	340.05	HES-1.1	CLN	2395	21

Appendix C Shear Wave Velocity for Beams

Appendix C presents the average shear wave velocity (SWV) collected in beams at the laboratory.

Table A. 10: Shear Wave Velocity for LLCP beams

Date	Time	Time from construction (h)	Section	Position	Avg. SWV (m/s)
7/14/20	10:23	23.89	D1B7	A	2617
7/14/20	10:25	23.92	D1B7	B	2590
7/14/20	10:27	23.96	D1B7	C	2620
7/14/20	10:29	23.99	D1B7	D	2617
7/14/20	10:31	24.02	D1B5	A	2670
7/14/20	10:33	24.05	D1B5	B	2587
7/14/20	10:34	24.07	D1B5	C	2660
7/14/20	10:35	24.09	D1B5	D	2553
7/14/20	10:37	24.12	D1B9	A	2670
7/14/20	10:38	24.14	D1B9	B	2617
7/14/20	10:40	24.17	D1B9	C	2647
7/14/20	10:41	24.19	D1B9	D	2613
7/16/20	11:04	72.57	D1B12	A	2727
7/16/20	11:06	72.61	D1B12	B	2730
7/16/20	11:08	72.63	D1B12	C	2730
7/16/20	11:09	72.65	D1B12	D	2730
7/16/20	11:14	72.74	D1B11	A	2730
7/16/20	11:17	72.79	D1B11	B	2670
7/16/20	11:20	72.84	D1B11	C	2730
7/16/20	11:24	72.90	D1B11	D	2730
7/16/20	11:28	72.97	D1B13	A	2730
7/16/20	11:31	73.02	D1B13	B	2670
7/16/20	11:33	73.06	D1B13	C	2730
7/16/20	11:36	73.10	D1B13	D	2730

Table A. 11: Shear Wave Velocity for LLCP beams Part II

Date	Time	Time from construction (h)	Section	Position	Avg. SWV (m/s)
7/18/20	7:20	116.84	D1B15	A	2730

7/18/20	7:21	116.86	D1B15	B	2720
7/18/20	7:23	116.88	D1B15	C	2733
7/18/20	7:24	116.90	D1B15	D	2660
7/18/20	7:26	116.94	D1B4	A	2730
7/18/20	7:28	116.98	D1B4	B	2730
7/18/20	7:30	117.01	D1B4	C	2773
7/18/20	7:32	117.03	D1B4	D	2730
7/18/20	7:36	117.10	D1B8	A	2733
7/18/20	7:38	117.14	D1B8	B	2673
7/18/20	7:40	117.17	D1B8	C	2730
7/18/20	7:42	117.20	D1B8	D	2703
7/20/20	10:13	167.72	D1B18	A	2747
7/20/20	10:14	167.73	D1B18	B	2737
7/20/20	10:16	167.77	D1B18	C	2833
7/20/20	10:17	167.79	D1B18	D	2747
7/20/20	10:20	167.84	D1B14	A	2733
7/20/20	10:22	167.87	D1B14	B	2720
7/20/20	10:24	167.91	D1B14	C	2747
7/20/20	10:26	167.94	D1B14	D	2730
7/20/20	10:28	167.98	D1B10	A	2870
7/20/20	10:30	168.01	D1B10	B	2737
7/20/20	10:32	168.03	D1B10	C	2857
7/20/20	10:33	168.06	D1B10	D	2740
7/27/20	10:51	336.35	D1B6	A	2770
7/27/20	10:52	336.37	D1B6	B	2730
7/27/20	10:53	336.38	D1B6	C	2730
7/27/20	10:54	336.40	D1B6	D	2693
7/27/20	10:59	336.49	D1B17	A	2880
7/27/20	11:01	336.52	D1B17	B	2740
7/27/20	11:02	336.53	D1B17	C	2883
7/27/20	11:03	336.55	D1B17	D	2760
7/27/20	11:11	336.68	D1B16	A	2890
7/27/20	11:12	336.71	D1B16	B	2737
7/27/20	11:13	336.72	D1B16	C	2890
7/27/20	11:14	336.74	D1B16	D	2870

Table A. 12: Shear Wave Velocity for HES beams

Date	Time	Time from construction (h)	Section	Position	Avg. SWV (m/s)
7/13/20	14:43	7.14	D2B3	D	2253
7/13/20	14:45	7.17	D2B3	A	2280
7/13/20	14:47	7.20	D2B3	B	2253
7/13/20	14:48	7.23	D2B3	C	2323
7/13/20	14:50	7.26	D2B1	A	2200
7/13/20	14:53	7.30	D2B1	B	2227
7/13/20	14:54	7.32	D2B1	C	2250
7/13/20	14:56	7.35	D2B1	D	2170
7/13/20	14:59	7.41	D2B4	A	2267

7/13/20	15:00	7.43	D2B4	B	2307
7/13/20	15:02	7.46	D2B4	C	2307
7/13/20	15:04	7.49	D2B4	D	2260
7/13/20	15:08	7.56	D2B2	A	2243
7/13/20	15:09	7.57	D2B2	B	2237
7/13/20	15:11	7.60	D2B2	C	2270
7/13/20	15:12	7.62	D2B2	D	2210

Appendix D Setting Information Provided on the National Website

Early Opening to Traffic Analysis Web Tool – National Version

Setting Explanations

Strength Models

The user must provide the calibration coefficients for the strength models. Only the maturity model coefficients are needed **(a_m, b_m, c_m, d_m)**.

Maturity Models:

$$M_r = a_m \ln TTF - b_m$$

$$f'_c = c_m \ln TTF - d_m$$

where:

TTF is the maturity index or temperature-time factor at age t, degree-days or degree-hours

M_r is the flexural strength (modulus of rupture), psi

f'_c is the compressive strength, psi

a_m, b_m, c_m, and d_m are calibration coefficients.

Note that in the web tool, M_r can either be specified directly or calculated using the above equation by adjusting a_m and b_m under the settings. On the other hand, f'_c is calculated from c_m and d_m and cannot be directly set by the user.

Concrete Properties Variability

The spatial variability of the concrete strength at an early age is much higher than for mature concrete. The following model is used to account for this concern. The user can provide specific calibration coefficients **C, D, and E** for their project. The standard default values are 0.25, 0.001, and 0.075, respectively

$$COV_R = Ce^{(-D \times TTF)+E}$$

where:

TTF is the maturity index or temperature-time factor at age t, degree-days or degree-hours

C, D, E are calibration coefficients.

Number of Simulations

The user can change the number of simulations the model performs. Increasing the number will increase the accuracy of the model but requires a longer run time. The standard default value is 100.

Built-In-Curl

Built-in-curling is a permanent curve in a concrete slab caused by moisture or temperature gradients during concrete setting. The user can change this value based on previous work in their area. The standard default value is -10°F.

Concrete Thickness Variability

The user can change the concrete thickness variation based on previous work in the area. This ensures that even the lowest possible thickness is considered in the reliability. The standard default value is 0.03.

Dynamic k-value

The dynamic k-value is the compressibility of underlaying layers that support the concrete layer. The user can change this value based on previous work in their area. The standard default value is 200 psi/in.

Strength Coefficient

The strength coefficient is defined as the true strength at a true strain of 1. The user can change this value based on previous work. The standard default value is 1.

Appendix E Setting Information Provided on the Regional Website

Early Opening to Traffic Analysis Web Tool – Regional Version

Setting Explanations

Strength Ranges

The user must provide the ultimate or design strength for both flexural and compressive strength **(M_{ru}, f'_{cu})**. The user must also provide the minimum flexural and compressive strength tested in a laboratory **($M_{r,min}$, $f'_{c,min}$)**. This ensures the model will not consider untested strengths.

Strength Models

The user must provide the calibration coefficients for the strength models. If maturity method is chosen as the nondestructive evaluation method, only the maturity model coefficients are needed **(a_m, b_m, c_m, d_m)**. If shear wave velocity is chosen, the maturity and shear wave velocity model coefficients are needed **(a_m, b_m, c_m, d_m, a_s, b_s)**.

1. *Maturity Models:*

$$M_r = M_{ru} e^{-\left(\frac{a_m}{TTF}\right)^{b_m}}$$

$$f'_c = f'_{cu} e^{-\left(\frac{c_m}{TTF}\right)^{d_m}}$$

where:

TTF is the maturity index or temperature-time factor at age t, degree-days or degree-hours

M_r is the flexural strength (modulus of rupture), psi

M_{ru} is the ultimate expected flexural strength, psi

f'_c is the compressive strength, psi

f'_{cu} is the ultimate expected compressive strength, psi

a_m, b_m, c_m, and d_m are calibration coefficients.

2. *Shear Wave Velocity Model*

$$M_r = M_{ru} \times e^{a_s SWV + b_s}$$

where:

SWV is the shear wave velocity, m/s

a_s and b_s are calibration coefficients.

Concrete Properties Variability

The spatial variability of the concrete strength at an early age is much higher than for mature concrete. The following model is used to account for this concern. The user can provide specific calibration coefficients **C, D, and E** for their project. The standard default values are 0.25, 0.001, and 0.075, respectively

$$COV_R = Ce^{(-D \times TTF) + E}$$

where:

TTF is the maturity index or temperature-time factor at age t, degree-days or degree-hours

C, D, E are calibration coefficients.

Number of Simulations

The user can change the number of simulations the model performs. Increasing the number will increase the accuracy of the model but requires a longer run time. The standard default value is 100.

Built-In-Curl

Built-in-curling is a permanent curve in a concrete slab caused by moisture or temperature gradients during concrete setting. The user can change this value based on previous work in their area. The standard default value is -10°F.

Concrete Thickness Variability

The user can change the concrete thickness variation based on previous work in the area. This ensures that even the lowest possible thickness is considered in the reliability. The standard default value is 0.03.

Dynamic k-value

The dynamic k-value is the compressibility of underlaying layers that support the concrete layer. The user can change this value based on previous work in their area. The standard default value is 200 psi/in.

Strength Coefficient

The strength coefficient is defined as the true strength at a true strain of 1. The user can change this value based on previous work in their area. The standard default value is 1.

Bibliography

[1] B. Ostendorf, A.E. Retallack, Current Understanding of the Effects of Congestion on Traffic Accidents, International Journal of Environmental Research and Public Health. (2019) 1–19.

[2] M. Barth, K. Boriboonsomsin, Real-world carbon dioxide impacts of traffic congestion, Transportation Research Record. (2008) 163–171. https://doi.org/10.3141/2058-20.

[3] E.B. Lee, C.W. Ibbs, D. Thomas, Minimizing Total Cost for Urban Freeway Reconstruction with Integrated Construction/Traffic Analysis, Journal of Infrastructure Systems. 11 (2005) 250–257. https://doi.org/10.1061/(ASCE)1076-0342(2005)11.

[4] Work Zone Fatal Crashes and Fatalities, American Road and Transportation Builders Association. (2020). https://www.workzonesafety.org/crash-information/work-zone-fatal-crashes-fatalities/#national.

[5] J. Walls, M. Smith, Life-Cycle Cost Analysis in Pavement Design, 1998.

[6] W. Uddin, K.P. George, User cost methodology for investment planning and maintenance. Management of roads and highways, Transportation Research Record. (1993) 65–72.

[7] J. Olek, M. Cohen, C. Scholer, D.R. Mandrekar, Use of Modulus of Rupture, Fatigue Resistance and Maturity in Determining Opening to Traffic Time for Concrete Pavements, Indianapolis, IN, 2002.

[8] G.I. Crawford, Guide to Nondestructive Testing of Concrete, 1997. FHWA-SA-97-105.

[9] A. Zayed, Performance Improvement of High Early Strength (HES) Concrete for Pavement Replacement, 2018. https://doi.org/10.20961/ge.v4i1.19180.

[10] Commonwealth of Pennsylvania Department of Transportation Publication 408, 2021.

[11] Fast-Track Concrete Pavements, Concrete Paving Technology. (1994) 1–3.

[12] L.W. Cole, P.A. Okamoto, Flexural strength criteria for opening concrete roadways to traffic, Transportation Research Record. (1995) 53–61.

[13] D. Yuan, S. Nazarian, A Nondestructive Methodology for Optimizing Opening of PCC Pavements to Traffic, 2004.

[14] J. Crovetti, L. Khazanovich, Early Opening of Portland Cement Concrete (PCC) Pavements to Traffic, 2005. WHRP 05-13.

[15] N. Ghafoori, M.W. Tays, Abrasion Resistance of Early-Opening-to-Traffic Portland Cement Concrete Pavements, Journal of Materials in Civil Engineering. 19 (2007). https://doi.org/ISSN 0899-1561/2007/11-925–935/$25.00.

[16] F.C. Antico, I. De la Varga, H.S. Esmaeeli, T.E. Nantung, P.D. Zavattieri, W.J. Weiss, Using accelerated pavement testing to examine traffic opening criteria for concrete pavements, Construction and Building Materials. 96 (2015) 86–95.

[17] K. Freeseman, K. Hoegh, B.I. Izevbekhai, L. Khazanovich, Effect of early opening to traffic on fatigue damage to concrete pavement, Transportation Research Record. 2590 (2016) 94–103. https://doi.org/10.3141/2590-11.

[18] Y.-F. Su, G. Han, N. (Luna) Lu, Determining the Optimal Traffic Opening Timing Through an In-Situ NDT Method for Concrete Early Age Properties, (2020) 66. https://doi.org/10.5703/1288284317113.

[19] J. Helal, M. Sofi, P. Mendis, Non-destructive Testing of Concrete: A Review of Methods, Electronic Journal of Structural Engineering. 14 (2015) 97–105.

[20] ASTM C293-Flexural Strength of Concrete (Using Simple Beam With Center-Point Loading), ASTM International. i (2013) 9–11. https://doi.org/10.1520/C0293.

[21] ASTM C78-Flexural Strength of Concrete (using Simple Beam with Third Point Testing), ASTM International. 4 (1995) 1–7. https://doi.org/10.1520/C0078.

[22] ASTM C39-Compressive Strength of Cylindrical Concrete Specimens, ASTM Standards. (2015) 1–7. https://doi.org/10.1520/C0039.

[23] K. Freeseman, K. Hoegh, L. Khazanovich, Concrete Strength Required to Open to Traffic, 2016. MN/RC 2016-01.

[24] N.J. Carino, H.S. Lew, The Maturity Method: From Theory to Application, in: P. Chang (Ed.), Structures Congress & Exposition, American Society of Civil Engineers, Washington, D.C, 2001: p. 19.

[25] T.C. Powers, A discussion of cement hydration in relation to the curing of concrete, Proc of the Highway Research Board. 27 (n.d.) 178–188.

[26] P.K. Mehta, P.J.M. Monteiro, Concrete: Microstructure, Properties and Materials, 2001.

[27] M. Soutsos, F. Kanavaris, M. Elsageer, Accuracy of maturity functions' strength estimates for fly ash concretes cured at elevated temperatures, Construction and Building Materials. 266 (2021). https://doi.org/10.1016/j.conbuildmat.2020.121043.

[28] J. Hong, R. Kim, C. Hoon, H. Choi, Evaluation of stiffening behavior of concrete based on contactless ultrasonic system and maturity method, Construction and Building Materials. 262 (2020). https://doi.org/10.1016/j.conbuildmat.2020.120717.

[29] M. Mancio, J.T. Harvey, A. Ali, J. Zhang, Evaluation of the Maturity Method for Flexural Strength Estimation in Concrete Pavement, 2004.

[30] P. Mynarcik, Technology and Trends of Concrete Industrial Floors, Procedia Engineering. 65 (2013) 107–112. https://doi.org/10.1016/j.proeng.2013.09.019.

[31] S. Nazarian, D. Yuan, A. Medichetti, Optimizing Opening of Portland Cement Concrete

Pavements Using Integrated Maturity and Nondestructive Tests, Transportation Research Record. (2003) 3–9. https://doi.org/10.3141/1861-01.

[32] ASTM 1074-Standard Practice for Estimating Concrete Strength by the Maturity Method 1, (2013) 1–10. https://doi.org/10.1520/C1074-11.2.

[33] M. Soutsos, F. Kanavaris, Compressive strength estimates for adiabatically cured concretes with the Modified Nurse-Saul (MNS) maturity function, Construction and Building Materials. 255 (2020). https://doi.org/10.1016/j.conbuildmat.2020.119236.

[34] P.A. Okamoto, D. Whiting, Use of Maturity and Pulse Velocity Techniques to Predict Strength Gain of Rapid Concrete Pavement Repairs During the Curing Period, Transportation Research Record. (1994) 85–90.

[35] C. Wilson, W.J. Weiss, Improving the Durability of High Early Strength (HES) Concrete Patching Materials for Concrete Pavements, Transportation Research Record. 8 (2020) 12–23. https://doi.org/10.1177/0361198120917374.

[36] K. Nandhini, J. Karthikeyan, The early-age prediction of concrete strength using maturity models: a review, Journal of Building Pathology and Rehabilitation. 6 (2021). https://doi.org/10.1007/s41024-020-00102-1.

[37] M. Cho, S. Joh, S.A. Kwon, T. Kang, P. Fellow, Nondestructive In-Place Strength Profiling of Concrete Pavements by Resonance Search Technique, Transportation Research Board 86th Annual Meeting. (2007).

[38] J.-H. An, J. Nam, S.-H. Joh, S.-A. Kwon, Estimation of the Compressive Strength of Concrete Using Shear Wave Velocity, 2009.

[39] K. Hoegh, L. Khazanovich, H.T. Yu, Ultrasonic tomography for evaluation of concrete pavements, Transportation Research Record. (2011) 85–94. https://doi.org/10.3141/2232-

09.

[40] K. Hoegh, Ultrasonic Linear Array Evaluation of Concrete Pavements, University of Minnesota, 2013.

[41] M. Vancura, L. Khazanovich, R. Barnes, Concrete pavement thickness variation assessment with cores and nondestructive testing measurements, Transportation Research Record. (2013) 61–68. https://doi.org/10.3141/2347-07.

[42] P. Choi, D.-H. Kim, B.-H. Lee, M.C. Won, Application of ultrasonic shear-wave tomography to identify horizontal crack or delamination in concrete pavement and bridge, Construction and Building Materials. 121 (2016) 81–91.

[43] L. Salles de Salles, L. Khazanovich, T. Balbo, Non-Destructive Evaluation of Crack Initiation and Propagation in Continuously Reinforced Concrete Pavements, Journal of Transportation Research Board. 2673 (2019) 375–385. https://doi.org/10.1177/0361198119833672.

[44] L.S. de Salles, R. Conway, L. Khazanovich, R. Barnes, K. Hoegh, D. da Silva Pereira, T. Burnham, Non-destructive ultrasonic evaluation of construction variability effect on concrete pavement performance, International Journal of Pavement Research and Technology. 14 (2021) 385–396. https://doi.org/10.1007/s42947-020-1198-2.

[45] J. Brožovský, O. Matejka, P. Martinec, Concrete interlocking paving blocks compression strength determination using non-destructive methods, 8th International Conference of the Slovenian Society for Non-Destructive Testing: Application of Contemporary Non-Destructive Testing in Engineering. (2005) 91–97.

[46] S. Akçaözoğlu, K. Akçaözoğlu, C.D. Atiş, Thermal conductivity, compressive strength and ultrasonic wave velocity of cementitious composite containing waste PET lightweight

aggregate (WPLA), Composites Part B: Engineering. 45 (2013) 721–726. https://doi.org/10.1016/j.compositesb.2012.09.012.

[47] S. Liu, J. Zhu, S. Seraj, R. Cano, M. Juenger, Monitoring setting and hardening process of mortar and concrete using ultrasonic shear waves, Construction and Building Materials. 72 (2014) 248–255.

[48] S. Hannachi, M.N. Guetteche, Review of the ultrasonic pulse velocity Evaluating concrete compressive strength on site, (2014) 103–112.

[49] T. Mandal, J.M. Tinjum, T.B. Edil, Non-destructive testing of cementitiously stabilized materials using ultrasonic pulse velocity test, Transportation Geotechnics. 6 (2016) 97–107. https://doi.org/10.1016/j.trgeo.2015.09.003.

[50] Z. Zou, J.N. Meegoda, A Validation of the Ultrasound Wave Velocity Method to Predict Porosity of Dry and Saturated Cement Paste, Advances in Civil Engineering. 2018 (2018). https://doi.org/10.1155/2018/3251206.

[51] K.F. Bompan, V.G. Haach, Ultrasonic tests in the evaluation of the stress level in concrete prisms based on the acoustoelasticity, Construction and Building Materials. 162 (2018) 740–750. https://doi.org/10.1016/j.conbuildmat.2017.11.153.

[52] R. E, S. Hatanaka, P. Palamy, S. Kurita, Experimental study on the porosity evaluation of pervious concrete by using ultrasonic wave testing on surfaces, Construction and Building Materials. 300 (2021) 123959. https://doi.org/10.1016/j.conbuildmat.2021.123959.

[53] M. Kaczmarek, B. Piwakowski, R. Drelich, Noncontact Ultrasonic Nondestructive Techniques: State of the Art and Their Use in Civil Engineering, Journal of Infrastructure Systems. 23 (2017). https://doi.org/10.1061/(asce)is.1943-555x.0000312.

[54] C. Yang, J. Chen, Fully noncontact nonlinear ultrasonic characterization of thermal damage

in concrete and correlation with microscopic evidence of material cracking, Cement and Concrete Research. 123 (2019) 105797. https://doi.org/10.1016/j.cemconres.2019.105797.

[55] R. Kim, J. Min, E. Ahn, H. Choi, Assessment of degradation index in freeze-thaw damaged concrete using multi-channel contactless ultrasound, Construction and Building Materials. 349 (2022) 128815. https://doi.org/10.1016/j.conbuildmat.2022.128815.

[56] D. Kim, R. Kim, J. Min, H. Choi, Early-Age Freeze–Thaw Damage Detection in Concrete Using Two-Dimensional Non-Contact Ultrasonic Sensors, SSRN Electronic Journal. 364 (2022) 129854. https://doi.org/10.2139/ssrn.4202041.

[57] Q. Tran, J.R. Roesler, Noncontact Ultrasonic and Computer Vision Assessment for Sawcut Initiation Time, Journal of Transportation Engineering, Part B: Pavements. 146 (2020) 04020055. https://doi.org/10.1061/jpeodx.0000207.

[58] K. Freeseman, L. Khazanovich, K. Hoegh, A. Nojavan, A.E. Schultz, S.H. Chao, Nondestructive monitoring of subsurface damage progression in concrete columns damaged by earthquake loading, Engineering Structures. 114 (2016) 148–157. https://doi.org/10.1016/j.engstruct.2016.02.017.

[59] K. Hoegh, L. Khazanovich, H. Yu, Concrete pavement joint diagnostics with ultrasonic tomography, Transportation Research Record. (2012) 54–61. https://doi.org/10.3141/2305-06.

[60] A. De La Haza, A.A. Samokrutov, P.A. Samokrutov, Assessment of concrete structures using the Mira and Eyecon ultrasonic shear wave devices and the SAFT-C image reconstruction technique, Construction and Building Materials. 38 (2013) 1276–1291. https://doi.org/10.1016/j.conbuildmat.2011.06.002.

[61] Y.H. Lee, T. Oh, The Measurement of P- , S- , and R-Wave Velocities to Evaluate the

Condition of Reinforced and Prestressed Concrete Slabs, 2016 (2016).

[62] N.J. Carino, The impact-echo method: An overview, Structures - A Structural Engineering Odyssey, Structures 2001 - Proceedings of the 2001 Structures Congress and Exposition. 109 (2004). https://doi.org/10.1061/40558(2001)15.

[63] A. Asadollahi, L. Khazanovich, Numerical investigation of the effect of heterogeneity on the attenuation of shear waves in concrete, Ultrasonics. 91 (2019) 34–44. https://doi.org/10.1016/j.ultras.2018.07.011.

[64] D. Van Deusen, T. Burnham, B. Izevbekhai, M. Vrtis, B. Worel, Report on 2017 MnROAD Construction Activities, 2018. MN/RC 2018-16.

[65] MnDOT, Standard Specification for Construction, Minnesota-Section 2353, Minnesota Department of Transportation. 1–2 (2020).

[66] L. Khazanovich, K. Kosar, H. Li, Evaluation of Long-Term Impacts of Early Opening of Concrete Pavements, 2021.

[67] D. Janisch, An Overview of MnDOT's Pavement Condition Rating Procedures and Indices, 2015. https://www.dot.state.mn.us/materials/pvmtmgmtdocs/Rating_Overview_State_2015V.pdf.

[68] J.R. Roesler, Fatigue of concrete beams and slabs, University of Illinois at Urbana-Champaign, 1998.

[69] J. Roesler, C. Gaedicke, Flexural Behavior of Concrete Specimens on Various Support Conditions, in: 7th International DUT-Workshop on Design and Performance of Sustatinable and Durable Concrete, Sevilla, Spain, 2010.

[70] J.R. Roesler, Fatigue resistance of concrete pavements, 6th International DUT - Workshop

on Fundamental Modelling of Design and Performance of Concrete Pavements. (2006).

[71] W.J. Weiss, P. Zavattieri, J. Olek, C. Wilson, H.S. Esmaeeli, N. Todd, C. Wilson, Concrete Patching Materials and Techniques and Guidelines for Hot Weather Concreting, 2019. https://doi.org/FHWA/IN/JTRP-2019/11.

[72] E.A. Larmie, C.C. Fu, Rehabilitation and maintenance of road pavements using high early strength concrete, University of Maryland, 2005. https://doi.org/10.1017/CBO9781107415324.004.

[73] V. Vongvorakarn, S. Punurai, C.T.T. Hsu, A. Luke, P. Balaguru, V. Vongvorakarn, S. Punurai, Optimization of VES Concrete Final Report, Washington D.C, 2002. FHWA NJ 2002-004.

[74] State of Ohio: Construction and Material Specifications, Ohio Department of Transportation, Columbus, Ohio, 2022.

[75] Standard Specifications for Construction and Maintenance of Highways, Streets, and Bridges, Texas Department of Transportation, 2014.

[76] Standard Specification for Construction, Minnesota Department of Transportation, St. Paul, Minnesota, 2018.

[77] Standard Specification for Road and Bridge Construction, New Jersey Department of Transportation, 2019.

[78] S. Ghahri Saremi, D. Goulias, Concrete strength gain monitoring with non-destructive methods for potential adoption in quality assurance, Construction and Building Materials. 260 (2020) 120464. https://doi.org/10.1016/j.conbuildmat.2020.120464.

[79] L. Salles, K. Kosar, J. Vandenbossche, L. Khazanovich, Determination of Concrete Strength for Concrete Pavement Opening Decision-Making, International Journal of Pavement

Research and Technology. (2022). https://doi.org/10.1007/s42947-022-00176-9.

[80] J.W. Zhang, J. Murton, S.J. Liu, L.L. Sui, S. Zhang, L. Wang, L.H. Kong, H. Ding, Sensitivity and regression analysis of acoustic parameters for determining physical properties of frozen fine sand with ultrasonic test, Quarterly Journal of Engineering Geology and Hydrogeology. 54 (2020). https://doi.org/10.1144/qjegh2020-021.

[81] D.R. Biswal, U.C. Sahoo, S.R. Dash, Non-destructive strength and stiffness evaluation of cement-stabilised granular lateritic soils, Road Materials and Pavement Design. 21 (2018) 835–849. https://doi.org/10.1080/14680629.2018.1511458.

[82] T. Mohammed, A. Ghanizadeh, C.R. Clarkson, Z. Yang, Profile Ultrasonic Velocity Measurements Performed on Slabbed Core: Implications for High-Resolution Permeability Prediction in Low-Permeability Rocks, Society of Petroleum Engineers - SPE Canadian Energy Technology Conference. (2022). https://doi.org/10.2118/208901-MS.

[83] AASHTO, Mechanistic Empirical Pavement Design Guide: A Manual Practice, 2008.

[84] L. Salles, K. Kosar, J. Vandenbossche, L. Khazanovich, Determination of Concrete Strength for Concrete Pavement Opening Decision-Making, International Journal of Pavement Research and Technology. (2022) 1–12. https://doi.org/10.1007/s42947-022-00176-9.

[85] J. Cheeke, N. David, Fundamentals and Applications of Ultrasonic Wave, Taylor & Francis Group, 2012. https://ebookcentral.proquest.com/lib/pitt-ebooks/detail.action?docID=945471.

[86] E.E. Franco, M. a B. Andrade, R.T. Higuti, J.C. Adamovski, F. Buiochi, Acoustic transmission with mode conversion phenomenon, Proceedings of COBEM 2005. 2 (2006) 113–120.

http://www.abcm.org.br/symposiumSeries/SSM_Vol2/Section_II_Industrial_Instrumentat

ion/SSM2_II_07.pdf.

[87] A. Sadri, K. Mirkhani, Wave Propagation Concrete NDT Techniques for Evaluation of Structures and Materials, ASPNDE 2009 6th International WorkshopNDT Signal Processing. (2009) 1–8. http://www.ndt.net/article/aspnde2009/papers/07.pdf.

[88] S.A. Altoubat, D.A. Lange, Tensile basic creep: Measurements and behavior at early age, ACI Materials Journal. 98 (2001) 386–393. https://doi.org/10.14359/10728.

[89] J.H. Jeong, D.G. Zollinger, Early-age curling and warping behavior insights from a fully instrumented test-slab system, Transportation Research Record. 2000 (2004) 66–74. https://doi.org/10.3141/1896-07.

[90] J.H. Jeong, D.G. Zollinger, Environmental effects on the behavior of jointed plain concrete pavements, Journal of Transportation Engineering. 131 (2005) 140–148. https://doi.org/10.1061/(ASCE)0733-947X(2005)131:2(140).

[91] L. Østergaard, D.A. Lange, S.A. Altoubat, H. Stang, Tensile basic creep of early-age concrete under constant load, Cement and Concrete Research. 31 (2001) 1895–1899. https://doi.org/10.1016/S0008-8846(01)00691-3.

[92] W. Hansen, Y. Wei, Tensile Creep Behavior of Concrete Subject to Constant Restraint at Very Early Ages, (2013). https://doi.org/10.1061/(ASCE)MT.1943-5533.0000671.

[93] A. Hilaire, F. Benboudjema, A. Darquennes, Y. Berthaud, G. Nahas, Modeling basic creep in concrete at early-age under compressive and tensile loading, Nuclear Engineering and Design. 269 (2014) 222–230. https://doi.org/10.1016/j.nucengdes.2013.08.034.

[94] S. Liang, Y. Wei, Modelling of creep effect on moisture warping and stress developments in concrete pavement slabs, International Journal of Pavement Engineering. 19 (2018) 429–438. https://doi.org/10.1080/10298436.2017.1402595.

[95] R. Rodden, D. Lange, Moisture and Temperature Curling Stresses in Airfield Concrete Pavements, Center of Excellence for Airport Technology, 2006.

[96] L. Khazanovich, M.I. Darter, H.T. Yu, Mechanistic-empirical model to predict transverse joint faulting, Transportation Research Record. (2004) 34–45. https://doi.org/10.3141/1896-04.

[97] A.M. Ioannides, M.R. Thompson, E.J. Barenberg, Westergaard Solutions Reconsidered, (1985) 13–23.

[98] L. Khazanovich, O.I. Selezneva, H. Thomas Yu, M.I. Darter, Development of rapid solutions for prediction of critical continuously reinforced concrete pavement stresses, Transportation Research Record. (2001) 64–72. https://doi.org/10.3141/1778-08.

[99] J. Thomlinson, Temperature Variations and Consequent Stresses Produced by Daily and Seasonal Temperature Cycles in Concrete Slabs, Concrete and Construction Engineering. 36 (1940) 298–307.

[100] M.W. Kumara, M. Tia, M. Bergin, B. Choubane, Evaluation of Early Strength Requirement of Concrete for Slab Replacement Using Accelerated Pavement Testing, Journal of Transportation Engineering. 2 (2006) 482–488. https://doi.org/10.1061/(ASCE)0733-947X(2006)132.

[101] A.M. Ioannides, L. Khazanovich, Nonlinear temperature effects on multilayered concrete pavements, Journal of Transportation Engineering. 124 (1998) 128–136. https://doi.org/10.1061/(ASCE)0733-947X(1998)124:2(128).

[102] L. Khazanovich, Structural Analysis of Multi-Layered Concrete Pavement Systems, University of Illinois, 1994.

[103] J.E. Hiller, J.R. Roesler, Simplified nonlinear temperature curling analysis for jointed

concrete pavements, Journal of Transportation Engineering. 136 (2010) 654–663. https://doi.org/10.1061/(ASCE)TE.1943-5436.0000130.

[104] L. Khazanovich, D. Tompkins, Incorporating Slab/Underlying Layer Interaction into the Concrete Pavement Analysis Procedures, The National Academies Press, 2017. https://doi.org/10.17226/24842.

[105] L. Khazanovich, J.M. Vandenbossche, J. DeSantis, S.G. Sachs, Development of an Improved Design Procedure for Unbonded Concrete Overlays, Minnesota Department of Transportation, 2020. MN 2020-08.

[106] Regional Offices, Pennsylvania Department of Transporation. (2022). https://www.penndot.pa.gov/RegionalOffices/Pages/default.aspx.

[107] A.M. Tabatabaie, E.J. Barenberg, Structural Analysis of Concrete Pavement Systems, Journal of Transportation Engineering. 106 (1980) 493–506.

[108] M. Banan, K. Hjelmstad, Data-Based Mathematical Modeling: Development and Application, University of Illinois, Urbana, IL, 1994. SRS No. 590.

[109] J.R. Roesler, L. Khazanovich, Finite-element analysis of portland cement concrete pavements with cracks, Transportation Research Record. 1568 (1997) 1–9. https://doi.org/10.3141/1568-01.